UNIVERSIDADE ESTADUAL DE CAMPINAS
Faculdade de Engenharia Elétrica e de Computação

Juan Camilo Lopez Amezquita

Designing and Implementation of a Self-Healing Scheme for Modern Electrical Distribution Systems

Estudo e Implementação de um Esquema de Self-Healing em Sistemas Modernos de Distribuição de Energia Elétrica

Campinas

2019

UNIVERSIDADE ESTADUAL DE CAMPINAS
Faculdade de Engenharia Elétrica e de Computação

Juan Camilo Lopez Amezquita

Designing and Implementation of a Self-Healing Scheme for Modern Electrical Distribution Systems

Estudo e Implementação de um Esquema de Self-Healing em Sistemas Modernos de Distribuição de Energia Elétrica

Thesis presented to the School of Electrical and Computer Engineering of the University of Campinas in partial fulfillment of the requirements for the degree of Doctor in Electrical Engineering, in the area of Electrical Energy.

Tese apresentada à Faculdade de Engenharia Elétrica e de Computação da Universidade Estadual de Campinas como parte dos requisitos exigidos para a obtenção do título de Doutor em Engenharia Elétrica, na Área de Energia Elétrica.

Supervisor: Prof. Dr. Marcos Julio Rider Flores

Este exemplar corresponde à versão final da tese defendida pelo aluno Juan Camilo Lopez Amezquita, e orientada pelo Prof. Dr. Marcos Julio Rider Flores

____

Campinas

2019

Agência(s) de fomento e nº(s) de processo(s): FAPESP 2015/12564-1; FAPESP 2017/02196-0; CNPq 154097/2015-2

Ficha catalográfica
Universidade Estadual de Campinas
Biblioteca da Área de Engenharia e Arquitetura
Rose Meire da Silva - CRB 8/5974

L881d López Amézquita, Juan Camilo, 1989-
Designing and implementation of a self-healing scheme for modern electrical ditribution systems / Juan Camilo López Amézquita. – Campinas, SP : [s.n.], 2019.

Orientador: Marcos Julio Rider Flores.
Tese (doutorado) – Universidade Estadual de Campinas, Faculdade de Engenharia Elétrica e de Computação.

1. Sistemas de energia elétrica - Distribuição. 2. Otimização matemática. 3. Estimação de estado generalizado. 4. Energia - Consumo - Previsão. I. Rider Flores, Marcos Julio, 1975-. II. Universidade Estadual de Campinas. Faculdade de Engenharia Elétrica e de Computação. III. Título.

Informações para Biblioteca Digital

Título em outro idioma: Estudo e implementação de um esquema de self-healing em sistemas modernos de distribuição de energia elétrica
Palavras-chave em inglês:
Electrical systems - Distribution
Mathematical optimization
Generalized state estimation
Energy - Consumption - Forescat
Área de concentração: Energia Elétrica
Titulação: Doutor em Engenharia Elétrica
Banca examinadora:
Marcos Julio Rider Flores [Orientador]
João Bosco Augusto London Junior
Jônatas Boas Leite
Fernanda Caseño Trindade Arioli
Madson Cortes de Alemida
Data de defesa: 31-07-2019
Programa de Pós-Graduação: Engenharia Elétrica

Identificação e informações acadêmicas do(a) aluno(a)
- ORCID do autor: http://orcid.org/0000-0001-5646-8612
- Currículo Lattes do autor: http://lattes.cnpq.br/3208899900567376

COMISSÃO JULGADORA – TESE DE DOUTORADO

Candidato: Juan Camilo López Amézquita RA: 180564
Data da Defesa: 31 de julho de 2019
Título da Tese: "Designing and Implementation of a Self-Healing Scheme for Modern Electrical Distribution Systems".

Prof. Dr. Marcos Julio Rider Flores
Prof. Dr. João Bosco Augusto London Junior
Prof. Dr. Jônatas Boas Leite
Profa. Dra. Fernanda Caseño Trindade Arioli
Prof. Dr. Madson Cortes de Almeida

A ata de defesa, com as respectivas assinaturas dos membros da Comissão Julgadora, encontra-se no SIGA (Sistema de Fluxo de Dissertação/Tese) e na Secretaria de Pós-Graduação da Faculdade de Engenharia Elétrica e de Computação.

To Maria, Manuela and Mario.

Acknowledgements

This work has been possible thanks to my parents, Maria del Socorro Amézquita Ospina and Mario Hernán López Becerra, and my sister Manuela López Amézquita. Without their love and caring I will be a drifting empty bottle.

Thanks to my supervisor, Prof. Dr. Marcos Julio Rider for his excellent orientation and vast knowledge, and to Prof. Dr. Qiuwei Wu in the center for Electric Power and Energy (CEE) at the Technical University of Denmark (DTU) in Copenhaguen, for allow me to stay and work with his excellent research group for a year.

I am also thankful to all my family and friends in Colombia and Brazil. Specially, Maria Nataly Bañol, Miguel Leandro Ocampo, Hernán Darío Ocampo, Oscar López Becerra, Leonardo Grand, Sergio Torres, Andrés Diaz, and too many others. To my teachers and colleagues at the Universidad Nacional de Colombia, Sede Manizales, and at the Universidade Estadual Paulista (UNESP), faculdade de Engenharia de Ilha Solteira.

To my friends and colleagues here at the Departamento de Sistemas e Energia (DSE), Faculdade de Engenharia Elétrica e Computação (FEEC), Universidade Estadual de Campinas (UNICAMP).

I would like to thank the Programa de Pós-graduação em Engenharia Elétrica da FEEC for the infrastructure and high-quality education that they provide. To Centro de Pesquisa e Desenvolvimento em Telecomunicações (CPqD), industrial research project *PD-0063-3010/2014: Self Healing - Sistema para reconfiguração automática de rede e alocação ótima de religadores automáticos telecomandados*, Prof. Dr. Arivaldo Garcia and CPFL Energia for the systems' data.

Finally, I would like to thank the Fundação de Amparo à Pesquisa do Estado de São Paulo (FAPESP), grants 2015/12564-1 and 2017/02196-0, and Conselho Nacional de Desenvolvimento Científico e Tecnológico (CNPq), grant 154097/2015-2, for the financial support.

Sincerely,
Juan Camilo López Amézquita
2019

"Todo arde si le aplicas la chispa adecuada."
Héroes del Silencio - La Chispa Adecuada - 1995

Abstract

The main objective of this theses is to design and to implement a centralized self-healing software for unbalanced three-phase electrical distribution systems (EDS), using the information provided by smart meters and considering distributed generation (DG). Self-healing is the ability of the EDS to automatically restore themselves in case of a permanent fault. According to the data gathered by smart meters and the EDS's parameters, the proposed self-healing software is able to: a) estimate the nodal demands during the pre and post-fault status, using a three-phase state estimator and a short-term load forecasting method, b) identify the zone wherein a permanent fault is located, and c) generate the sequence of operations that must be deployed by the remote-controlled switches installed along the system. Ultimately, the self-healing scheme will isolate the faulty section of the network and restore the service of as many customers as possible, in the least amount of time and with minimal human intervention. The proposed self-healing software will have a friendly graphical user interface to simplify the data acquisition process and to present the results, considering geographic data, dispatchable DG units, smart meters and remote-controlled switching devices. A three-phase state estimator will continuously calculate the power demands at the nodes. In case of a permanent fault, the fault location algorithm will use the smart meters' data and the fault indicators signals to establish the zone where a permanent fault is most probably located. After finding the faulty section of the system and the estimated post-fault demands, an optimal service restoration will be deployed in order to determine the sequence of switch operations. Mathematical optimization models will be used to represent the three-phase state estimator and the service restoration process. An enhanced bus-impedance-matrix-based fault-location method will be also implemented. The methodology used to solve the optimization models will be the metaheuristic *Tabu Search*. The short-term load forecasting method will be an adaptation of the seasonal ARIMA models. The proposed self-healing scheme will be tested using real EDS.

Keywords: Electrical distribution system, fault-location method, mathematical programming, self-healing scheme, service restoration, short-term load forecasting.

Resumo

O objetivo deste trabalho é projetar e implementar um software eficiente de *self-healing* em sistemas de distribuição de energia elétrica trifásicos, usando as leituras dos medidores inteligentes instalados na rede e considerando a operação dos geradores distribuídos (GD). *Self-healing* é a capacidade de um sistema de distribuição para se restaurar automaticamente após a identificação e isolamento de uma falta permanente na rede. Em função dos parâmetros do sistema e das medidas, o esquema de *self-healing* proposto deve: a) estimar as demandas dos nós, no estado de pré e pós-falta, através de um estimador de estado trifásico e um modelo de previsão da demanda ao curto prazo, b) identificar a zona da rede onde existe uma falta permanente, e c) gerar a sequência de operações das chaves instaladas ao longo do sistema para isolar a zona com falta e restaurar o serviço de energia do maior número de usuários desenergizados, no menor tempo possível, e com mínima intervenção humana. Foi desenvolvida uma ferramenta computacional com um entorno gráfico amigável capaz de ler e processar os dados elétricos e geográficos das redes trifásicas, os parâmetros das fontes de GD, as leituras dos medidores inteligentes, e o estado de operação das chaves remotamente controláveis. Um algoritmo de estimação de estado trifásico determinará continuamente as injeções de potência nos nós em função das medidas registradas pelos medidores. Em caso de falta permanente, um modelo de localização de faltas, baseado nas leituras dos medidores e dos indicadores de falta instalados na rede, fornecerá o local aproximado da falta. Após localizar a falta e, segundo o valor das demandas estabelecidas pelo estimador de estado, o esquema de restauração fornecerá a sequência de operações das chaves para levar o sistema até um estado restaurativo eficiente. Modelos de otimização matemática serão desenvolvidos para representar o estimador de estado e o problema de restauração trifásica, respectivamente. O método de localização de falta utilizado será uma versão melhorada do método basedo em medida esparsas e a matriz de impedância das barras. A meta-heurística *Tabu Search* será utilizada para resolver os modelos de otimização propostos. O modelo ARIMA será utilizado para a previsão da demanda. O software de *self-healing* será testado utilizando sistemas reais.

Palavras-chaves: Estimação de estado, meta-heurísticas, otimização matemática, previsão do consumo de energia, sistemas de distribuição de energia elétrica.

List of Figures

List of Tables

Table of Contents

1 Introduction

Acronyms of Chapter 1

ARIMA Autoregressive integrated moving average

DG Distributed generation

EDS Electrical distribution system

GIS Geographic information system

GUI Graphical user interface

MAS Multi-agent system

MILP Mixed-integer linear programming

MINLP Mixed-integer nonlinear programming

MISOCP Mixed-integer second-order conic programming

NLP Nonlinear programming

OLTC On-load tap changer

SCADA Supervisory control and data acquisition

1.1 Background

In the context of modern electrical distribution systems (EDS), a centralized self-healing system is a set of equipment, software and communication technologies that, after a permanent fault, can determine and deploy a sequence of restorative actions to isolate the faulted section of the network and to minimize the total number of unsupplied customers (AGUERO, 2012). Among the restorative actions, the most commonly used are the operation of remote-controlled switching devices and the outputs of the dispatchable distributed generation (DG) resources. A truly automated self-healing system not only restores the EDS in case of a fault, but also is able to identify the approximated location of the fault and to estimate the total amount of unsupplied demand that needs to be minimized by the service restoration process. As shown in Fig. 1, the centralized self-healing scheme uses the information gathered by the SCADA system (e.g., field measurements and status of the control/protection devices) to identify the most probable location of a permanent fault and respond to it as soon as possible, with minimal human intervention. Finally, once the faulted section of the zone has been cleared, the maintenance crews can be sent to find and repair the interruption (LIU *et al.*, 2014).

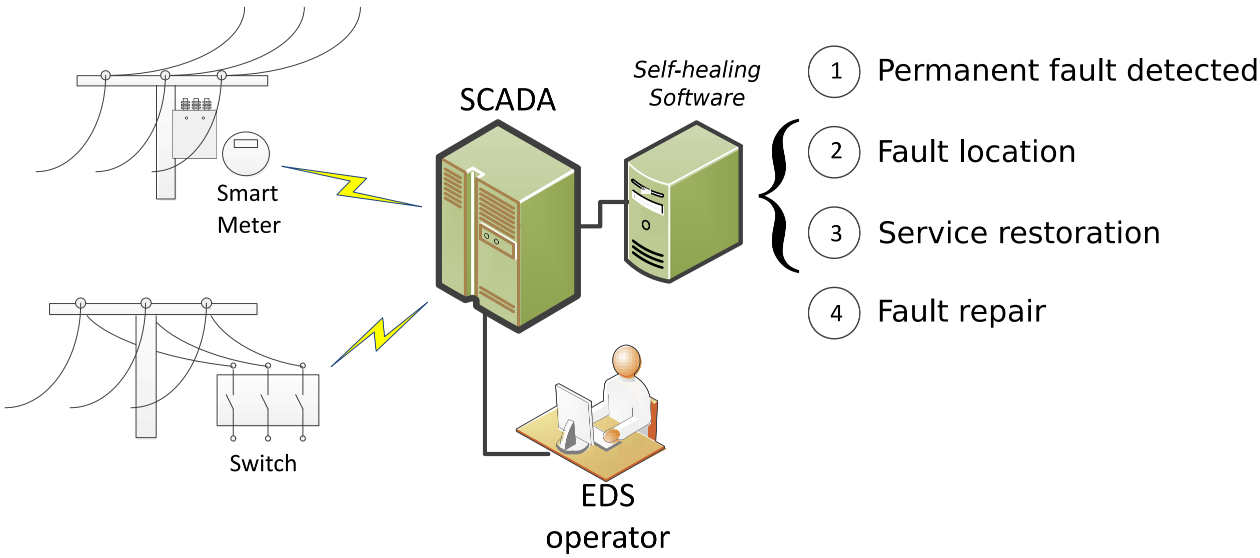

Figure 1 – Centralized self-healing system.

Source: author.

Based on the former description, the flowchart in Fig. 2 summarizes the steps of a truly centralized self-healing system. Using data gathered by smart meters and the EDS's topological and electrical parameters, a centralized self-healing scheme: a) estimates the nodal demands during the pre and pos-fault conditions, using a three-phase steady-state estimation algorithm and a short-term load forecasting method; b) identifies the zone wherein a permanent fault is located; and c) generates the sequence of switching actions and dispatchable DG outputs that minimize the total unsupplied demand (ZIDAN *et al.*, 2017). Thus, the modules of the proposed self-healing system work in tandem: once the measurements from the SCADA system have been processed by the data processing module, the state estimator module establishes the pre and the post-fault operating point of the EDS. If a permanent fault has been identified by the protection coordination, the fault location algorithm establishes the zone of the network where the outage is, most probably, located; a.k.a., the faulty zone. Finally, given a faulty zone and the estimation of the demands after the fault, an optimal restoration algorithm is deployed.

Clearly, the main module of any self-healing system is the service restoration algorithm. In general, service restoration adapts the classic system reconfiguration problem in which, instead of active power losses, the objective is to minimize the unsupplied demand

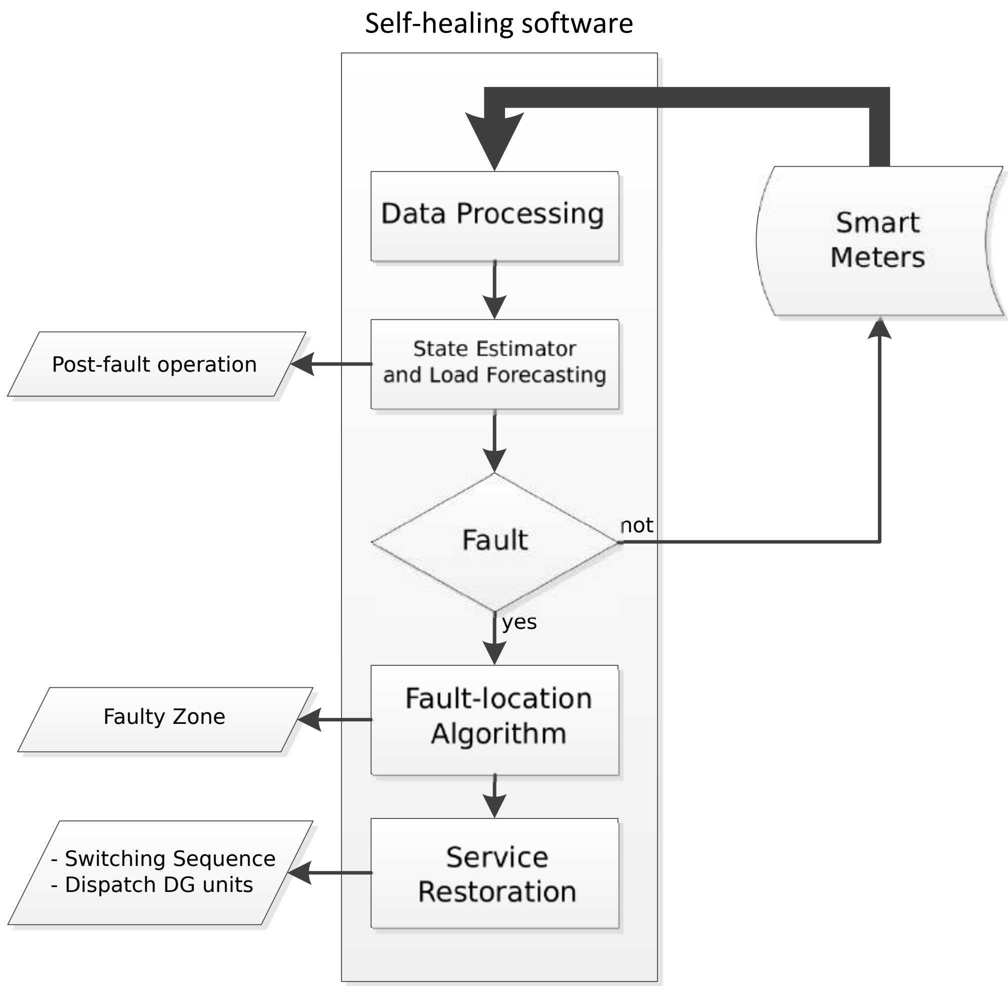

Figure 2 – Flowchart of the proposed self-healing system.

Source: author.

after a permanent fault. In order to exemplify the service restoration scheme consider the restoration sequence shown in Fig. 3. Given a permanent fault at any component of Zone 2 in the test system at Fig. 3, a simple protection scheme would open the circuit-breaker S2 to extinguish the fault (Step 1). Eventually, all loads at Zones 2 and 5 will be de-energized. Then, a simple restoration algorithm can be deployed to restore all loads at Zone 5 by opening Switch S6 and transferring Zone 5 to another feeder by closing Switch S8. (Steps 2 and 3) Finally, the faulty Zone 2 will be isolated and ready to be repaired, and the amount of unsupplied demand will be minimal.

In summary, the service restoration problem is a computationally complex optimization problem (LATARE *et al.*, 2017) for the following reasons: 1) it is combinatorial since there exists a large number of possible configurations depending on the number of remote-controlled switches; 2) it is a non-linear non-convex problem due to the equations used to

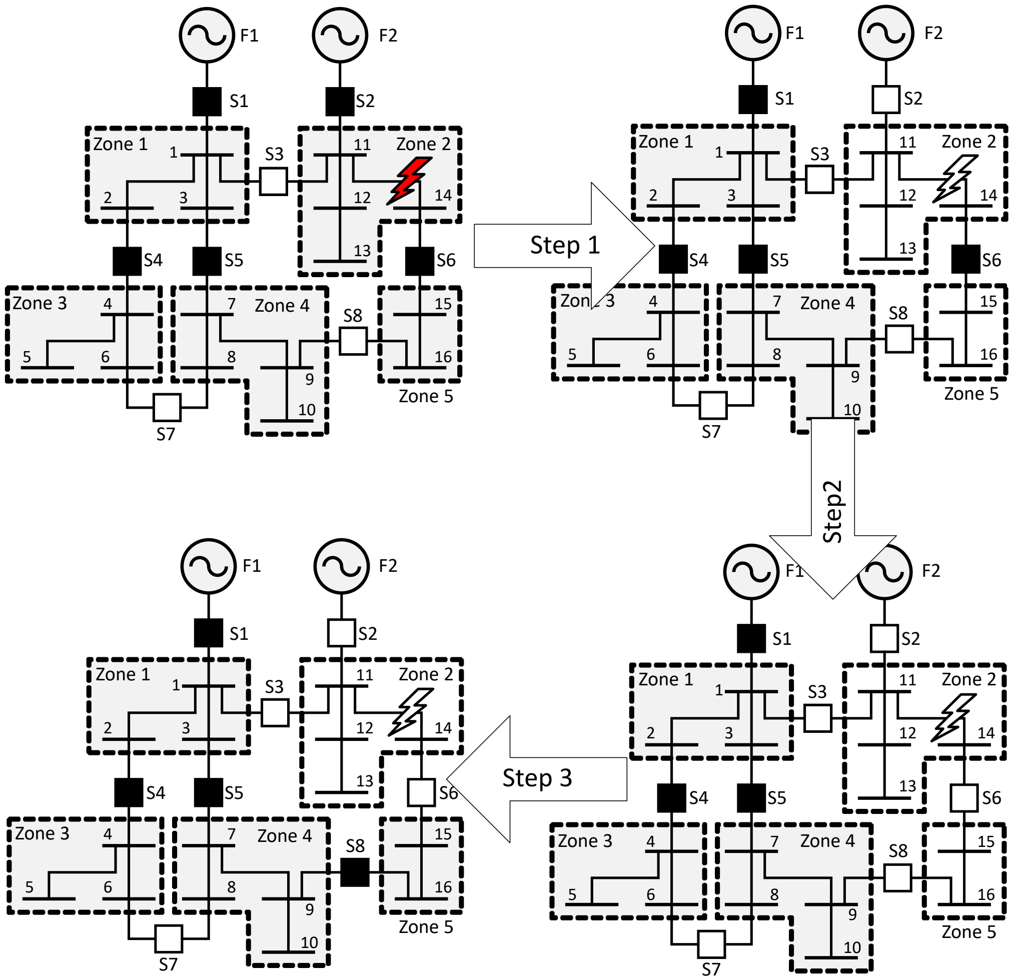

Figure 3 – Restoration sequence for a fault in Zone 2.

Source: Lopez *et al.* (2018).

represent the steady-state operation of unbalanced three-phase EDS; 3) it can be multi-objective; and 4) it is a constrained problem, in terms of electromechanical limits, switching sequence and radial topology.

1.2 State-of-the-art

Since the early nineties, multiple centralized approaches for the optimal service restoration have been proposed in the specialized literature. In this work, we have classified the service restoration methods in the following groups: expert systems, heuristic and metaheuristic algorithms, fuzzy set-based methods, graph theory-based methods, mathematical programming, and multi-agent systems (SHEN *et al.*, 2018).

1.2.1 Expert Systems

Expert systems are knowledge or field-based experience techniques. They are used to transfer experts' knowledge into a set of *if-then-else* rules, and uses them as decision-making tools to establish a set of restorative actions (SRIVASTAVA; BUTLER-BURRY, 2006). For instance, authors in Liu *et al.* (1988) developed an expert system with 180 different rules that are gathered from the specialized literature and from discussions among operators. Authors in Lee *et al.* (1992) proposed a knowledge-based restoration system with different rules that are able to separate the outage areas into a single group or multiple groups, based on feeder margins, branch points, and tie switches. Authors in Chen *et al.* (2002) developed an expert system using a colored Petri net model. This inference method can be solved in parallel processors, hence, it is very efficient for numerous switching scenarios. In addition, load priority was also considered by Chen *et al.* (2002). The author in Tsai (2008) developed an expert system using an object-oriented programming technique. In this case, the feeder configuration data is organized in a hierarchical structure that improves the performance of the inference tool. Furthermore, the proposal in Tsai (2008) considered time-dependent loads.

Although the above-mentioned expert system techniques can be very efficient in terms of computational performance, they are not suitable when more than one fault is considered, and when the electrical and topological constraint of the EDS are taken into account. Furthermore, experience can be very subjective; thus, it can be difficult to transfer into logic rules.

1.2.2 Heuristic Algorithms

Heuristic algorithms use domain-specific rules that guide the searching for quality solutions of combinatorial optimization problems. In Hsu *et al.* (1992), Miu *et al.* (1999), Kleinberg *et al.* (2011), Shirmohammadi (1992) the service restoration problem has been solved problem using distinctive heuristic approaches. Authors in Hsu *et al.* (1992) presented an heuristic multi-step procedure that makes use of feeders and lateral branches to perform full restoration or partial restoration in case of a fault. In Miu *et al.* (1999), a multi-tier algorithm was developed. In there, a tier1 is a set of tie switches, switch pairs and feeders incident to the out-of-service areas, whereas tier2 is a set of tie switches, switch pairs and feeders incident to tier1. At first, all switches and feeders in tier1 attempt to restore all the de-energized loads. If this fails, then tier2 is used to solve the problem. A similar approach considering load curtailment was proposed in Kleinberg *et al.* (2011). The author in Shirmohammadi (1992) developed a service restoration based on load flow analysis. Initially, all available switches are treated as ideal current sources and then they are closed to create a meshed grid. Then, a compensation-based power flow is executed to calculate the current magnitudes at each branch of the network. Once the current magnitudes are known, the switch carrying the least amount of current is opened to eliminate a loop. Switches are iteratively opened using the same procedure until a radial network with acceptable operating requirements is obtained.

Authors in Morelato and Monticelli (1989), Wu *et al.* (1991), Botea *et al.* (2012) constructed search spaces and decision trees of the combinatorial problem and used them in different search techniques. Clearly, domain-specific knowledge can be used to avoid unnecessary search. Thus, authors in Morelato and Monticelli (1989) developed a binary search tree in which each node is a partial assignment of a binary decision variable given by the switches' status, either open or closed. Starting from any parent node, a switch in the network is selected for branching the tree. Each possible binary value produces a child node. After the binary tree has been built, a depth-fist search technique is used to search for the optimal solution. Authors in Wu *et al.* (1991) proposed a different decision tree, in which a node represents a configuration of the network. The transition from a parent node to a child node is given by the opening of a sectionalizing switch or the closing of a tie-switch. In this work, breadth-first search is used to travel through the decision tree. Finally, authors in Botea *et al.* (2012) built a similar decision tree than Morelato and Monticelli (1989) disregarding load transference among healthy feeders. A specialized A* search technique was used in Botea *et al.* (2012) to search for the optimal reconfiguration.

While heuristic algorithms can obtain fast solutions, they still require specialists' knowledge and they are not based on classical mathematical optimization, thus optimality and feasibility are not guaranteed.

1.2.3 Metaheuristic Algorithms

Metaheuristic algorithms (or simply, metaheuristics) are optimization methods that use dissimilar strategies to avoid local minima in the search for the optimal solution of combinatorial problems (LOPES *et al.*, 2013). Many metaheuristics have been developed for solving the service restoration problem, including genetic algorithms (AUGUGLIARO *et al.*, 1998; LUAN *et al.*, 2002), tabu search (TOUNE *et al.*, 2002a), particle swarm optimization (CHEN *et al.*, 2011), parallel simulated annealing (TOUNE *et al.*, 2002b), among others. These algorithms have similar objectives with different search strategies and systems for encoding the solutions.

Thus, in Toune *et al.* (2002b), four metaheuristics were built and compared considering the average execution time and the quality of the final solution. In most metaheuristics (AUGUGLIARO *et al.*, 1998; LUAN *et al.*, 2002), a multi-objective problem is converted into an equivalent single objective problem via weighting factors, and the admissible switching sequence is usually omitted. To overcome these disadvantages, some improvements have been proposed as in Kumar *et al.* (2008), where authors adopted a non-dominated sorting genetic algorithm-II (NSGA-II) to solve the restoration problem. The objectives are the minimization of the out of service areas, switching operations and network losses. The utilization of non-dominated sorting techniques deals with multiple objectives without using weighting factors. Authors in Marques *et al.* (2018) proposed a multi-objective revolutionary algorithm that considers priority in loads and switches, and also determines the optimized switching sequence. In addition, the methodology uses a node-depth encoding method that guarantees radiality of each solution.

Metaheuristic algorithms can be very fast and do not require specialists' knowledge. However, global optimality cannot be guaranteed by any of the aforementioned techniques.

1.2.4 Fuzzy Theory

Fuzzy theory (a.k.a., fuzzy logic or fuzzy set theory) has been successfully used to address the multi-objective nature of the service restoration problem (LEE *et al.*, 1998; HSIAO; CHIEN, 2000), to consider the imprecise linguistic terms of some heuristic rules (HSU; KUO, 1994; HUANG, 2003) and to characterize uncertainties in the optimization problem (KUO; HSU, 1993; POPOVIC; POPOVIC, 2004). In these works, loads, the number of switching actions, line flows, bus voltage, etc., are treated as fuzzy variables and the solution is attained based on a maximum membership function.

Authors in Lee *et al.* (1998) developed fuzzy evaluation criteria to deal with the multi-objective nature of the restoration problem. First, a set of feasible plans is generated by a heuristic algorithm. Then, four predefined fuzzy criteria are used to evaluate these plans and to choose the one with the highest membership value. In Hsiao and Chien (2000), an interactive fuzzy satisfying method was proposed. Initially, multiple objectives are normalized by their corresponding membership functions, and the decision maker establishes a satisfaction value between 0 and 1 for each objective. Then, a genetic algorithm is used to find the solution whose membership values are closer to the established satisfaction value. Finally, according to satisfactory level of the solution, the decision maker can redefine the objectives and find a new solution.

Fuzzy set theory can also be used to represent imprecise linguistic terms of heuristic rules. In Hsu and Kuo (1994), some objectives and constraints, such as capacity limits of the supporting feeders and lateral branches, are transformed into fuzzy objectives and fuzzy constraints. Then, a *maxmin* problem is adapted to determine the best solution. In Huang

(2003), heuristic rules are transformed into a fuzzy cause-effect network, which is used to evaluate all feasible cases and find the solution with best objective value.

Uncertainties in loads were modeled in Kuo and Hsu (1993), Popovic and Popovic (2004) via fuzzy theory. In Kuo and Hsu (1993) stochastic demands are represented by fuzzy variables. According to mathematical operations on fuzzy variables, a heuristic algorithm is used to find the solution with the lowest number of required switching actions. In Popovic and Popovic (2004), uncertainties at loads and payback value are modeled as fuzzy variables, and a fuzzy mixed-integer model is developed to perform a risk-averse service restoration.

Fuzzy theory is suitable when an analytical representation of the problem is not straightforward. However, service restoration can be represented using mathematical expressions and well-known physical equations. Thus, the use of fuzzy logic seems unnecessary in most practical cases.

1.2.5 Graph Theory

Distribution networks can be represented using a graph in which nodes are seen as vertices and circuits are seen as edges of the network. Thus, the service restoration problem can be considered as the problem of finding the spanning tree that bests represents the structure of a graph in which the faulty section has been isolated, satisfying a set of operational constraints. Different graph-oriented techniques have been proposed in the specialized literature (LI *et al.*, 2014; DRAYER *et al.*, 2018; ZADSAR *et al.*, 2017; SARMA *et al.*, 1994; DIMITRIJEVIC; RAJAKOVIC, 2015). In Li *et al.* (2014), authors proposed a spanning tree search procedure based on the cut set theory. According to this theory, a new tree can be generated by operating a pair of switches with different status. Then, power flows can be executed to evaluate the feasibility of all newly formed trees and find the desired tree. In Drayer *et al.* (2018) the concept of fundamental loops is used. In theory, a tree can be derived by removing one edge from every fundamental loop. As before, power flow calculations are used to evaluate the quality of the obtained trees. In Zadsar *et al.* (2017), fundamental loops are used again to form microgrids and the particle swarm optimization is used to find the optimal solution. Author in Sarma *et al.* (1994) proposed the concept of *interested trees*. An interested tree is a graph in which all vertices are supplied by a given source. After evaluating all interested trees, a service restoration plan can be obtained. In Dimitrijevic and Rajakovic (2015), any energized node that can be connected to a de-energized area is considered as a possible root, which means that the process of restoring faulted areas can be treated as a process of identifying multiple spanning trees.

Although the optimal solution can be obtained through exhaustive search in graph theory, the number of spanning trees can be considered as a NP-hard problem. Thus, graph theory approaches suffer from scalability issues.

1.2.6 Mathematical Programming

In mathematical programming, the service restoration problem is formulated as a combinatorial optimization problem. In Nagata *et al.* (1995), Ciric and Popovic (2000), an heuristic algorithm and an expert system were merged with combinatorial optimization. Authors in Nagata *et al.* (1995) used generic experts knowledge to separate a network into several sub-networks. Then, each sub-network is analyzed with a mixed-integer linear programming (MILP) problem, solved via branch and bound. In Ciric and Popovic (2000), the combinatorial optimization is used when a simple heuristic algorithm is unable to find a feasible solution. In this context, a smaller version of the original network is used to formulate the MILP problem.

In Khushalani *et al.* (2007), Romero *et al.* (2016), Cavalcante *et al.* (2016), Lopez *et al.* (2018) more sophisticated mathematical programming models for service restoration have been proposed. Authors in Khushalani *et al.* (2007) developed two different mixed-integer nonlinear programming (MINLP) models for distribution network restoration in unbalance three-phase EDS. The first formulation uses a classical bus injection model and the second uses a branch flow model (a.k.a., DistFlow model). A nonlinear optimization solver was used to solve both MINLP models. It is well-known that solving MINLP models is difficult due to their non-convex non-linear nature. Authors in Romero *et al.* (2016) relaxed the original MINLP problem into a mixed-integer second-order cone programming (MISOCP) model, which can be efficiently solved and whose optimality is guaranteed by commercial solvers. In Cavalcante *et al.* (2016), a two-stage procedure was proposed. The first stage uses a piece-wise linearization method to transform the original MINLP problem into a convex MILP problem to calculate the value of the binary decision variables. In the second stage, a nonlinear programming (NLP) problem is solved to adjust the steady-state operating point of the network and to further optimized the load curtailment. In Lopez *et al.* (2018), the authors proposed a multi-stage MINLP problem, considering dispathchable DG units and the optimal switching sequence. Likewise, the MINLP problem is transformed into a convex MILP problem via a set of linearization techniques.

Furthemore, dynamic programming has also been used to solve the service restoration problem with switching sequence. Authors in Perez-Guerrero *et al.* (2008) used dynamic programming to determine the restoration sequence that minimizes the usupplied energy during the service restoration. In Carvalho *et al.* (2007), a two-phase strategy was proposed. In the first phase, genetic algorithm is used to find the optimal configuration. Then, in the second phase, the optimal sequence of switching operations is calculated using dynamic programming.

Uncertainties of the DG units and loads have also been studied in the specialized literature. Authors in Chen *et al.* (2016) proposed a robust restoration model that uses a two-terms objective and it takes the form of a *minmax* problem. Then, the MILP problem is solved by a column-and-constrained generation method and an optimized configuration that tries to restore as much unsupplied demand as possible, in the worst-case scenario of possible DG dispatch. Authors in Chen *et al.* (2015) formulated a robust restoration decision-making model based on information gap decision theory. This method considers uncertainties at renewable resources and loads. For a given bounded uncertainty set, the solution guarantees that the operational constraints will not be violated, and the supplied load will not fall below a selected threshold.

Some mathematical optimization models have been developed to solve the service restoration problem considering the assistance of microgrids. Authors in Wang and Wang (2015) proposed a holistic strategy that uses DG units and energy storage systems (ESS), in which normal and restorative operation are considered. In the normal operation, a rolling-horizon MINLP model is proposed to minimize the total operational costs and to deal with uncertainties. On the other hand, during restorative operation, sectionalizers are used to break the network into self-sustained microgrids. Authors in Chen *et al.* (2018) proposed a sequential restoration strategy to break the network into microgrids. Moreover, typical components of EDS, such as voltage regulators and capacitor banks, are modelled. In Guo and Wang (2016), authors used Bender's decomposition technique to solve the service restoration problem. The master problem minimizes the load shedding during the reconfiguration, and the slave problem minimizes active power losses in each generated microgrid.

Although convex mathematical programming can obtain the optimal solution under diverse operating constraints, execution times often exceed practical implementation, specially for large-scale EDS.

1.2.7 Multi-agent Systems

Multi-agent systems (MAS) are decentralized control methods that use procedural programming at each individual agent of the system to achieve a common goal. Authors in Nagata and Sasaki (2002) proposed a MAS-based service restoration process in which each bus is considered as a single agent with a central facilitator agent. Each bus agent is responsible for monitoring and restoring its own load, whereas the facilitator runs a negotiation process to guarantee overall feasibility. Clearly, the previous work is not totally decentralized due to the presence of a central facilitator agent. Authors in Solanki *et al.* (2007) proposed a fully decentralized MAS-based restoration using three types of agents: switch, load, and generation agents. Each agent has restricted access to local measurements and limited communication with neighboring agents. Full restoration and partial restoration can be achieved in Solanki *et al.* (2007) thanks to the inclusion of load priority at each load agent. Likewise, authors in Zidan and El-Saadany (2012) proposed a MAS-based restoration using zone and feeder agents, considering the presence of dispatchable DG resources. A two-step process is considered by each agent at Zidan and El-Saadany (2012); first, zone agents monitor the EDS in search for permanent faults or under-fault operation, and deploy a set of control actions according to the impact of the fault. Then, in the second step, a negotiation among agents is carried out to reduce the amount of unsupplied demand. Multiple faults are also considered by the method in Zidan and El-Saadany (2012). Working above the previous proposal, authors in Hafez *et al.* (2018) proposed four different types of zone agents, namely, faulted zone agent, unsupplied zone agent, tie zone agent, and healthy zone agent. After a permanent fault, each zone of the network identify itself as one of the previous types depending on the location of the fault. Authors in Elmitwally *et al.* (2015) included a new type of agent associated to voltage control. Such devices, voltage regulators, capacitor banks and OLTCs, are used to improve the voltage profile of the system and, therefore, the restorative capacity of the EDS. Fuzzy set theory was used to carry out the decision-making process at each agent.

More recently, energy storage systems and microgrids have been adapted to provide service restoration services., as in Nguyen and Flueck (2012). Under normal operation, storage units are used to provide voltage support and active power losses reduction. Then, in case of a permanent fault, storage and switch agents are deployed in order to reduce the impact of the outage by transferring loads among healthy feeders and the creation of microgrid islands. Finally, electric vehicles with vehicle-to-grid (V2G) capabilities are employed to support the grid in case of a fault, as in Sharma *et al.* (2015). In this work, a new aggregator agent is proposed and used by the MAS-based restoration service to improve the restorative capacity of the grid.

1.3 Objectives

The main objective of this thesis is to develop a software dedicated to the design and implementation of a centralized *self-healing system* in modern EDS. Based on the measurements gathered by smart meters and the operation of remote-controlled switches installed throughout the network, and considering the presence of dispatchable DG units, the proposed software can be used to locate the fault, to estimate the state and to restoration the grid in case of a permanent fault. Hence, the overall reliability and resilience of the network will be enhanced. The use of real time measurements will make it possible to forecast the moment of maximum consumption after a fault, which is necessary to deploy a robust restoration sequence that minimizes the un-supplied demand and isolates the faulted section of the network.

A straightforward geographic information system (GIS)-based graphical user interface (GUI) will be developed to represent the real EDS. On the other hand, the proposed software will be flexible enough to allow the application of different networks with a specific data-set format. Operational limits, such as three-phase current and voltage limits, source capacities and maximum number of switching actions can be adjusted by the user, and they will be considered as constraints of the service restoration module.

Finally, the proposed self-healing system will require the following set of modules and methods that will be explained and tested in the subsequent chapters:

- Three-phase state estimator based on smart meters' measurements and SCADA data.
- Short-term load forecasting module to determine the moment of maximum consumption after a permanent fault.
- Fault location and identification algorithm based on smart meters' measurements and SCADA data.
- Optimal restoration sequence of unbalanced three-phase EDS.
- A GIS-based GUI for visualizing and deploying the proposed self-healing system in real EDS.

1.4 Motivation

The motivation behind the proposed research project was originated during the execution of the industrial research project (a.k.a., P&D project) *PD-0063-3010/2014: Self Healing - Sistema para reconfiguração automática de rede e alocação ótima de religadores automáticos telecomandados* coordinated by the Centro de Pesquisa e Desenvolvimento em Telecomunicações (CPqD), Prof. Dr. Arivaldo Garcia, financed by the Companhia Paulista de Força e Luz (CPFL Energia) and technically supported by the supervisor Prof. Dr. Marcos Julio Rider. The challenge was to implement a practical self-healing scheme in real electrical distribution systems, considering the unreliable and sometimes non-existing data, which can be fully deployed within reasonable amount of time and limited computational resources. To this date, and thanks to some of the results presented in this PhD thesis, the industrial research project was successfully implemented and many of the tests presented throughout this thesis are part of the real CPFL's distribution network.

1.5 Organization

This thesis has been structured using a paper-based approach, in which each chapter is a complete paper with abstract, introduction, state-of-the-art, contributions, methodology, tests, results and conclusions. Thus, the rest of this document is organized as follows: Chapter 2 explains and shows the performance of the proposed service restoration method for unbalanced three-phase EDS, considering the operation of dispatchable DG units and an optimized switching sequence. Chapter 3 shows the proposed fault location algorithm used to establish the most probable location of a permanent fault, based on the smart meters' measurements and the bus impedance matrix. Chapter 4 shows the adaptation of a short-term load forecasting method via seasonal autoregressive integrated moving average (ARIMA) models to estimate the moment of maximum consumption after the fault, used to deploy a robust restoration plan. Chapter 5 illustrates the resulting self-healing software and shows a practical implementation in a real EDS. Finally, conclusions and future works are addressed in Chapter 6.

2 Optimal Restoration/Maintenance Switching Sequence of Unbalanced Three-Phase Distribution Systems

Abstract

This chapter presents a mixed-integer non-linear programming (MINLP) model for the optimal restoration/maintenance switching sequence of unbalanced three-phase electrical distribution systems. Once the protection coordination has identified and cleared the faulty zone, the proposed MINLP model determines the status of the remote-controlled switches and the dispatchable distributed generation (DG) units, used to de-energized the troubled section of the network and supply as much demand as possible. The optimal restoration considers the switching sequence over a discrete horizon, guaranteeing that the operational constraints of the distribution system are not violated in every step of the sequence. Furthermore, a set of linearization strategies are presented to transform the proposed MINLP model into a mixed-integer linear programming (MILP) model. The use of MILP models guarantees convergence to optimality by applying convex optimization techniques. Tests are performed over an unbalanced three-phase radial distribution system comprising 123 nodes, 12 switches, and three dispatchable DG units. A real network with more then 5,000 nodes is also tested. Results show that the proposed optimization model is a holistic procedure that can be used to efficiently manage power restoration or to minimize isolated areas in case of scheduled maintenance in modern electrical distribution systems.

Notation of Chapter 2

The notation used throughout this chapter is as follows:

Sets:

Ω_b Set of nodes

Ω_g Set of dispatchable DG units

Ω_l Set of circuits

Ω_s	Set of sequence steps $\{1, \ldots, s^{\max}\}$
$\Omega_{\mathbf{sw}}$	Set of switches
Ω_z	Set of zones
Ω_z^S	Set of source zones
Ω_f	Set of phases $\{a, b, c\}$
$\Omega_z \setminus \Omega_z^S$	Set of load zones, disregarding the source zones

Functions:

$g\left(V_{i,f,s}^r, V_{i,f,s}^i\right)$	Function of the real part of the load current at node i, phase f, and step s
$h\left(V_{i,f,s}^r, V_{i,f,s}^i\right)$	Function of the imaginary part of the load current at node i, phase f, and step s

Parameters:

θ_f	Reference angle at phase f [rad]
θ_+	Maximum positive deviation of the voltage phase angle around the reference for each phase [rad]
θ_-	Maximum negative deviation of the voltage phase angle around the reference for each phase [rad]
Λ	Number of discrete blocks used in the square current linearization
$\phi_{ij,\lambda}$	Slope of the λ-th discrete block used to linearize the square current through circuit ij
$c_{z,s}^{\mathbf{U}}$	Cost of de-energizing a given zone z at step s [m.u.]
$c^{\mathbf{sw}}$	Cost of operating a switch during the restoration [m.u.]
$\bar{I}_{ij}$	Maximum current magnitude through circuit ij [A]
$\bar{I}_{ij}^{\mathbf{sw}}$	Maximum current magnitude through switch ij [A]
M_I	Big-M number
$\hat{n}_g$	Node of DG unit g

$P_{i,f}^{D}$ Active power demand at node i and phase f [kW]

$\underline{P}_{g}^{DG}$ Active power capacity of DG unit g [kW]

$\mathbf{pf}_{g}$ Minimum power factor of DG unit g

$Q_{i,f}^{D}$ Reactive power demand at node i and phase f [kvar]

$\overline{Q}_{g}^{DG}$ Upper reactive power capacity of DG unit g [kvar]

$\underline{Q}_{g}^{DG}$ Lower reactive power capacity of DG unit g [kvar]

$R_{ij,f,k}$ Resistance of circuit ij between phase f and phase k [mΩ]

$s^{\mathbf{max}}$ Maximum number of sequenced switching operations

$s_{ij}^{\mathbf{ini}}$ Initial status of switch ij

$\overline{V}$ Upper voltage magnitude [kV]

$\underline{V}$ Lower voltage magnitude [kV]

$V_{i,f}^{r*}$ Real part of the estimated voltage at node i and phase f [kV]

$V_{i,f}^{i*}$ Imaginary part of the estimated voltage at node i and phase f [kV]

$X_{ij,f,k}$ Reactance of circuit ij between phase f and phase k [mΩ]

$\hat{z}_{i}$ Zone of node i

$\hat{z}_{ij}$ Zone of circuit ij

Continuous Variables:

$\Delta_{ij,f,s,\lambda}^{r}$ Value of the λ-th auxiliary variable used to linearize the real current through circuit ij, phase f, and step s

$\Delta_{ij,f,s,\lambda}^{i}$ Value of the λ-th auxiliary variable used to linearize the imaginary current through circuit ij, phase f, and step s

$b_{ij,s^{\mathbf{max}}}$ Continuous auxiliary variable related to $y_{ij,s^{\max}}$

$b_{i,f,s}^{r}$ Continuous auxiliary variable related to $I_{i,f,s}^{r^D}$

$b_{i,f,s}^{i}$ Continuous auxiliary variable related to $I_{i,f,s}^{i^D}$

$I_{ij,f,s}^{r}$ Real part of the current through circuit ij, at phase f, and step s [A]

$I^{i}_{ij,f,s}$ Imaginary part of the current through circuit ij, at phase f, and step s [A]

$I^{r+}_{ij,f,s}$ Positive amount of current's real part through circuit ij, at phase f, and step s [A]

$I^{r-}_{ij,f,s}$ Negative amount of current's real part through circuit ij, at phase f, and step s [A]

$I^{i+}_{ij,f,s}$ Positive amount of current's imaginary part through circuit ij, at phase f, and step s [A]

$I^{i-}_{ij,f,s}$ Negative amount of current's imaginary part through circuit ij, at phase f, and step s [A]

$I^{r\mathbf{D}}_{i,f,s}$ Real part of the current demanded at node i, phase f, and step s [A]

$I^{i\mathbf{D}}_{i,f,s}$ Imaginary part of the current demanded at node i, phase f, and step s [A]

$I^{r\mathbf{DG}}_{g,f,s}$ Real part of the current generated by the DG unit g, phase f, and step s [A]

$I^{i\mathbf{D}}_{g,f,s}$ Imaginary part of the current generated by the DG unit g, phase f, and step s [A]

$I^{r\mathbf{S}}_{i,f,s}$ Real part of the current generated at node i, phase f, and step s [A]

$I^{i\mathbf{S}}_{i,f,s}$ Imaginary part of the current generated at node i, phase f, and step s [A]

$I^{r\mathbf{sw}}_{ij,f,s}$ Real part of the current through switch ij, phase f, and step s [A]

$I^{i\mathbf{sw}}_{ij,f,s}$ Imaginary part of the current through switch ij, phase f, and step s [A]

$P^{\mathbf{DG}}_{g,s}$ Active power generated at DG unit g, and step s [kW]

$Q^{\mathbf{DG}}_{g,s}$ Reactive power generated at DG unit g, and step s [kvar]

$V^{r}_{i,f,s}$ Real part of the voltage at node i, phase f, and step s [kV]

$V^{i}_{i,f,s}$ Imaginary part of the voltage at node i, phase f, and step s [kV]

Binary Variables:

$y_{ij,s}$ Status of switch ij, where $y_{ij,s} = 1$ if switch ij is closed at step s, or $y_{ij,s} = 0$, if open.

$x_{z,s}$ Binary variable that indicates the state of zone z. If $x_{z,s} = 1$, then zone z is energized at step s; if $x_{z,s} = 0$, then zone z is de-energized.

$\Delta y^{+}_{ij,s}$ Opening of switch ij at step s, where $\Delta y^{+}_{ij,s} = 1$ if switch ij has been opened at the step s, or $\Delta y^{+}_{ij,s} = 0$, otherwise.

$\Delta y^{-}_{ij,s}$ Closing of switch ij at step s, where $\Delta y^{-}_{ij,s} = 1$ if switch ij has been opened at the step s, or $\Delta y^{-}_{ij,s} = 0$, otherwise.

2.1 Introduction

After a permanent fault has been identified and cleared by the protection coordination system, or if a specific zone needs to be isolated for scheduled maintenance, the restoration/maintenance sequence of electrical distribution systems (EDS) can be deployed in order to establish a set of sequenced switching operations that de-energizes the faulty zone and that minimizes the unsupplied demand (WILLIS, 2004). Execution of the restoration process can be integrated into a centralized distributed automation (DA) scheme or a SCADA system in order to obtain the location and time of the fault, whereas the nodal demands can be gathered via measurements, state estimation or statistically, through short-term demand forecasting. The restoration must satisfy a set of constraints related to the electrical and physical limits of the EDS, such as the current and voltage magnitude limits, the operational constraints of the dispatchable distributed generation (DG) units, and radiality (ZIDAN *et al.*, 2017). The restoration of EDS is a combinatorial optimization problem; since the operation of remotely-controlled switches, as well as the status of each load zone at the end of the restoration process can be represented using binary decision variables. Furthermore, the restoration is also a non-linear programming problem, since the equations that represent the steady-state operation of unbalanced AC electrical networks are non-linear, non-convex mathematical expressions.

The first computational efforts for solving the optimal restoration problem relied mostly on the operator's experience, and heuristic strategies (LIU *et al.*, 1988; HSU *et al.*, 1992). Further works considered the topological and operational constraints of the EDS by using power flow analysis and heuristic approaches to provide optimized restoration schedules in a reasonable amount of time (AOKI *et al.*, 1989; MORELATO; MONTICELLI, 1989; SARMA *et al.*, 1994). With the advent of meta-heuristic algorithms, these techniques have been widely applied to provide quality solutions to the restoration problem; they have been used to deal with conflicting objective functions (KUMAR *et al.*, 2008), comparative studies (TOUNE *et al.*, 2002a), unbalanced networks (MANJUNATH; MOHAN, 2007), and large networks (SANCHES *et al.*, 2014). Fuzzy sets have also been applied to improve the decision-making process (HUANG, 2003; CHEN, 2010). More recently, in the context of DA and smart grids, new and specialized approaches have been proposed, taking advantage of modern computational and telecommunication resources spread along the EDS. A restoration algorithm, considering direct load control and demand response is presented in Kleinberg *et al.* (2011). Distributed alternatives are presented in Solanki *et al.* (2007), Nguyen and Flueck (2012), Eriksson *et al.* (2015) via multi-agent systems. A spanning-tree search algorithm is proposed in Li *et al.* (2014) in order to restore three-phase microgrids after a fault, considering dispatchable resources and islanded operation. None of these techniques guarantee optimality and none of them are either flexible or easy to develop and adapt in case of new or unexpected conditions (e.g., different objective functions, new constraints or parameters).

Mathematical optimization (or exact methods) has also been applied for solving the restoration problem. In Butler *et al.* (2001) a mixed-integer linear programming (MILP) model, based on a simplified DC power flow, is used to restore critical shipboard power feeders. Furthermore, a mixed-integer nonlinear programming (MINLP) model with the aim of restoring unbalanced EDS is proposed in Khushalani *et al.* (2007); a non-linear optimization solver was applied to obtain the solution for the MINLP formulation in Khushalani *et al.* (2007). On the other hand, in Romero *et al.* (2016) and Hijazi and Thiebaux (2014), authors present a mixed integer second-order cone programming model to solve the restoration problem, which is convex and can be solved efficiently using classical optimization techniques. Chen *et al.* (2016) formulate a MILP robust model, considering uncertain DG and demand. However, none of the aforementioned solutions have taken into account switching sequence operation and DG resources as part of the restoration process of unbalanced EDS.

This chapter proposes a generalized MINLP model for the optimal restoration/ maintenance switching sequence in unbalanced EDS, considering operational and topological constraints. The solution provided by the proposed MINLP model determines the operation of remotely-controlled switches and dispatchable DG units in each step of the sequence. The solution de-energizes the faulty or maintenance zone, and minimizes the total unsupplied demand, whilst guaranteeing a feasible steady-state operation. In each step of the sequence, only a single switch would be able to change its status. Thus, the proposed MINLP model defines a sequence of switching and dispatchable DG actions that isolates the trouble portion of the network, whilst supplying most of the remaining demand. In case of a permanent fault, the restoration process is deployed shortly after the protection coordination and DG protection have been triggered. A set of linearization strategies is used to transform the proposed MINLP model into a convex MILP model. Despite other enumerative, heuristic or metaheuristic approaches, MILP models are flexible, easy to reproduce and represent using mathematical programming languages such as AMPL (FOURER *et al.*, 2003). Additionally, convergence to optimality is guaranteed by convex optimization solvers such as CPLEX (CPLEX, 2009), which uses binary search algorithms (e.g., branch and bound) to solve MILP models. The main contributions of this chapter are as follows:

1. A holistic and flexible MINLP model for the optimal restoration of unbalanced three-phase EDS, considering the switching sequence, dispatchable DG resources and operational constraints.
2. A MILP model for the restoration/maintenance switching sequence that can be solved efficiently using convex optimization solvers.

2.2 Optimal Restoration/Maintenance Switching Sequence of EDS

The optimal restoration sequence of the EDS is an event-based problem that determines the optimal switching sequence, with the double aim of de-energizing the faulty section of the network and minimizing the amount of de-energized consumers during and after the restoration. The restoration process is independent from the protection coordination, and it is executed immediately after the fault has been totally cleared and located. Meanwhile, all the operational constraints must be guaranteed in every step of the sequence (WILLIS, 2004). Moreover, zones can also be isolated for maintenance purposes, by setting the zones to be de-energized at the last step of the switching sequence (CHOWDHURY; KOVAL, 2011).

The 16-node test system, shown in Fig. 4, is used here to exemplify the proposed sequence restoration. During the pre-fault status, the EDS is totally energized, having two radial feeders (associated with sources F1 and F2), five load zones (wherein each load zone is a section of the system, delimited by switches), and eight remotely controlled switches represented by black-colored squares, if closed; and white-colored squares, if open. If a permanent fault occurs in any branches of Zone 2, then a basic protection scheme would open the circuit-breaker S2 to extinguish the fault (Step 0). However, the opening of S2 also de-energizes Zone 5 and increases the amount of unsupplied demand. Eventually, an optimized restoration scheme would determine that the demand in Zone 5 can be transferred to feeder F1 by opening switch S6 (Step 1), followed by the closing of switch S8 (Step 2). This load transference considers the operational constraints of the system, such as voltage and current limits, and executes one switch operation at a time. In general, Step 0 is associated to the operation of the protection scheme; Step 1, is associated to the isolation of the zones that cannot be restored, and further steps are associated to load transference and minimization of the unsupplied demand by the restoration/maintenance switching sequence.

In addition to the load transference and the switching operation, the optimal restoration/maintenance process can be enhanced by considering the contribution of the dispatchable DG resources. If a DG unit is available and connected to an energized zone, it can be used

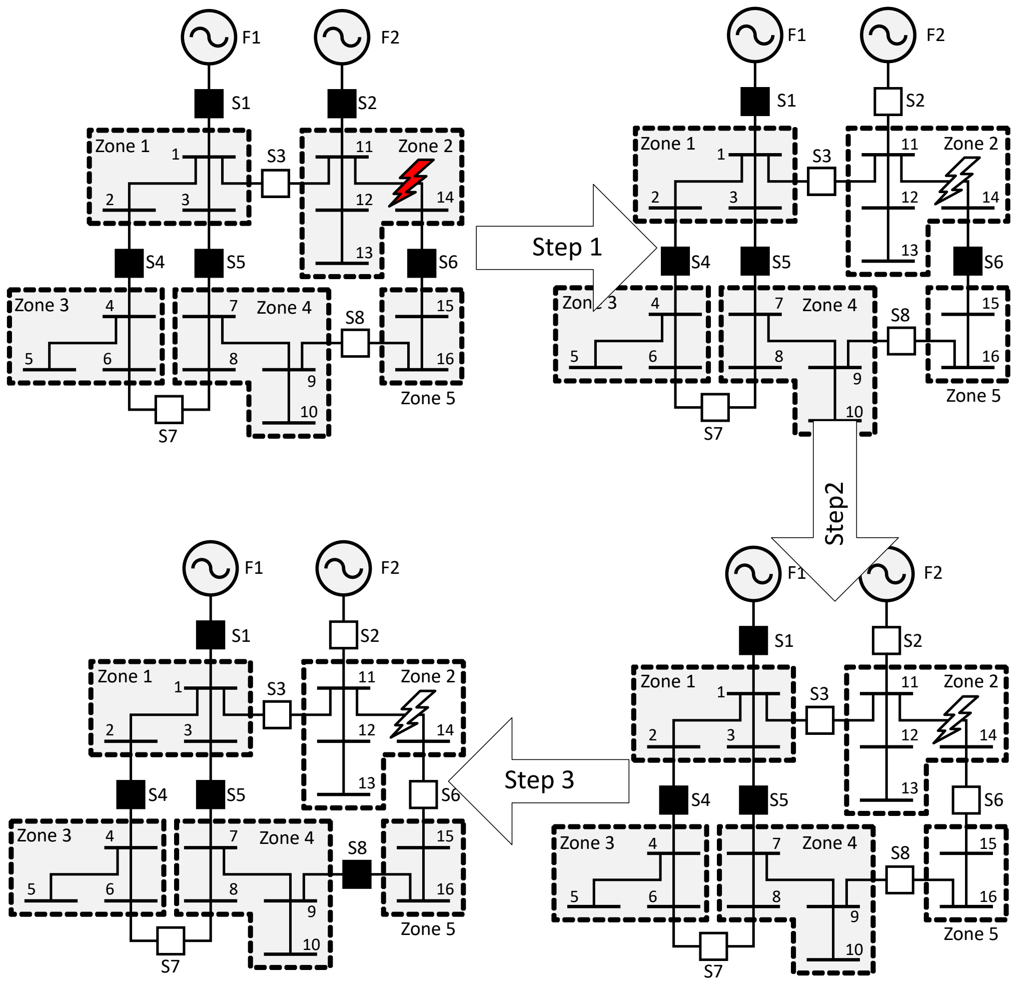

Figure 4 – Restoration sequence for a fault in Zone 2: Step 0, open switch S2 to extinguish the fault. Step 1, open switch S6. Step 2, close switch S8 to transfer the demand in Zone 5 to the feeder supplied by F1.

Source: Lopez *et al.* (2018).

to improve the service restoration. Finally, if none of the former strategies are sufficient, the restoration process can de-energize other zones of the system to meet the system constraints.

2.3 Mathematical Programming Approach

This section discusses the hypotheses and the proposed MINLP model used to represent the optimal restoration sequence of unbalanced three-phase EDS.

2.3.1 Hypotheses

The mathematical functions used to calculate the steady-state operating point of unbalanced EDS are based on the analytical formulation that represents the unbalanced three-phase current flow (CHENG; SHIRMOHAMMADI, 1995), used in Franco *et al.* (2015) and Sabillon-Antunez *et al.* (2016) to solve other related EDS operation problems. In order to formulate the optimization model, the following hypotheses are considered:

1. Electrical loads in the EDS are represented as three-phase constant active and reactive power demands.
2. Switches are considered short-length circuits with negligible impedance and limited current capacity.
3. The sequence of switching operations is discretized over a horizon of $s^{\max}$ steps.
4. Parameters, such as three-phase circuit impedances, limits, and DG capacities are established once and remain constant.
5. The location of the fault and nodal demands are gathered externally, e.g., via field measurements, state estimation or statistically.

2.3.2 Mixed-Integer Non-Linear Programming (MINLP) Model

The MINLP model that represents the optimal restoration/maintenance switching sequence of unbalanced EDS is shown in (2.1)-(2.22). Note that every node and circuit of the network must belong to a unique zone $z \in \Omega_z$, wherein each zone is an interconnected section of the network delimited by the remote-controlled switches.

$$\min \left\{ \sum_{z\in\Omega_z} \sum_{s\in\Omega_s} c^{\mathrm{U}}_{z,s} \left(1 - x_{z,s}\right) + c^{\mathrm{sw}} \sum_{ij\in\Omega_{\mathrm{sw}}} \sum_{s\in\Omega_s} \left(\Delta y^{+}_{ij,s} + \Delta y^{-}_{ij,s}\right) \right\} \tag{2.1}$$

Subject to:

$$\sum_{ji\in\Omega_l} I^{r}_{ji,f,s} - \sum_{ij\in\Omega_l} I^{r}_{ij,f,s} + \sum_{ji\in\Omega_{\mathrm{sw}}} I^{r^{\mathrm{sw}}}_{ji,f,s} - \sum_{ij\in\Omega_{\mathrm{sw}}} I^{r^{\mathrm{sw}}}_{ij,f,s} + \sum_{g\in\Omega_g|\hat{n}_g=i} I^{r^{\mathrm{DG}}}_{g,f,s} + I^{r^{\mathrm{S}}}_{i,f,s} = I^{r^{\mathrm{D}}}_{i,f,s} x_{\hat{z}_i,s} \quad \forall i\in\Omega_b, f\in\Omega_f, s\in\Omega_s \tag{2.2}$$

$$\sum_{ji\in\Omega_l} I^{i}_{ji,f,s} - \sum_{ij\in\Omega_l} I^{i}_{ij,f,s} + \sum_{ji\in\Omega_{\mathrm{sw}}} I^{i^{\mathrm{sw}}}_{ji,f,s} - \sum_{ij\in\Omega_{\mathrm{sw}}} I^{i^{\mathrm{sw}}}_{ij,f,s} + \sum_{g\in\Omega_g|\hat{n}_g=i} I^{i^{\mathrm{DG}}}_{g,f,s} + I^{i^{\mathrm{S}}}_{i,f,s} = I^{i^{\mathrm{D}}}_{i,f,s} x_{\hat{z}_i,s} \quad \forall i\in\Omega_b, f\in\Omega_f, s\in\Omega_s \tag{2.3}$$

$$V^r_{i,f,s} - V^r_{j,f,s} = \sum_{k \in \Omega_f} \left(R_{ij,f,k} I^r_{ij,k,s} - X_{ij,f,k} I^i_{ij,k,s} \right) \qquad \forall ij \in \Omega_l, f \in \Omega_f, s \in \Omega_s \quad (2.4)$$

$$V^i_{i,f,s} - V^i_{j,f,s} = \sum_{k \in \Omega_f} \left(X_{ij,f,k} I^r_{ij,k,s} + R_{ij,f,k} I^i_{ij,k,s} \right) \qquad \forall ij \in \Omega_l, f \in \Omega_f, s \in \Omega_s \quad (2.5)$$

$$I^{r^{\mathrm{D}}}_{i,f,s} = g\left(V^r_{i,f,s}, V^i_{i,f,s}\right) = \frac{P^{\mathrm{D}}_{i,f} V^r_{i,f,s} + Q^{\mathrm{D}}_{i,f} V^i_{i,f,s}}{\left(V^r_{i,f,s}\right)^2 + \left(V^i_{i,f,s}\right)^2} \qquad \forall i \in \Omega_b, f \in \Omega_f, s \in \Omega_s \quad (2.6)$$

$$I^{i^{\mathrm{D}}}_{i,f,s} = h\left(V^r_{i,f,s}, V^i_{i,f,s}\right) = \frac{P^{\mathrm{D}}_{i,f} V^i_{i,f,s} - Q^{\mathrm{D}}_{i,f} V^r_{i,f,s}}{\left(V^r_{i,f,s}\right)^2 + \left(V^i_{i,f,s}\right)^2} \qquad \forall i \in \Omega_b, f \in \Omega_f, s \in \Omega_s \quad (2.7)$$

$$\left| V^r_{i,f,s} - V^r_{j,f,s} \right| \leq 2\overline{V} \left(1 - y_{ij,s}\right) \qquad \forall ij \in \Omega_{\mathrm{sw}}, f \in \Omega_f, s \in \Omega_s \quad (2.8)$$

$$\left| V^i_{i,f,s} - V^i_{j,f,s} \right| \leq 2\overline{V} \left(1 - y_{ij,s}\right) \qquad \forall ij \in \Omega_{\mathrm{sw}}, f \in \Omega_f, s \in \Omega_s \quad (2.9)$$

$$P^{\mathrm{DG}}_{g,s}/3 = V^r_{\hat{n}_g,f,s} I^{r^{\mathrm{DG}}}_{g,f,s} + V^i_{\hat{n}_g,f,s} I^{i^{\mathrm{DG}}}_{g,f,s} \qquad \forall g \in \Omega_g, f \in \Omega_f, s \in \Omega_s \quad (2.10)$$

$$Q^{\mathrm{DG}}_{g,s}/3 = -V^r_{\hat{n}_g,f,s} I^{i^{\mathrm{DG}}}_{g,f,s} + V^i_{\hat{n}_g,f,s} I^{r^{\mathrm{DG}}}_{g,f,s} \qquad \forall g \in \Omega_g, f \in \Omega_f, s \in \Omega_s \quad (2.11)$$

$$0 \leq P^{\mathrm{DG}}_{g,s} \leq \overline{P}^{\mathrm{DG}}_g x_{\hat{z}_g,s} \qquad \forall g \in \Omega_g, s \in \Omega_s \quad (2.12)$$

$$\underline{Q}^{\mathrm{DG}}_g x_{\hat{z}_g,s} \leq Q^{\mathrm{DG}}_{g,s} \leq \overline{Q}^{\mathrm{DG}}_g x_{\hat{z}_g,s} \qquad \forall g \in \Omega_g, s \in \Omega_s \quad (2.13)$$

$$\left| Q^{\mathrm{DG}}_{g,s} \right| \leq P^{\mathrm{DG}}_{g,s} \tan\left(\cos^{-1} \mathrm{pf}_g\right) \qquad \forall g \in \Omega_g, s \in \Omega_s \quad (2.14)$$

$$\underline{V}^2 x_{\hat{z}_i,s} \leq \left(V^r_{i,f,s}\right)^2 + \left(V^i_{i,f,s}\right)^2 \leq \overline{V}^2 x_{\hat{z}_i,s} \qquad \forall i \in \Omega_b, f \in \Omega_f, s \in \Omega_s \quad (2.15)$$

$$0 \leq \left(I^r_{ij,f,s}\right)^2 + \left(I^i_{ij,f,s}\right)^2 \leq \overline{I}^2_{ij} x_{\hat{z}_{ij},s} \qquad \forall ij \in \Omega_l, f \in \Omega_f, s \in \Omega_s \quad (2.16)$$

$$0 \leq \left(I^{r^{\mathrm{sw}}}_{ij,f,s}\right)^2 + \left(I^{i^{\mathrm{sw}}}_{ij,f,s}\right)^2 \leq \left(\overline{I}^{\mathrm{sw}}_{ij}\right)^2 y_{ij,s} \qquad \forall ij \in \Omega_{\mathrm{sw}}, f \in \Omega_f, s \in \Omega_s \quad (2.17)$$

$$y_{ij,s} - y_{ij,s-1} = \Delta y^+_{ij,s} - \Delta y^-_{ij,s} \qquad \forall ij \in \Omega_{\mathrm{sw}}, s \in \Omega_s |_{y_{ij,0} = s^{\mathrm{ini}}_{ij}} \quad (2.18)$$

$$\sum_{ij \in \Omega_{\mathrm{sw}}} \left(\Delta y^{+}_{ij,s} + \Delta y^{-}_{ij,s} \right) \leq 1 \qquad \forall s \in \Omega_s \quad (2.19)$$

$$\left| x_{\hat{z}_i,s} - x_{\hat{z}_j,s} \right| \leq 1 - y_{ij,s} \qquad \forall ij \in \Omega_{\mathrm{sw}}, s \in \Omega_s \quad (2.20)$$

$$\sum_{ij \in \Omega_{\mathrm{sw}}} y_{ij,s^{\max}} x_{\hat{z}_{ij},s^{\max}} = \sum_{z \in (\Omega_s \setminus \Omega_s^{\mathrm{S}})} x_{z,s^{\max}} \quad (2.21)$$

$$y_{ij,s}, x_{z,s}, \Delta y^{+}_{ij,s}, \Delta y^{-}_{ij,s} \qquad \forall ij \in \Omega_{\mathrm{sw}}, z \in \Omega_z, s \in \Omega_s \quad (2.22)$$

The objective function in (2.1) is comprised by two terms. The first term aims at minimizing the total cost of de-energizing the zone $z \in \Omega_z$, at each step of the sequence $s \in \Omega_s$, using parameter $c^{\mathrm{U}}_{z,s}$. The second term of the objective function minimizes the total cost of the switching operations throughout the sequence, using parameter c^{sw}. Note that the objective function in (2.1) is a straightforward expression that can be easily adapted to consider other objectives, such as priorities, switching times, energy not supplied, total amount of de-energized demand, among others.

Equations (2.2) and (2.3) represent the nodal balance equations for the real and the imaginary part of the currents, respectively. Both equations are defined for each node $i \in \Omega_b$ and discrete step $s \in \Omega_s$; and they consider the three-phase injections of DG units (given by the set Ω_g) and switch currents (given by the set Ω_{sw}). The nodal voltages for unbalanced three-phase EDSs are calculated using (2.4) and (2.5), as shown in Cheng and Shirmohammadi (1995). Since loads are represented as constant active and reactive demands (see hypothesis 1 in Section 2.3.1), (2.6) and (2.7) determine the three-phase current injections at each node i and step s, as functions of the nodal voltage components $V^{r}_{i,f,s}$ and $V^{i}_{i,f,s}$. Moreover, since the impedances of the switches are negligible, (2.8) and (2.9) guarantee that the voltage difference of a closed switch ij (i.e., if $y_{ij,s} = 1$) is equal to zero. Otherwise, if the switch ij is open (i.e., if $y_{ij,s} = 0$), both nodal voltage components can vary freely within their limits, given by $2\overline{V}$.

The operation of the DG units is represented by (2.10)–(2.14). Equations (2.10) and (2.11) establish the relationship between the active and reactive generations at each phase and the steady-state variables (i.e., voltages and currents) of the three-phase DG units. In case dispatchable DG units were considered as single-phase units, then, variables $P^{\mathrm{DG}}_{g,s}$ and $Q^{\mathrm{DG}}_{g,s}$ will be calculated as the addition of each single-phase generation, and the division by three will not be necessary. Total active and reactive generations are limited by (2.12) and (2.13), respectively. As shown by (2.14), each DG unit is also limited by the minimum power factor, pf_g. Note that all DG units can only operate if the zone which they are connected to is energized (i.e., if $x_{\hat{z}_g,s} = 1$); otherwise, the DG injections are set to zero. Other operational constraints related to DG units' operation, such as ramping rates, capability curves, or turning on/off limits, can be included in the proposed formulation.

Constraint (2.15) limits the voltage magnitudes of the energized nodes; if node i is not energized, i.e., if $x_{\hat{z}_i,s} = 0$, then the voltage at node i will be zero. Likewise, (2.16) limits the current magnitudes of the energized circuits and the current capacities of the feeders and transformers. The current limits of the switching devices are given by (2.17). If switch $ij \in \Omega_{\text{sw}}$ is open (i.e., if $y_{ij,s} = 0$), then no current will flow through it. Otherwise, ij is closed (i.e., if $y_{ij,s} = 1$), the current magnitude will be limited by the switch's maximum current.

Constraints (2.18) and (2.19) model the sequenced operation of the switching devices. Both binary auxiliary variables in (2.18), $\Delta y^+_{ij,s}$ and $\Delta y^-_{ij,s}$, represent a switching transition from open-to-closed and closed-to-open, respectively. Both variables are used to calculate the number of switching operations at the end of the restoration process. Constraint (2.19) guarantees that only one transition will be made in each step of the switching sequence. Furthermore, (2.20) defines the relationship between the binary variable that represents each switch's status, $y_{ij,s}$, and the binary variable that represents each zone's status, $x_{z,s}$: if a switch ij is closed at step s (i.e., if $y_{ij,s} = 1$), then both zones, $\hat{z}_i$ and $\hat{z}_j$, must share the same status (energized or de-energized). Constraint (2.20) guarantees that an energized zone will not be connected to a de-energized zone, and vice-versa. In case a switch cannot change its status (e.g., a sectional switch), the binary decision variable associated to that switch ($y_{ij,s}$) can be fixed.

At the final step of the restoration, it is desired that the energized portion of the system has a radial topology. Radiality is made possible by equation (2.21), along with the current flow balance equations in (2.2) and (2.3). As demonstrated by Lavorato *et al.* (2012), a radial network is obtained if the number of energized switches is equal to the number of energized load zones. In this case, (2.21) guarantees that the number of closed and energized switches - hence the product between the binary decision variables $y_{ij,s^{\text{sw}}}$ and $x_{\hat{z}_i,s^{\max}}$ - must be equal to the number of energized load zones at the end of the restoration process, given by the expression $\sum_{z \in (\Omega_z \setminus \Omega_z^S)} x_{z,s^{\max}}$. Finally, the binary nature of the decision variables is given by (2.22).

2.4 MILP Model for the Optimal Restoration/Maintenance Sequence of Unbalanced EDS

The proposed MINLP in (2.1)–(2.22) is non-convex and optimality can be guaranteed by neither classical optimization techniques nor by modern heuristic approaches. Thus, this section presents a set of linearization strategies used to transform the proposed MINLP into a MILP model. This kind of formulation is desirable because there are tools (e.g., commercial solvers) available for its solution, which are more efficient and scalable than the ones used for MINLP formulations.

2.4.1 Linear Equivalents of the Binary Products

The product between binary variables and continuous variables can be represented using a single continuous variable via disjunctive constraints (FORTUNY-AMAT; MCCARL, 1981). Thus, the products between the real and imaginary load currents ($I^{r\mathrm{D}}_{i,f,s}$ and $I^{i\mathrm{D}}_{i,f,s}$) and the zone status ($x_{\hat{z}_i,s}$) in constraints (2.2) and (2.3) is replaced by the continuous auxiliary variables $b^r_{i,f,s}$ and $b^i_{i,f,s}$, using the linear equivalent equations (2.23)–(2.26), where M_I is a big-M number.

$$\left|b^r_{i,f,s}\right| \leq M_I x_{\hat{z}_i,s} \qquad \forall i \in \Omega_b, f \in \Omega_f, s \in \Omega_s \quad (2.23)$$

$$\left|I^{r\mathrm{D}}_{i,f,s} - b^r_{i,f,s}\right| \leq M_I \left(1 - x_{\hat{z}_i,s}\right) \qquad \forall i \in \Omega_b, f \in \Omega_f, s \in \Omega_s \quad (2.24)$$

$$\left|b^i_{i,f,s}\right| \leq M_I x_{\hat{z}_i,s} \qquad \forall i \in \Omega_b, f \in \Omega_f, s \in \Omega_s \quad (2.25)$$

$$\left|I^{i\mathrm{D}}_{i,f,s} - b^i_{i,f,s}\right| \leq M_I \left(1 - x_{\hat{z}_i,s}\right) \qquad \forall i \in \Omega_b, f \in \Omega_f, s \in \Omega_s \quad (2.26)$$

Similarly, the product between the binary variables $y_{ij,s^{\max}}$ and $x_{\hat{z}_i,s^{\max}}$ in (2.21) can be replaced with yet another continuous auxiliary variable $b_{ij,s^{\max}}$ as shown in (2.27)–(2.29).

$$y_{ij,s^{\max}} + x_{\hat{z}_i,s^{\max}} - 1 \leq b_{ij,s^{\max}} \qquad \forall ij \in \Omega_{\mathrm{sw}} \quad (2.27)$$

$$0 \leq b_{ij,s^{\max}} \leq y_{ij,s^{\max}} \qquad \forall ij \in \Omega_{\mathrm{sw}} \quad (2.28)$$

$$0 \leq b_{ij,s^{\max}} \leq x_{\hat{z}_i,s^{\max}} \qquad \forall ij \in \Omega_{\mathrm{sw}} \quad (2.29)$$

2.4.2 Linearization of the Load Currents

Non-linear rational equations (2.6) and (2.7) can be linearized using an approximation based on Taylor series expansion. Considering estimated values for the real and imaginary parts of the nodal voltages ($V_{i,f}^{r*}$ and $V_{i,f}^{i*}$), the linear equations for the nodal load currents are given by the first-order approximations in (2.30) and (2.31).

$$I_{i,f,s}^{r^{\mathrm{D}}} \approx g^{*} + \frac{\partial g}{\partial V_{i,f,s}^{r}}|^{*}\left(V_{i,f,s}^{r} - V_{i,f}^{r*}\right) + \frac{\partial g}{\partial V_{i,f,s}^{i}}|^{*}\left(V_{i,f,s}^{i} - V_{i,f}^{i*}\right) \qquad \forall i \in \Omega_b, f \in \Omega_f, s \in \Omega_s \quad (2.30)$$

$$I_{i,f,s}^{i^{\mathrm{D}}} \approx h^{*} + \frac{\partial h}{\partial V_{i,f,s}^{r}}|^{*}\left(V_{i,f,s}^{r} - V_{i,f}^{r*}\right) + \frac{\partial h}{\partial V_{i,f,s}^{i}}|^{*}\left(V_{i,f,s}^{i} - V_{i,f}^{i*}\right) \qquad \forall i \in \Omega_b, f \in \Omega_f, s \in \Omega_s \quad (2.31)$$

This approximation results in a relatively low error because the voltage magnitudes at each node are limited by a narrow interval. The estimated values $V_{i,f}^{r*}$ and $V_{i,f}^{i*}$, can be selected using an initial three-phase load flow analysis, experience-based values, or even a flat-start power flow.

2.4.3 Linearization of the DG Units

The three-phase operation of DG units given by the nonlinear equations (2.10) and (2.11) can be approximated using estimated values for the real and imaginary parts of the nodal voltages ($V_{i,f}^{r*}$ and $V_{i,f}^{i*}$) as shown by (2.32) and (2.33).

$$P_{g,s}^{\mathrm{DG}}/3 \approx V_{\hat{n}_g,f}^{r*} I_{g,f,s}^{r^{\mathrm{DG}}} + V_{\hat{n}_g,f}^{i*} I_{g,f,s}^{i^{\mathrm{DG}}} \qquad \forall g \in \Omega_g, f \in \Omega_f, s \in \Omega_s \quad (2.32)$$

$$Q_{g,s}^{\mathrm{DG}}/3 \approx -V_{\hat{n}_g,f}^{r*} I_{g,f,s}^{i^{\mathrm{DG}}} + V_{\hat{n}_g,f}^{i*} I_{g,f,s}^{r^{\mathrm{DG}}} \qquad \forall g \in \Omega_g, f \in \Omega_f, s \in \Omega_s \quad (2.33)$$

2.4.4 Linearization of the Voltage Limits

As shown in Fig. 5, the nodal voltage constraint in (2.15) can be linearized by selecting a maximum positive and negative deviation around the reference angle for each phase, given by θ_+ and θ_-, respectively. Thus, a set of linear constraints are used to approximate (2.15) as follows:

$$V_{i,f,s}^{i} \lesseqgtr \frac{\sin\left(\theta_f + \theta_+\right) - \sin\left(\theta_f - \theta_-\right)}{\cos\left(\theta_f + \theta_+\right) - \cos\left(\theta_f - \theta_-\right)} \left[V_{i,f,s}^{r} - x_{\hat{z}_i,s}\underline{V}\cos\left(\theta_f + \theta_+\right)\right] + x_{\hat{z}_i,s}\underline{V}\sin\left(\theta_f + \theta_+\right)$$
$$\forall i \in \Omega_b, f \in \Omega_f, s \in \Omega_s \quad (2.34)$$

$$V_{i,f,s}^{i} \lesseqgtr \frac{\sin\left(\theta_f + \theta_+\right) - \sin\theta_f}{\cos\left(\theta_f + \theta_+\right) - \cos\theta_f} \left[V_{i,f,s}^{r} - x_{\hat{z}_i,s}\overline{V}\cos\theta_f\right] + x_{\hat{z}_i,s}\overline{V}\sin\theta_f$$
$$\forall i \in \Omega_b, f \in \Omega_f, s \in \Omega_s \quad (2.35)$$

$$V^i_{i,f,s} \lesseqgtr \frac{\sin(\theta_f - \theta_-) - \sin\theta_f}{\cos(\theta_f - \theta_-) - \cos\theta_f}\left[V^r_{i,f,s} - x_{\hat{z}_i,s}\overline{V}\cos\theta_f\right] + x_{\hat{z}_i,s}\overline{V}\sin\theta_f$$
$$\forall i \in \Omega_b, f \in \Omega_f, s \in \Omega_s \quad (2.36)$$

$$V^i_{i,f,s} \lesseqgtr V^r_{i,f,s}\tan(\theta_f + \theta_+) \qquad \forall i \in \Omega_b, f \in \Omega_f, s \in \Omega_s \quad (2.37)$$

$$V^i_{i,f,s} \lesseqgtr V^r_{i,f,s}\tan(\theta_f - \theta_-) \qquad \forall i \in \Omega_b, f \in \Omega_f, s \in \Omega_s \quad (2.38)$$

The inequality symbols in (2.34)–(2.38) are chosen according to Table I, assuming θ_+ and θ_- lower than 30°.

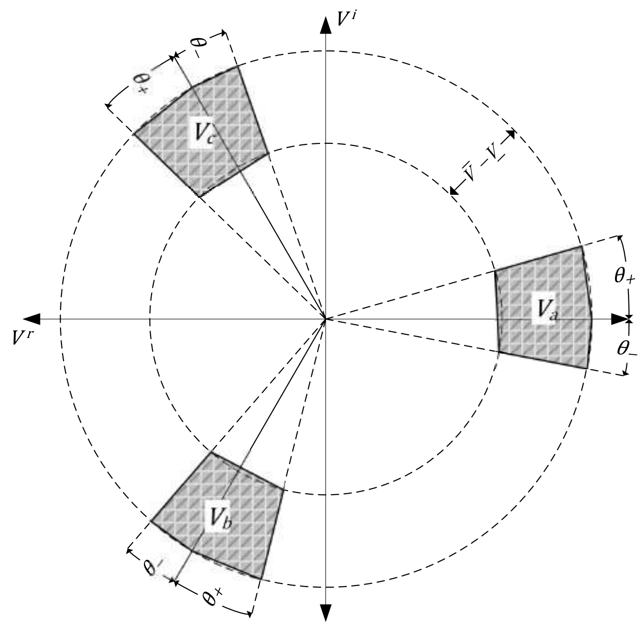

Figure 5 – Linearization of the voltage limits.

Source: Lopez *et al.* (2018).

Table 1 – Inequality symbols for (2.34)–(2.38) assuming θ_+ and θ_- lower than 30°.

Equation	$f = a$	$f = b$	$f = c$
(2.34)	$\leq$	$\leq$	$\geq$
(2.35)	$\leq$	$\geq$	$\leq$
(2.36)	$\geq$	$\geq$	$\leq$
(2.37)	$\leq$	$\geq$	$\geq$
(2.38)	$\geq$	$\leq$	$\leq$

2.4.5 Linearization of the Current Limits

To linearize the quadratic terms in (2.16) and (2.17), a piecewise linear approximation function is used (FRANCO *et al.*, 2015). Thus, the square magnitude of the real and imaginary current through each circuit is approximated by the set of linear equations in (2.39)-(2.46). Similarly, the square magnitudes of the current through the switches in (2.17) are linearized using the same piecewise approach.

$$\left(I_{ij,f,s}\right)^2 \approx \sum_{\lambda=1}^{\Lambda} \phi_{ij,\lambda} \left(\Delta^r_{ij,f,s,\lambda} + \Delta^i_{ij,f,s,\lambda}\right) \qquad \forall ij \in \Omega_l, f \in \Omega_f, s \in \Omega_s \quad (2.39)$$

$$I^r_{ij,f,s} = I^{r+}_{ij,f,s} - I^{r-}_{ij,f,s} \qquad \forall ij \in \Omega_l, f \in \Omega_f, s \in \Omega_s \quad (2.40)$$

$$I^i_{ij,f,s} = I^{i+}_{ij,f,s} - I^{i-}_{ij,f,s} \qquad \forall ij \in \Omega_l, f \in \Omega_f, s \in \Omega_s \quad (2.41)$$

$$I^{r+}_{ij,f,s} + I^{r-}_{ij,f,s} = \sum_{\lambda=1}^{\Lambda} \Delta^r_{ij,f,s,\lambda} \qquad \forall ij \in \Omega_l, f \in \Omega_f, s \in \Omega_s \quad (2.42)$$

$$I^{i+}_{ij,f,s} + I^{i-}_{ij,f,s} = \sum_{\lambda=1}^{\Lambda} \Delta^i_{ij,f,s,\lambda} \qquad \forall ij \in \Omega_l, f \in \Omega_f, s \in \Omega_s \quad (2.43)$$

$$0 \le \Delta^r_{ij,f,s,\lambda} \le \bar{I}_{ij}/\Lambda \qquad \forall ij \in \Omega_l, f \in \Omega_f, s \in \Omega_s, \lambda = 1 \ldots \Lambda \quad (2.44)$$

$$0 \le \Delta^i_{ij,f,s,\lambda} \le \bar{I}_{ij}/\Lambda \qquad \forall ij \in \Omega_l, f \in \Omega_f, s \in \Omega_s, \lambda = 1 \ldots \Lambda \quad (2.45)$$

$$\phi_{ij,\lambda} = (2\lambda - 1)\, \bar{I}_{ij}/\Lambda \qquad \forall ij \in \Omega_l, \lambda = 1 \ldots \Lambda \quad (2.46)$$

2.4.6 Optimization Process

The following steps and the flowchart in Fig. 6 summarize the proposed optimization process used to solve the optimal restoration/maintenance switching sequence of unbalanced, three-phase EDS:

Step 1 Based on experience, technical assessments or switching operation policies, define $s^{\max}$ as the maximum number of steps of the restoration process. Define the faulty zone $z_f \in \Omega_z$, and fix the zone status $x_{z_f,s} = 0$. Define s^{ini}_{ij} as the initial status of the remotely controlled switches. Define the estimated values of the voltage components ($V^{r*}_{i,f}$ and $V^{i*}_{i,f}$) by solving a relaxed version of the MINLP model in (2.1)-(2.22). To do so, all binary decision variables in (2.1)-(2.22) are transformed into continuous, bounded variables, and a non-linear solver is used to find the estimation of $V^{r*}_{i,f}$ and $V^{i*}_{i,f}$.

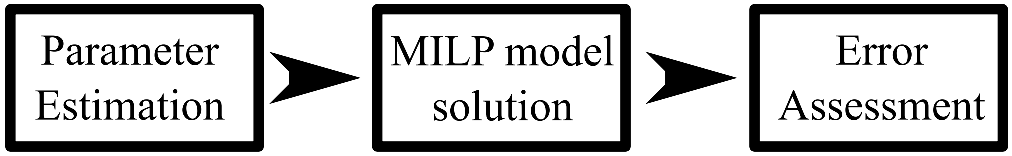

Figure 6 – Proposed optimization process.

Source: Lopez *et al.* (2018).

Step 2 Solve the restoration problem given by (2.1)-(2.22), considering the linearization strategies in Section 2.4. The resulting MILP model can be solved using a MILP solver, such as CPLEX, which uses a branch-and-bound/branch-and-cut algorithm to find the optimal solution (CPLEX, 2009). Once the solver has finished, save the decision variables, i.e., the optimal switching sequence and the DG units' operation.

Step 3 If necessary, fix the values of the decision variables and execute a three-phase load flow algorithm, such as the one in Cheng and Shirmohammadi (1995), to assess the linearization error of the proposed methodology.

2.5 Tests and Results

The unbalanced 123-node test system shown in Fig. 7 has been adapted to demonstrate the performance of the proposed restoration process. The nominal voltage is 4.16 kV. Three-phase circuit parameters and node demands can be obtained in PES (2013). As shown in Fig. 7, the voltage regulation and the capacitor banks from the original test system have been removed, and additional switches have been installed. Under normal operation, considering DGs, the minimum voltages at each phase are: $V_a = 0.9575$ p.u. at node 151, $V_b = 0.9755$ p.u. at node 96, and $V_c = 0.9623$ p.u. at node 66. The current limit for all circuits is 600 A. For the sake of simplicity, the costs in the objective function are chosen using a hierarchical criterion: the cost of de-energizing a given zone during the switching sequence is $c^U_{z,s} = 1 \cdot 10^3$ m.u. for $s < s^{\max}$, and the cost of de-energizing a zone at the end of the restoration process is $c^U_{z,s} = 10 \cdot 10^3$ m.u. The cost of each switching operation is $c^{\text{sw}} = 0.1 \cdot 10^3$ m.u. In practice, these costs are selected based on operational, reliability, or financial criteria. The maximum number of switching operations is defined as $s^{\max} = 5$, which corresponds to the maximum number of steps necessary to perform a complete restoration of any zone. If forecasted demands are accurate, a technical assessment of $s^{\max}$ can be obtained by iteratively increasing its value until no more restored demand is obtained.

The system in Fig. 7 has two feeders, 7 radial load zones, and 12 remotely controlled switches, indicated with black-colored squares, if initially closed and white-colored squares,

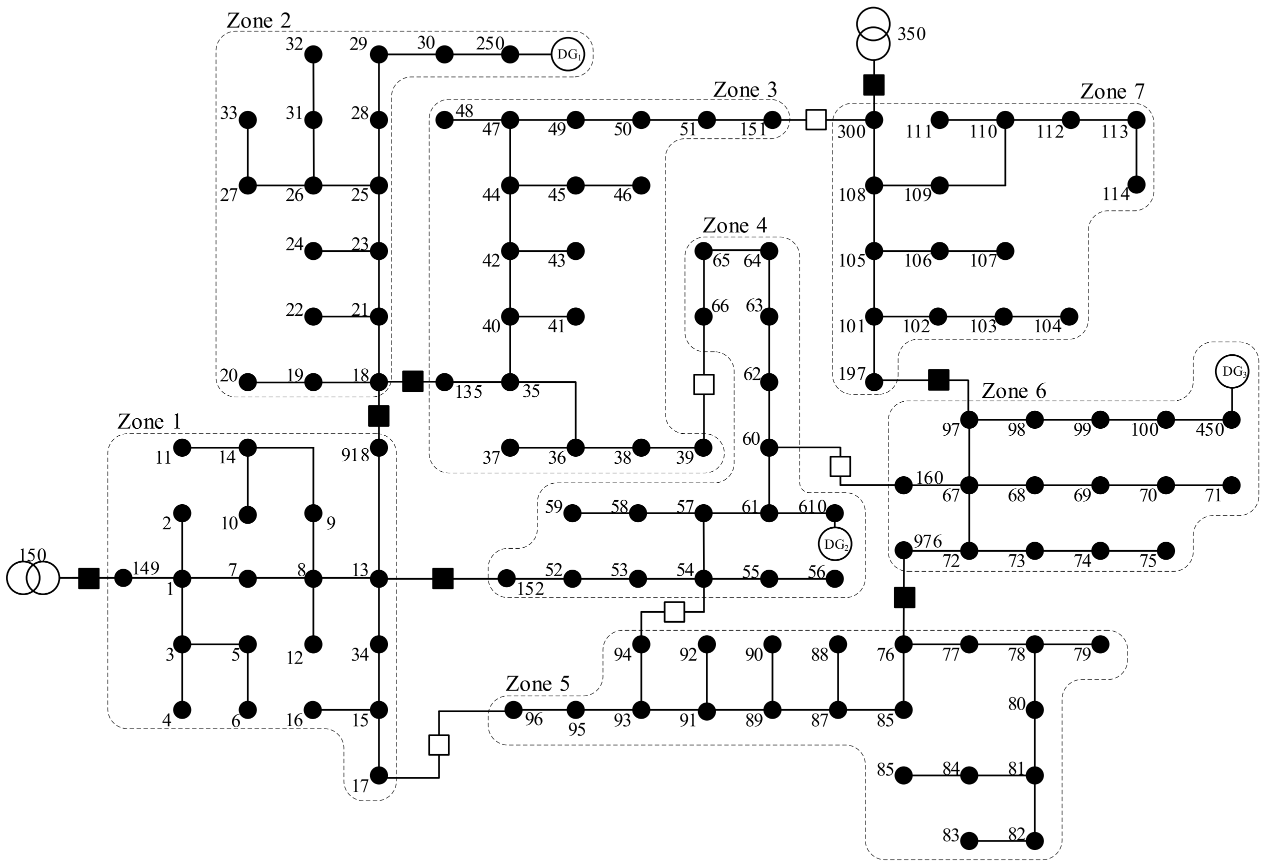

Figure 7 – Unbalanced 123-node test system.

Source: Lopez *et al.* (2018).

if initially open. The topology shown in Fig. 7 corresponds to the pre-fault state of the EDS. The maximum current magnitudes of the system during pre-fault are 387 A, 215 A and 313 A, for phases a, b, and c, respectively.

Three case studies are used here to demonstrate the adaptability of the proposed restoration process for different scenarios. In Case 1, the objective is to de-energize a faulty zone and minimize the unsupplied demand as soon as the protective scheme has located the fault, i.e., the faulty zone must be de-energized during the entire restoration sequence. The objective of Case 2 is to isolate a given zone for scheduled maintenance, thus the EDS operator would like to de-energize a zone in the last step of the switching sequence while reducing the number of de-energized customers in the process. Finally, Case 3 is identical to Case 1, but with no DG units available. In summary, for Case 1 and 3, $x_{z_f,s} = 0$, $\forall s \in \Omega_s$, and for Case 2, $x_{z_f,s^{\max}} = 0$. The voltage magnitude limits for both cases are set to $\overline{V} = 1.02\,\text{p.u.}$ and $\underline{V} = 0.95\,\text{p.u.}$ Capacity limits of the three dispatchable DG units in Fig. 7 are $\overline{P}_g^{\text{DG}} = 100\,\text{kW}$, $\underline{Q}_g^{\text{DG}} = -50\,\text{kvar}$, $\overline{Q}_g^{\text{DG}} = 50\,\text{kvar}$, and $\text{pf}_g = 0.9$, for all units. The dispatchable DG units are located at nodes 250, 450, and 610, respectively.

Table 2 – Case 1 (Restoration): Switching sequence, total unsupplied demand and optimization results.

Zone	Restoration Sequence					PU	O.F.	$V_{\min}$ [p.u.]			$I_{\max}$ [A]			Time
z_f	$s=1$	$s=2$	$s=3$	$s=4$	$s=5$	[kW]	[m.u.]	$f=a$	$f=b$	$f=c$	$f=a$	$f=b$	$f=c$	[s]
1	150-149↑	918-18↑	151-300↓	13-152↑	60-160↓	0.0	22.5	0.9616	0.9689	0.9619	569	379	418	9.6
2	918-18↑	18-135↑	151-300↓	–	–	0.0	16.3	0.9696	0.9755	0.9713	407	309	300	5.6
3	18-135↑	–	–	–	–	0.0	14.1	0.9696	0.9755	0.9672	260	182	211	1.4
4	13-152↑	–	–	–	–	0.0	14.1	0.9627	0.9755	0.9730	306	182	236	1.3
5	976-76↑	–	–	–	–	0.0	14.1	0.9817	0.9918	0.9673	273	168	211	1.4
6	97-197↑	976-76↑	96-17↓	–	–	0.0	16.3	0.9645	0.9804	0.9581	367	227	307	2.8
7	300-350↑	976-76↑	96-17↓	–	–	360	30.3	0.9575	0.9752	0.9530	525	357	410	25.7

The optimization process shown in Section 2.4.6 was implemented using the mathematical modeling language AMPL (FOURER *et al.*, 2003), whereas the MILP problem was solved via CPLEX 12.6 (CPLEX, 2009). The optimization gap of the MILP solver has been set to zero. The number of discrete blocks used in the current linearization was set to $\Lambda = 40$ blocks. All simulations were executed using a workstation with an Intel Core processor i7-6700 (3.40 GHz), and 8.00 GB of RAM.

2.5.1 Case 1: Restoration

The results of the proposed restoration process are summarized in Table 2, in which each line indicates the simulated faulty zone (z_f). As shown in Fig. 7, all load zones have been tested. The second column indicates the switching sequence generated by the proposed methodology. The symbols "↑" and "↓" represent the "opening" and "closure" of the specified switch, and "–" indicates no switching action required. The column marked as PU determines the amount of unsupplied demand at the end of the restoration sequence, without considering the demand of the faulty zone. PU is calculated using (2.47), where $x^*_{\hat{z}_i,s^{\max}}$ represents the optimal status of the zone $\hat{z}_i$ at the end of the switching sequence. The column marked as "O.F." shows the value of the objective function at the end of the restoration process. Columns "$V_{\min}$" and "$I_{\max}$" show the minimum three-phase voltage magnitudes (in p.u.) and maximum currents (in Amperes) at the end of the restoration process. Finally, the execution time is shown in the last column of Table 2.

$$PU = \sum_{i \in \Omega_b | \hat{z}_i \neq z_f} \sum_{f \in \Omega_f} P^{\mathrm{D}}_{i,f} \left(1 - x^*_{\hat{z}_i,s^{\max}}\right) \tag{2.47}$$

All the solutions in Table 2 guarantee that the operational constraints are not violated, i.e., all the three-phase voltage magnitudes, circuit currents, switch currents, and DG capacities are within their operational limits in every step of the sequence and the energized section of the network has a radial topology at the end of the restoration process. Furthermore, after executing a three-phase load flow algorithm (CHENG; SHIRMOHAMMADI, 1995), the maximum relative error of the proposed MILP model in terms of nodal voltage magnitudes was 0.14%, and in terms of current magnitudes was 2.3%. These errors are low and similar to other linear three-phase load flow formulations (GAN; LOW, 2014; GARCES, 2016). A more comprehensive error assessment of the proposed linear three-phase load flow formulation can be found in Franco *et al.* (2015), Franco *et al.* (2013).

From Table 2, note that the restoration after faults in Zones 3, 4 and 5 requires only one switch action because, as shown in Fig. 7, the isolation of those zones is made possible by opening a single switch without de-energizing other zones. Thus, the optimal restoration sequence of Zones 3, 4 and 5 is trivial, and it can be achieved by opening a single switch. In contrast, the restoration of Zones 2 and 6 requires three steps because those zones are middle sections of the feeders; therefore, the restoration process uses at least two steps to totally isolate those zones, while one additional step is required to transfer the downstream unsupplied demand to other feeders. Finally, since Zones 1 and 7 are located at the initial section of the feeders, the restoration process would require all the steps of the sequence. Nevertheless, the switching sequence generated by the proposed methodology guarantees minimum unsupplied demand, whilst satisfying operations constraints. This is demonstrated by comparing the restoration process performed after faults in Zones 1 and 7 at Table 2. Zone 1 is completely isolated at the end of the switching sequence and no additional unsupplied demand exists (i.e., $PU = 0.0\,\text{kW}$). In contrast, at the end of the restoration of Zone 7, an amount of $PU = 360.0\,\text{kW}$ is caused due to the disconnection of Zone 6, which cannot be restored by the proposed optimization model without violating the voltage limits of the EDS.

As indicated by the "O.F." column in Table 2, the more steps are used, the higher the objective function is. This happens because each switching operation has an additional cost. To satisfy the radiality constraint, the proposed methodology initiates each restoration sequence by opening the upstream switch of the faulty zone, which de-energizes all the downstream zones. Then, it transfers the non-faulty zones to other feeders, whist maintaining the radial topology of the energized section of the network.

The contribution of the dispatchable distributed resources can be illustrated by comparing the operation of each DG unit during the restoration after a fault in Zone 1. As shown in Fig. 8, since DG3 is located at Zone 6 – which is not affected by the fault at Zone 1– it operates unchanged during the entire restoration sequence. DG2 operates at step 3 when Zone 2 is restored. Finally, DG1 only operates when the Zone 4 has been transferred to the other feeder at the final step. Thus, the proposed methodology does not allow any DG unit to operate if its zone has not been yet totally restored.

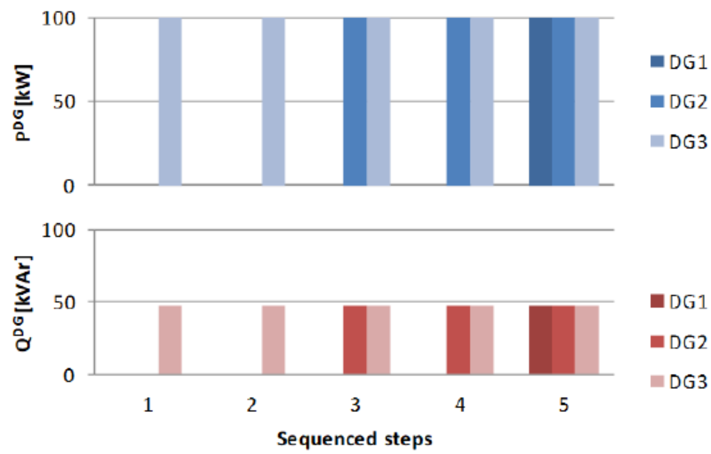

Figure 8 – Operation of the DG units during the restoration after a fault in Zone 1.

Source: Lopez *et al.* (2018).

Table 3 – Case 2 (Maintenance): Switching sequence, total unsupplied demand and optimization results.

Zone	Restoration Sequence					*PU*	O.F.	$V_{\min}$ [p.u.]			$I_{\max}$ [A]			Time
z_f	$s=1$	$s=2$	$s=3$	$s=4$	$s=5$	[kW]	[m.u.]	$f=a$	$f=b$	$f=c$	$f=a$	$f=b$	$f=c$	[s]
1	151-300↓	60-160↓	918-18↑	13-152↑	150-149↑	0.0	10.5	0.9616	0.9689	0.9619	569	379	418	5.5
2	–	–	151-300↓	18-135↑	918-18↑	0.0	10.3	0.9696	0.9755	0.9713	407	309	300	3.6
3	–	–	–	–	18-135↑	0.0	10.1	0.9696	0.9755	0.9672	260	182	211	2.3
4	–	–	–	–	13-152↑	0.0	10.1	0.9627	0.9755	0.9730	306	182	236	2.1
5	–	–	–	–	976-76↑	0.0	10.1	0.9817	0.9918	0.9673	273	168	211	2.3
6	–	–	96-17↓	976-76↑	97-197↑	0.0	10.3	0.9645	0.9804	0.9581	367	227	307	7.3
7	–	–	96-17↓	976-76↑	300-350↑	360	20.3	0.9575	0.9752	0.9530	525	357	410	13.0

2.5.2 Case 2: Scheduled Maintenance

As in the previous case, Table 3 summarizes the results of the proposed methodology applied to define the set of switching actions used to isolate each zone for maintenance.

As shown in Table 3, all switching operations are carried out at the end of the switching sequence because the binary decision variable that defines each zone status is fixed as $x_{z_f,s^{\max}} = 0$. Moreover, the radiality constraint is relaxed for $s < s^{\max}$ to consider the use of temporary loops during the switching sequence. As an example, considering the isolation of Zone 2, note that the switch 151-300 was closed first, which creates a temporary interconnection path between both feeders. Then, switches 918-18 and 18-135 were opened to isolate Zone 2 and to transfer Zone 3 to another feeder. This temporary loop minimizes the number of de-energized zones during the switching sequence. However, if meshed configurations are not desired by the EDS's operator, then the switching sequence can be reproduced

Table 4 – Case 3 (Restoration without DG): Switching sequence, total unsupplied demand and optimization results.

Zone	Restoration Sequence					PU	O.F.	$V_{\min}$ [p.u.]			$I_{\max}$ [A]			Time
z_f	$s=1$	$s=2$	$s=3$	$s=4$	$s=5$	[kW]	[m.u.]	$f=a$	$f=b$	$f=c$	$f=a$	$f=b$	$f=c$	[s]
1	150-149↑	918-18↑	151-300↓	–	–	550	32.3	0.9683	0.9740	0.9721	520	343	373	12.9
2	918-18↑	18-135↑	151-300↓	–	–	0.0	16.3	0.9683	0.9740	0.9693	423	325	316	8.7
3	18-135↑	–	–	–	–	0.0	14.1	0.9683	0.9740	0.9644	276	198	243	1.4
4	13-152↑	–	–	–	–	0.0	14.1	0.9612	0.9740	0.9715	323	198	252	1.4
5	976-76↑	–	–	–	–	0.0	14.1	0.9549	0.9853	0.9594	420	247	346	1.4
6	97-197↑	151-300↓	976-76↑	54-94↓	18-135↑	0.0	17.5	0.9501	0.9783	0.9590	402	259	338	30.3
7	300-350↑	–	–	–	–	1105	42.1	0.9549	0.9853	0.9594	420	247	346	25.8

“backwards” and the final solution would be the same.

2.5.3 Case 3: Restoration Without DG

Table 4 shows the results for the restoration of each zone without DG resources in the EDS. There are some noticeable differences between results in Table 2 and results in Table 4. First, note that after a fault in Zone 1, the proposed methodology will not transfer Zone 4 to another feeder due to current limits. Moreover, as shown in Table 4, in order to restore Zone 5 during an outage in Zone 6, an additional transference of Zone 3 must be done to alleviate the undervoltage of the feeder supplied by node 150. This additional switching sequence cannot be performed in less than five steps when simulating an outage in Zone 7. Thus, in case of a permanent fault in Zone 7, the proposed methodology only opens switch 300-350 and de-energizes the entire feeder. Comparing the simulations in Table 2 and 4, it is evident that dispatchable DG resources improve the restoration capacity of the system.

2.5.4 Real EDS

In order to demonstrate the performance of the proposed optimal restoration model, the real-size 13.2 kV EDS in Fig. 9 was used for tests. The system comprises five radial feeders that supply electricity to 38,000 users. The real-size EDS has 5,181 nodes, from which 955 are primary distribution transformers. Distribution transformers are represented by small circles in Fig. 9. Blue and magenta feeders are connected to a main substation of 40 MVA (nominal capacity), whereas red, yellow, and green feeders are connected to a different substation of 60 MVA. Moreover, the EDS has three 5 MVA dispatchable distributed generation (DG) units. The total installed capacity of the distribution transformers is approximately 81 MVA. Also, there are 32 remotely-controlled normally closed (NC) switches and 14 remotely-controlled normally open (NO) switches that participate in the switching sequence.

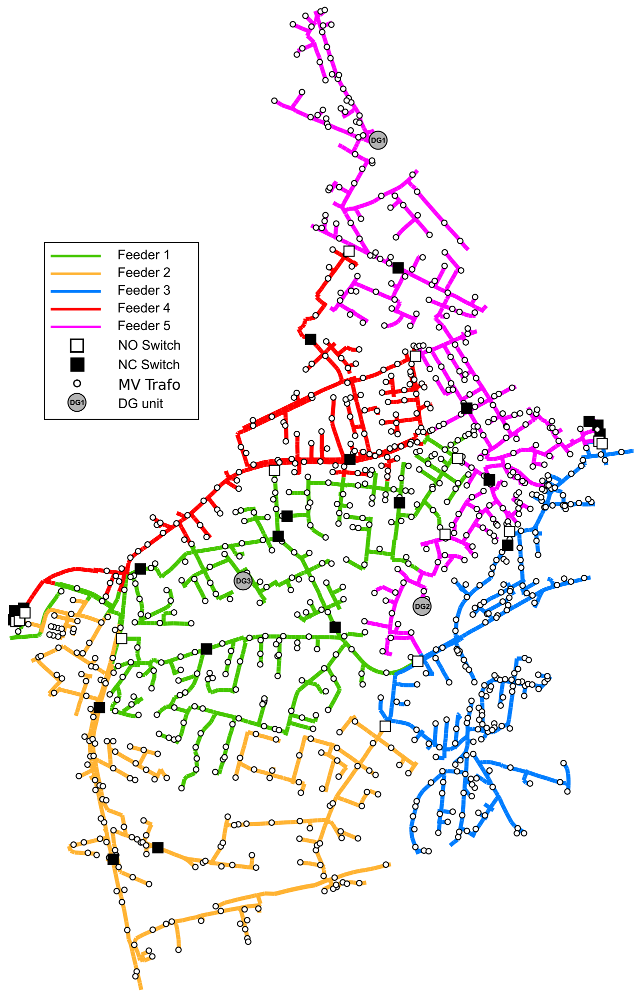

Figure 9 – Real 13.2 kV EDS with five feeders, 5,181 nodes, three DG units, 32 remotely-controlled NC switches and 14 remotely-controlled NO switches.

Source: author.

A permanent fault has been located at feeder 1 (green), close to the main substation. Then, after solving the proposed service restoration model with $s^{\max} = 5$, the resulting switching sequence is shown in Fig. 10. In order to extinguish the fault (depicted by the lightning bolt in Fig. 10), the first step of the service restoration was to open the feeder's main breaker at the substation. Then, a second NC switch was opened to isolate the faulty zone (Step 2) and a NO switch that interconnects feeder 1 (green) and 2 (yellow) was closed to restore most of the un-supplied demand (Step 3). Finally, in order to alleviate the burden at feeder 2 (yellow), part of its load was transferred to feeder 4 (red) by opening a NC switch (Step 4) and closing a NO tie switch at Step 5.

In this case, due to the size of the EDS, a 12 core server with Intel® Xeon® CPUs at 2.4 GHz and 32 GB of RAM was used to solve the model. Under these conditions, the MILP

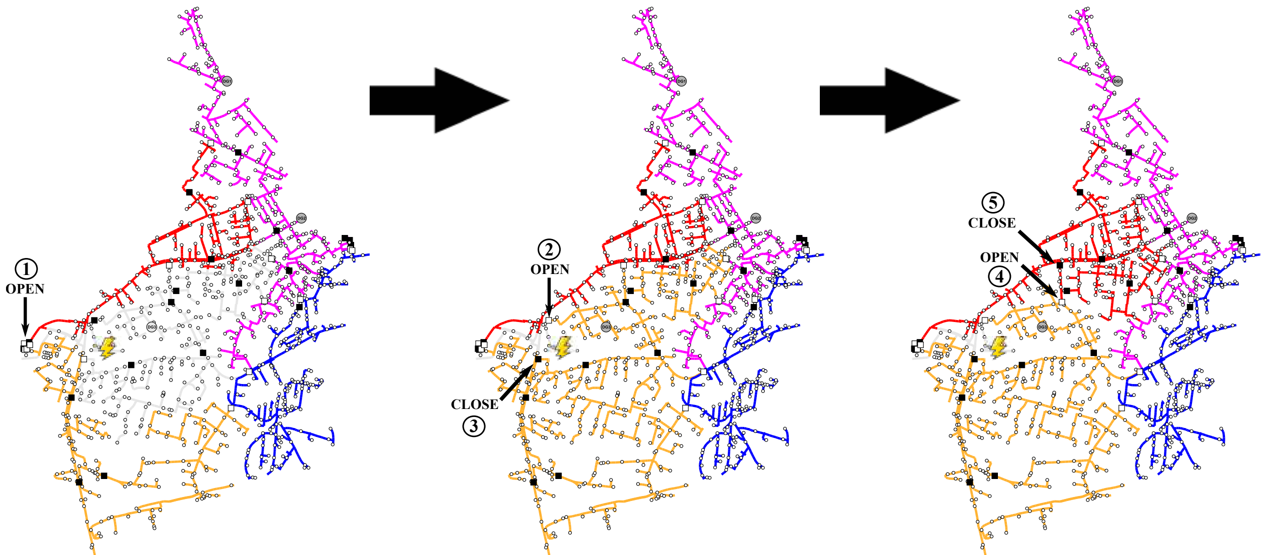

Figure 10 – Switching sequence of the proposed restoration applied to a real EDS in Fig. 9.

Source: author.

model was solved in approximately 16 minutes.

2.5.5 Computational Performance and Applicability

The execution time and the applicability of the proposed methodology can be improved using the following strategies:

1. Improve the processing capacity of the computer being used to solve the problem.
2. Reduce the number of discrete blocks Λ or use an optimization gap different from zero as a stopping criterion of the MILP solver.
3. Solve the model without the set Ω_s and constraints (2.18) and (2.19), i.e., disregard the switching sequence. Then, count the number of switching actions and use this value to establish $s^{\max}$ in Step 1 of the optimization process.

2.6 Conclusion

In this chapter, a new mixed-integer non-linear programming (MINLP) model for the optimal restoration sequence of unbalanced three-phase EDS, which considers a discrete switching sequence and the contribution of DG resources, has been presented. The proposed optimization methodology de-energizes the zone wherein a permanent fault has been identified – or for maintenance – and minimizes the total un-supplied demand, as well as the number of switching operations during the restoration process. The operational constraints of the system are not violated in every step of the sequence. The proposed MINLP was linearized using a set of efficient linearization strategies and solved by a convex optimization solver. The obtained results show that the proposed optimization model is a holistic procedure that can be used to efficiently manage power restoration or to minimize isolated areas in case of scheduled maintenance.

3 Enhanced Fault Location Method for Electrical Distribution Systems

Abstract

An essential aspect that contributes to the reliability of modern electrical distribution systems (EDS) is the deployment of efficient and fast fault location, isolation and service restoration (FDIR). Once the protection system has reacted to a fault, the next step in the FDIR philosophy is to assess, with maximum accuracy, the location of the fault. This chapter proposes an enhanced version of the fault location method based on asynchronous voltage measurements and the bus impedance matrix. Given a voltage drop sensed by each smart meter, the location of the fault is achieved by averaging the fault current as seen by each meter in each node of the system. Then, the node with the lowest difference between the average fault current and the individual fault currents will be regarded as the location of the fault. This method has proved to be easy to implement, fast and robust. The fault location algorithm has been enhanced in this chapter by using a weighted arithmetic mean instead of a regular arithmetic mean for averaging the fault current. As shown by the result, this simple enhancement makes the algorithm less susceptible to erroneous fault locations when some of the measurements are missing or unreliable.

3.1 Introduction

With the advent of smart meters and advanced metering infrastructure (AMI) in electrical distribution systems (EDS), distribution companies are becoming more aware of the status of their networks, in almost real-time basis (MOHASSEL *et al.*, 2014). AMI is of course expensive, and its cost must be justified by the applications that can be performed with such level of supervision. More accurate and timely billing, remote service connection and disconnection, short-term load and distributed generation (DG) forecasting, tamper and theft detection, voltage control, and load-side management programs are among the main benefits of AMI and smart meters (DOE, 2016).

Another benefit from advanced supervision in EDS is the deployment of efficient and fast fault detection, isolation and service restoration (FDIR) (ZIDAN *et al.*, 2017). Without smart meters, a truly automated and responsive FDIR will not be possible, specially because the location of the fault and the service restoration systems requires accurate and recent field measurements. Efficient fault-location techniques reduce outage management costs and increase the overall reliability of the EDS (KEZUNOVIC, 2011).

The proper identification and location of faults in distribution networks is an active research field. As discussed in CIRED WORKING GROUP WG03 (1999) there are three distinctive fault-location techniques for EDS in continuous development: techniques that use fault indication devices (SUN *et al.*, 2016a; JIANG *et al.*, 2016), techniques that use transient and traveling wave signal analysis (ROBSON *et al.*, 2019; ROBSON *et al.*, 2014; RUI *et al.*, 2017) and techniques that indicate the distance to the fault based on fault current/voltage estimation (KEZUNOVIC, 2011). In the last category, the fault location is done by comparing how well each calculated fault current/voltage matches up to what was actually observed at the meters in the network. In this case, a fault location index is defined. The pioneer method in Pereira *et al.* (2009) requires the direct calculation of a current fault which is highly influenced by the type of fault and the fault resistance. Robustness of the pioneer method was assessed in Chen *et al.* (2014).

Many techniques based on fault current/voltage estimation derived in large system of equations that require complex computational resources and slow iterative procedures. Many authors have proposed the application of reduced equivalent networks to deploy the fault location algorithms in a hierarchical structure (OROZCO-HENAO *et al.*, 2017; MORA-FLOREZ *et al.*, 2015; ZHANG *et al.*, 2018). Other authors have solve the fault location problem as a instance of the state estimation in EDS (MAJIDI *et al.*, 2015; MAJIDI *et al.*, 2015; MAJIDI; ETEZADI-AMOLI, 2018; JAMALI; BAHMANYAR, 2016). Moreover, highly sophisticated approaches have been proposed in the past, such as backward/forward calculation (BAHMANYAR; JAMALI, 2017), data-mining (RECHE *et al.*, 2019), data-driven (HOSSAN; CHOWDHURY, 2019), fuzzy logic (JARVENTAUSTA *et al.*, 1994) and modern heuristics (JAMALI *et al.*, 2015). Most of these techniques try to cope with the multiple estimation problem. However, these techniques require sophisticated programming and infrastructure, which inhibits the applicability and scalability of these methods. A comprehensive review on fault location methods in distribution systems up to 2017 can be found in Bahmanyar *et al.* (2017).

To the best of our knowledge, the simplistic impedance-based method proposed in Pereira *et al.* (2009) is still the most straightforward, robust and efficient fault location technique for practical distribution networks, considering scarce and asynchronous voltage measurements. Other authors have proposed different enhancements to deal with the multiple estimation problem (TRINDADE *et al.*, 2014; BISCARO *et al.*, 2016; CAVALCANTE; ALMEIDA, 2018). Similar to the aforementioned works, this chapter proposes a simple enhancement of the method presented in (TRINDADE *et al.*, 2014) to deal with missing or unreliable measurements in a simplistic way that do not compromise the straightforwardness, robustness and overall accuracy of the bus-impedance-matrix-based methods.

The fault-location methods in Trindade *et al.* (2014), Cavalcante and Almeida (2018) establish the location of the fault by minimizing an index δ_n. Based on the voltage drop measured by each smart meter after a fault, the node with the lowest δ_n is considered as the most probable location of the fault. In this chapter, the assessment of δ_n is enhanced by using a weighted arithmetic mean instead of a regular arithmetic mean for calculating the average fault current due to a voltage drop at each meter. As shown by the results, the proposed enhancement elevates the robustness of the methods presented in Trindade *et al.* (2014), Cavalcante and Almeida (2018) by making them less susceptible to erroneous fault locations when some of the measurements are missing or unreliable. Moreover, the scalability and practicality of the method is demonstrated by its simulation in real size distribution systems.

The rest of the chapter is organized as follows: Section 3.2 introduces the fault location method based on scarce, asynchronous voltage measurements and the bus impedance matrix. The proposed enhancement is illustrated in Section 3.2.1. Section 3.3 presents the tests and results obtained using a 135-bus 13.8 kV three-phase distribution system and a real size distribution system. Finally, conclusions are given in Section 3.4.

3.2 Fault-location method

Thanks to the ongoing reduction of their costs and the increasing set of capabilities of intelligent electronic devices (IED), smart electricity meters are now capable to participate in detection and diagnosis of outages in EDS (SUN *et al.*, 2016b). Nowadays, smart meters are able to provide two-way end-to-end communication, data storage and processing, and high rate sampling, within small, robust and affordable equipment. Thus, AMI applications, such as automatic fault-location methods, are becoming feasible solutions for distribution system operators (DSO).

Given a voltage drop perceived in each smart meter $m \in M$, the fault-location method in Trindade *et al.* (2014) is based on the short-circuit current at each node $n \in N$, calculated by the following expression:

$$\begin{bmatrix} |I_a|\, e^{j\theta_a^I} \\ |I_b|\, e^{j\theta_b^I} \\ |I_c|\, e^{j\theta_c^I} \end{bmatrix}_{n,m}^{\text{fault}} = \begin{bmatrix} Z_{aa} & Z_{ab} & Z_{ac} \\ Z_{ba} & Z_{bb} & Z_{bc} \\ Z_{ca} & Z_{cb} & Z_{cc} \end{bmatrix}_{n,m}^{-1} \begin{bmatrix} |\Delta V_a|\, e^{j\theta_a^{\Delta V}} \\ |\Delta V_b|\, e^{j\theta_b^{\Delta V}} \\ |\Delta V_c|\, e^{j\theta_c^{\Delta V}} \end{bmatrix}_{m} \qquad \forall n \in N, m \in M \quad (3.1)$$

In (3.1), the voltage drop at each meter $m \in M$ is calculated as follows:

$$\begin{bmatrix} |\Delta V_a| \, e^{j\theta_a^{\Delta V}} \\ |\Delta V_b| \, e^{j\theta_b^{\Delta V}} \\ |\Delta V_c| \, e^{j\theta_c^{\Delta V}} \end{bmatrix}_m = \begin{bmatrix} |V_a| \, e^{j\theta_a^{V}} \\ |V_b| \, e^{j\theta_b^{V}} \\ |V_c| \, e^{j\theta_c^{V}} \end{bmatrix}_m^{\text{pre-fault}} - \begin{bmatrix} |V_a| \, e^{j\theta_a^{V}} \\ |V_b| \, e^{j\theta_b^{V}} \\ |V_c| \, e^{j\theta_c^{V}} \end{bmatrix}_m^{\text{fault}} \qquad \forall m \in M \quad (3.2)$$

In case the smart meter $m \in M$ does not have voltage phasor capabilities, the angles in (3.1) can be replaced by their nominal values, i.e., $\theta_a^{\Delta V} = 0$, $\theta_b^{\Delta V} = -\frac{2\pi}{3}$ and $\theta_c^{\Delta V} = \frac{2\pi}{3}$, with comparable performance.

Based on the system parameters and topology, the three-phase bus impedance matrix in (3.1) can be obtained through analytical approaches or via simulations using an electromagnetic transient program, such as ATP/EMPT (ATP/EMPT, 1992), to assess and store all the three-phase bus impedance seen by each smart meter $m \in M$, given a solid three-phase fault at each node $n \in N$. Whatever the case, loads must be considered during the calculation of the impedance bus matrix as equivalent shunt elements. Load impedances can be obtain from average consumption, nominal values or smart electricity meters.

Thus, the fault-location index δ_n is calculated using (3.3) for each node of the system, where $\overline{\left|I_{f,n}^{\text{fault}}\right|}$ is the magnitude of the average fault current at each node $n \in N$ and phase $f \in \{a, b, c\}$, given by $\overline{\left|I_{f,n}^{\text{fault}}\right|} = \frac{1}{|M|} \sum_{m \in M} \left|I_{f,n,m}^{\text{fault}}\right|$.

$$\delta_n = \sum_{f \in \{a,c,b\}} \sum_{m \in M} \left| \overline{\left|I_{f,n}^{\text{fault}}\right|} - \left|I_{f,n,m}^{\text{fault}}\right| \right| \qquad \forall n \in N \quad (3.3)$$

The node with the lowest value of δ_n is considered to be the location of the fault. Implicitly, the fault-location index in (3.3) assesses the variance of the current faults as seen by the meters. Thus, the minimization of δ_n is a risk-averse estimator that selects the node with the lowest variability around the mean value.

3.2.1 Enhanced fault-location method

The robustness and accuracy of the previous fault-location method can be improved by considering a weighted arithmetic mean for the fault current $\overline{\left|I_{f,n}^{\text{fault}}\right|}$, instead of the regular arithmetic mean. In this case, the weight of each fault current is inversely proportional to the physical distance between the node and the meter, given by $d_{n,m}$. The proposed enhancement is shown in (3.4), where the weights $p_{n,m}$ are given by equation (3.5).

$$\overline{\left|I_{f,n}^{\text{fault}}\right|} = \sum_{m \in M} p_{n,m} \left|I_{f,n,m}^{\text{fault}}\right| \qquad \forall n \in N, f \in \{a, b, c\} \quad (3.4)$$

$$p_{n,m} = \frac{d_{n,m}^{-1}}{\sum_{n \in M} d_{n,m}^{-1}} \qquad \forall n \in N, m \in M \quad (3.5)$$

Once again, the fault-location index is calculated using (3.3). The proposed weighted arithmetic mean gives more importance to the meters closer to the estimated fault. Hence, it is expected that the impact from erroneous or unreliable measurements were reduced in those meters that perceive small voltage drops. A similar weighted approach was proposed in Cavalcante and Almeida (2018). However, the weights in Cavalcante and Almeida (2018) depend on the voltage drop at each meter, which might be an unreliable parameter in case of erroneous measurements. Since the distance is a constant value, it will not be affected by the quality of the measure. An empirical comparisons of the fault-location methods in Trindade *et al.* (2014), Cavalcante and Almeida (2018) and this work are carried out in the following section.

3.3 Tests and Results

Test and results are divided in two subsections. The first subsection compares the accuracy and robustness of the proposed fault-location method with similar bus impedance based location methods in Trindade *et al.* (2014) and Cavalcante and Almeida (2018). To do so, the real 135-nodes, 13.8 kV distribution system in Fig. 11 will be used for tests. The system comprises one feeder with 13 smart meters arbitrarily allocated along the network. Meters do not have voltage phasor capabilities, and they only provide three-phase phase-to-ground voltage magnitudes before and after the fault. Load and branch parameters can be obtained in Trindade *et al.* (2014), Pereira *et al.* (2009). The short-circuit analysis was performed in ATP/EMPT. Fig. 12 shows the schematic of the network in ATPDraw (ATP/EMPT, 1992). The second section shows the application of the proposed fault location method in a real size distribution system comprising thousands of nodes and branches.

3.3.1 Comparison of Fault-location Methods

In this case, the fault location methods in Trindade *et al.* (2014), Cavalcante and Almeida (2018) and this work, are analyzed to show their susceptibility to erroneous measurements. All three methods are based on the three-phase bus impedance matrix in (3.1), but the fault location index δ_n is calculated using dissimilar criteria. Considering a solid three-phase fault at nodes 14, 55, 75 and 114; Table 5 shows the average distance to the fault after executing the three fault-location methods for different levels of erroneous measurements. The average distance to the fault is computed using a set of Monte Carlo simulations with

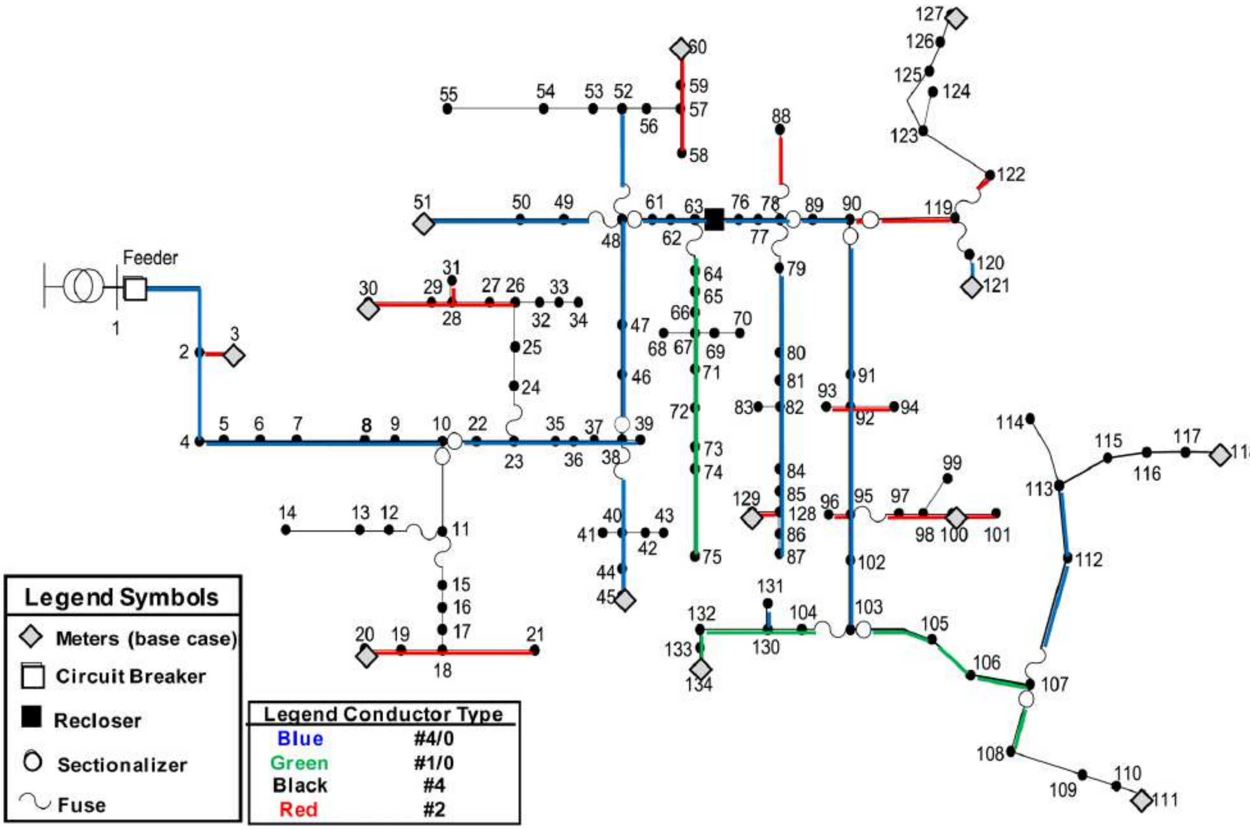

Figure 11 – Real 134-nodes, 13.8 kV distribution feeder (TRINDADE *et al.*, 2014; PEREIRA *et al.*, 2009).

Source: Trindade *et al.* (2014).

10,000 iterations for each test. The simulated error is adjusted by adding white Gaussian noise to the three-phase voltage magnitudes using different signal-to-noise ratios (SNR).

As shown by the results in Table 5, the proposed fault-location method has superior performance over the other methods when the SNR is low, i.e., when meters are unreliable. However, for reliable measurements (SNR = 40) all three method behave similarly with small distances to the faults. A more practical approach to assess the robustness of the methods is shown in Table 6. Based on the Monte Carlo simulations, Table 6 computes the percentage of positive locations of each method and SNR. The criterion for considering a location as "positive" is that the distance between the actual faulty node and the location provided by each method is lower than 500 m. Clearly, the proposed method is less susceptible to erroneous measurements, up to SNR = 30. However, for extremely noisy readings (SNR = 20) all methods are equally unable to locate the fault.

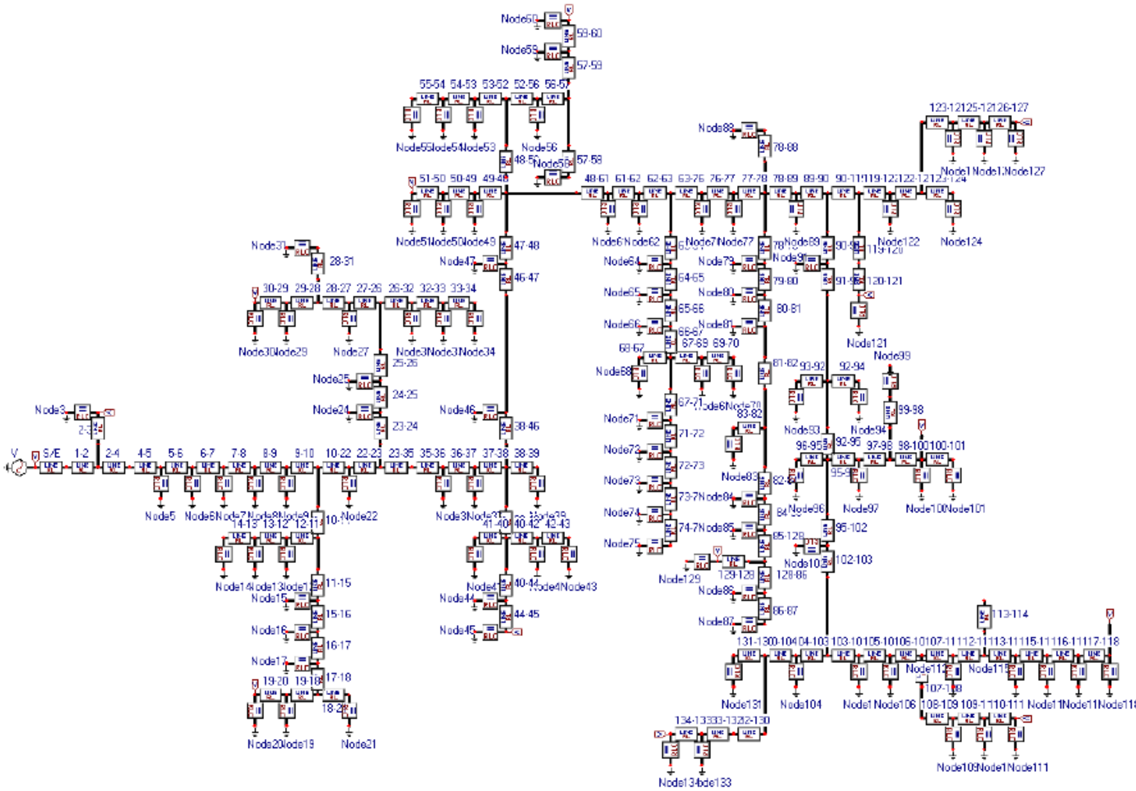

Figure 12 – 135-nodes test system in ATP/EMPT.

Source: author.

3.3.2 Real-size distribution system

To show the scalability of the proposed fault-location method, a real-size 13.2 kV EDS has been tested. The system comprises five radial feeders that supply electricity to 38,000 users of different types. The real-size EDS has 5,181 nodes, from which 955 are primary transformers. Also, there are 32 remotely-controlled NC switches and 14 remotely-controlled NO switches. Consider three three-phase faults at dissimilar nodes of the network. Fig. 13 depicts the performance of the proposed method if the voltage magnitude measurements, before and after the fault, are collected by the smart meters installed at the 32 remotely-controlled NC switches and 14 remotely-controlled NO switches, i.e., there are only 46 smart meters available. The magnifying glass in Fig. 13 represents a radius of 100 m from the location of the fault provided by the proposed method. The true location of the fault is represented by the thunderbolt. Note that, with only 46 smart meters available, locations are not accurate enough, but they can be used as rough indicators of the fault. Finally, results considering 955 smart meters participating in the fault-location method, i.e., AMI, are shown in Fig. 14. Note that all faults are within the 100 m range when AMI is implemented. Thus, an effective outage management system can be deployed.

Table 5 – Average distance (in meters) to the fault for different SNR and fault-location methods

Method	SNR=20	SNR=25	SNR=30	SNR=35	SNR=40
a) Three-phase fault at node 14					
(TRINDADE *et al.*, 2014)	2053	2046	1920	498	33
(CAVALCANTE; ALMEIDA, 2018)	2053	**2027**	1950	672	32
This work	**2052**	2035	**1270**	**48**	**2**
b) Three-phase fault at node 55					
(TRINDADE *et al.*, 2014)	2417	2313	984	**454**	**117**
(CAVALCANTE; ALMEIDA, 2018)	2417	2336	1136	456	**117**
This work	**2380**	**2000**	**676**	508	181
c) Three-phase fault at node 75					
(TRINDADE *et al.*, 2014)	2523	2233	482	19	**1**
(CAVALCANTE; ALMEIDA, 2018)	2527	2277	503	19	**1**
This work	**2438**	**1769**	**137**	**14**	**1**
d) Three-phase fault at node 114					
(TRINDADE *et al.*, 2014)	1197	815	567	237	54
(CAVALCANTE; ALMEIDA, 2018)	**1171**	812	546	221	46
This work	1352	**339**	**197**	**72**	**8**

3.3.3 Applicability Notes

1. The proposed fault-location method can be further improved by considering the performance of the distribution protection system. In practice, protection devices (circuit breakers, reclosers, fuses, etc.) are coordinated so that faults can be isolated with minimum impact. This creates an outage mapping that can be exploited to omit areas that should no be considered by the fault-location method.

2. The proposed fault-location method can be easily embedded into an optimization problem. Thus, it can be used for formulating the optimal allocation of smart meters that maximizes the accuracy of the fault-location process.

3. Finally, a major applicability issue of the proposed fault-location method is the delay or latency among measurements. This is a complex telecommunication-related problem, that must be addressed in future works.

3.4 Conclusion

This chapter proposed a enhanced version of the fault-location method based on asynchronous voltage measurements and the three-phase bus impedance matrix. The method is straightforward, fast, accurate and robust, in the sense that it is less susceptible to erroneous

Table 6 – Percentage of positive locations ($< 500\,\text{m}$) for different SNR and fault-location methods

Method	SNR=20	SNR=25	SNR=30	SNR=35	SNR=40
a) Three-phase fault at node 14					
(TRINDADE *et al.*, 2014)	0.0%	0.1%	3.2%	54.8%	93.4%
(CAVALCANTE; ALMEIDA, 2018)	0.0%	0.1%	2.4%	48.9%	93.5%
This work	0.0%	0.3%	27.7%	91.1%	99.7%
b) Three-phase fault at node 55					
(TRINDADE *et al.*, 2014)	0.0%	0.3%	15.2%	40.8%	85.2%
(CAVALCANTE; ALMEIDA, 2018)	0.0%	0.2%	13.9%	40.5%	85.1%
This work	0.0%	1.7%	17.3%	33.9%	77.4%
c) Three-phase fault at node 75					
(TRINDADE *et al.*, 2014)	0.0%	1.3%	66.6%	97.8%	99.8%
(CAVALCANTE; ALMEIDA, 2018)	0.0%	1.2%	66.3%	97.8%	99.8%
This work	0.0%	9.9%	88.5%	98.1%	99.8%
d) Three-phase fault at node 114					
(TRINDADE *et al.*, 2014)	0.4%	2.4%	20.4%	74.9%	99.3%
(CAVALCANTE; ALMEIDA, 2018)	0.4%	2.4%	21.8%	78.5%	99.3%
This work	19.3%	44.4%	91.7%	99.9%	100.0%

fault locations when some of the measurements are missing or unreliable. As demonstrated by the results, the proposed simple enhancement increases the performance of the fault-location method without compromising its applicability and scalability, which makes it suitable for outage management systems in AMI networks.

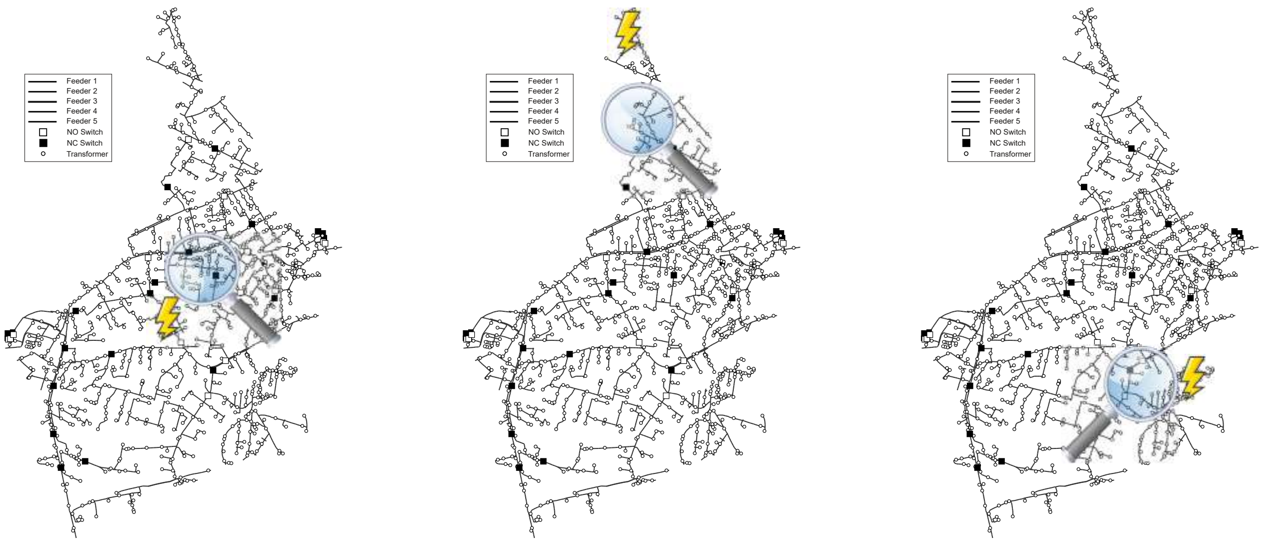

Figure 13 – Real-size EDS: Fault-locations for three different faults based on the measurements of 46 smart meters.

Source: authors.

Figure 14 – Real-size EDS: Fault-locations for three different faults based on the measurements of 955 smart meters, i.e., AMI.

Source: authors.

4 Parsimonious Short-Term Load Forecasting for Optimal Operation Planning of Electrical Distribution Systems

Abstract

The optimal operation planning (OOP) of electrical distribution systems (EDS) is very sensible to the quality of the short-term load forecasts. Assuming aggregated demands in EDS as univariate non-stationary seasonal time series, and based on historical measurements gathered by smart meters, this chapter presents a parsimonious short-term load forecasting method to estimate the expected outcomes of future demands, and the standard deviations of forecast errors. The chosen short-term load forecasting method is an adaptation of the multiplicative autoregressive integrated moving average (ARIMA) models. Seasonal ARIMA models are parsimonious forecasting techniques because they require very few parameters and low computational resources to provide an adequate representation of stochastic time series. Two approaches are used in this chapter to estimate the parameters that constitute the proposed multiplicative ARIMA model: a frequentist and a Bayesian approach. Advantages and disadvantages of both methods are compared by simulating a centralized self-healing scheme of a real EDS that uses the forecasts to deploy a robust restoration plan. Results shown that the proposed seasonal ARIMA model is a fast, precise, straightforward and adaptable load forecasting method, suitable for OOP of highly supervised EDS.

4.1 Introduction

Short-term load forecasting is of great importance in the operation planning of bulk energy systems. Regulation bids, energy arbitrage, and market-clearing mechanisms are conducted on hourly bases, which puts a lot of pressure on forecasting techniques to provide accurate and fast estimations of future demands (TAYLOR; MCSHARRY, 2017). With the advent of smart meters and advanced distributed automation, electrical distribution system (EDS) operators are also becoming active users of short-term operation planning (HONG, 2014). Based on the information gathered by meters, demand forecasts can be used as input data for the dynamic optimization of the EDS resources, a.k.a., optimized energy management systems. Moreover, in case of a fault, fast restoration methods can be deployed to minimize the total amount of expected unsupplied demand while the fault is being repaired, a.k.a., self-healing schemes (NORTHCOTE-GREEN; WILSON, 2017).

Optimal operation planning (OOP) problems, such as self-healing schemes, require fast and precise short-term load forecasts in order to compute their decisions. In many cases, only the expected value of the future consumption is not enough. Other statistical moments, such as the standard deviation of forecast errors, are also important to make robust and risk-averse decisions. Such is the case for self-healing schemes, in which EDS operators would be more interested in a restoration plan that not only minimizes the expected amount of unsupplied demand, but also guarantees that the energized portion of the network is able to operate within its operational constraints during the time required to repair the fault. Thus, when implementing a self-healing scheme, the accuracy of the expected outcomes, and the standard deviations of the forecast errors, are significant to the robustness of the final restoration plan (CHEN *et al.*, 2016).

Since the beginnings of electrical engineering, numerous short-term load forecasting techniques have been proposed and extensively tested (HONG; FAN, 2016; HERNANDEZ *et al.*, 2014). Most techniques use historical information to formulate and train different estimators: multiple linear regression models (PAPALEXOPOULOS; HESTERBERG, 1990), semi-parametric additive models (FAN; HYNDMAN, 2012; GOUDE *et al.*, 2014), exponential smoothing models (TAYLOR; MCSHARRY, 2007), autoregressive moving average models (HAGAN; BEHR, 1987; WERON, 2013), artificial neural networks (HIPPERT *et al.*, 2001; KHOTANZAD *et al.*, 1998), fuzzy regression models (SONG *et al.*, 2005; HONG; WANG, 2014), support vector machines (CHEN *et al.*, 2004), and gradient boosting (TAIEB; HYNDMAN, 2014; LLOYD, 2014); are among the most successful forecasting techniques proposed to this date.

In this context, the objective of this chapter is not to propose a new short-term load forecasting technique in an already saturated research area. Our goal is, in fact, to adapt one of the aforementioned methods for formulating and solving short-term OOP problems in highly supervised EDS. To achieve this, the forecasting technique must meet the following four requirements: a) its computational complexity must be low in order to be deployed in on-line on-site applications; b) it should be accurate in terms of expected values and residuals; c) it should contain as few tuning parameters and forecasting variables as possible; and d) it should be able to automatically adapt itself to the ever-charging stochastic nature of EDS demands. A short-term load forecasting technique that satisfies all these four requirements is said to be a *parsimonious* method (BOX *et al.*, 2008).

As shown in previous empirical studies, multiplicative autoregressive integrated moving average (ARIMA) models are simplistic and accurate analytical methods for short-term forecasting of aggregated demands (TAYLOR; MCSHARRY, 2017). All forecasting techniques are subject to error but, when dealing with univariate seasonal stochastic time series, regression models are regarded as the best option to provide fast and reliable forecasts (HONG *et al.*, 2014). Assuming aggregated demands as non-stationary seasonal time series, several univariate multiplicative ARIMA models (one for each electrical measurement) can be used to dynamically estimate future outcomes of power demands in each load node. In this chapter, a generalized parsimonious short-term load forecasting method based on seasonal ARIMA models and historical measurements gathered by smart meters is presented. Two approaches are used to estimate the parameters that constitute the proposed multiplicative ARIMA model: a frequentist and a Bayesian approach. The accuracy and efficiency of both estimation methods are tested by simulating a robust self-healing scheme in a real EDS that requires fast and precise short-term load forecasts to deploy its restoration plan. Results show that the proposed seasonal ARIMA model satisfies the four parsimonious requirements, and it is suitable for solving short-term OOP problems in highly supervised EDS.

The main contributions of this chapter are as follows:

- A parsimonious short-term load forecasting method, based on seasonal ARIMA models and historical measurements gathered by smart meters, is adapted and presented as the first-step for solving short-term OOP problems in highly supervised and automated EDS.

- A frequentist and a Bayesian approaches for estimating the parameters of the seasonal ARIMA models are used and compared. Advantages and disadvantages of both methods are discussed by simulating a centralized self-healing scheme that uses the forecasted demands to execute a robust restoration plan.

The rest of the chapter as organized as follows: Section 4.2 presents the application of forecasting techniques for the OOP of highly supervised EDS. Section 4.3 shows the process of model identification, preliminary estimation and forecasting, using the proposed seasonal ARIMA model. Section 4.4 deals with the estimation of the model's parameters using the frequentist and Bayesian approaches. Model adequacy is discussed in Section 4.5, and test and results are shown in Section 4.6, followed by conclusions.

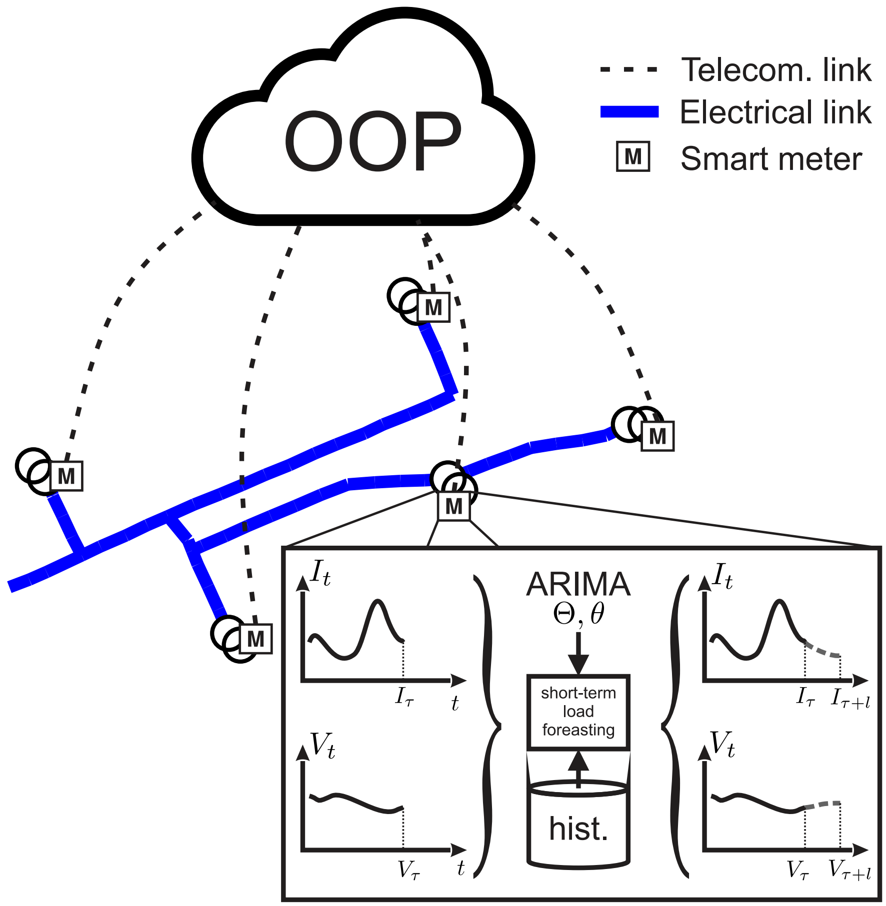

Figure 15 – Short-term load forecasting for OOP of highly supervised EDS.

Source: Lopez *et al.* (2019).

4.2 Short-term Load Forecasting for the Optimal Operation Planning of EDS

The optimal operation planning (OOP) of EDS requires fast, updated, and precise load forecasts to make informed decisions (HERNANDEZ *et al.*, 2014). As shown in Fig. 15, short-term load forecasting is the very first step for deploying an OOP method in distribution systems with an advanced metering infrastructure (AMI) (MOHASSEL *et al.*, 2014). Based on current measurements (i.e., at time τ) and historical information, the short-term load forecasting method (the ARIMA model in Fig. 15) estimates the expected values and the standard deviations of future demands at each load node, i.e., from time τ to $\tau + l$, where l is the time lag of the forecasts.

Electrical measurements, such as current and voltage magnitudes at distribution transformers, can be considered as non-stationary seasonal time series that depend on the aggregated demands of all users connected to each transformer. Thus, as shown in Fig. 15, these time series can be forecasted on-line and on-site by taking advantage of the limited storage and processing capabilities of smart meters in the field.

Using a small resolution (e.g., 5 minutes per sample), the short-term memory of regression models can capture slow consumption patterns affected by exogenous variables, such as temperature and humidity (TAYLOR; MCSHARRY, 2017). Moreover, control actions that affect the collective consumption in a seasonal fashion (e.g., demand response at certain hours of the day, scheduled charging of EVs, etc.) can be also captured by univariate seasonal methods.

Finally, it is worth mentioning that univariate load forecasting methods should be used to estimate pure aggregated consumption, i.e., their are neither suitable for forecasting individual demands (e.g., households) nor renewable generation resources, because these stochastic processes are highly influenced by rapid exogenous random events, such as micro-weather conditions or individual human behavior, that cannot be fully captured by univariate linear regression models (HONG, 2014).

4.2.1 OOP problem: Self-healing Scheme

In order to evaluate the efficiency of the proposed parsimonious load forecasting technique, a real-size EDS with an AMI will be used to simulate a centralized self-healing scheme. In case of a permanent fault, the function of the self-healing scheme is to automatically generate a set of control actions that minimize the impact of the outage while the fault is being repaired. Based on the short-term load forecasts and the location of the fault, the self-healing scheme is represented as an OOP problem whose solution aims at minimizing the expected unsupplied demand after the fault (CAVALCANTE *et al.*, 2016; AGUERO, 2012).

The quality of the self-healing scheme is highly influenced by the speed and precision of the load forecasts. The set of restorative actions must be deployed shortly after the fault has been identified in order to be effective. Thus, forecasts must be updated and available at any time. Moreover, poor forecasting can result in ill-conceived restoration plans. For example, too much load could be transferred to heavily loaded feeders or, on the contrary, feeders with enough capacity could be ignored by the self-healing scheme. Thus, in this case, not only the average values of the load forecasts are important, but also the standard deviation of the forecast errors are significant to the robustness of the restoration.

In this chapter, the optimization model in Lopez *et al.* (2018) is used to represent and deploy the restoration plan of the centralized self-healing scheme in unbalanced three-phase EDS. The model in Lopez *et al.* (2018) considers the operation of remotely-controlled switches for transferring de-energized sections of the system to other feeders and for isolating the

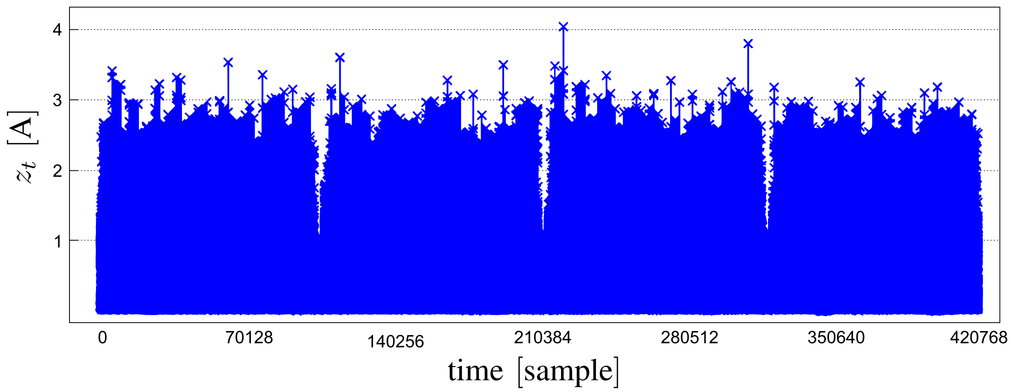

Figure 16 – Time series z_t: four years of single-phase current magnitudes recorded from the primary side of a distribution transformer.

Source: Lopez *et al.* (2019).

fault. Also, if available, dispatchable distributed generation (DG) units can be rescheduled to improve the impact of the restoration plan. The optimization model is shown in Chapter 2. Details regarding the optimization technique used to solve the restoration plan will be discussed in Section 4.6.

4.3 Seasonal ARIMA model

In this section, the use of a seasonal ARIMA model as a parsimonious short-term load forecasting technique is justified by analyzing the estimated autocorrelation function of a typical time series, associated to the magnitude of an aggregated single-phase demand current. Furthermore, the identification of the model, the initial estimation of its parameters, and the generation of forecasts will be discussed and validated through empirical analysis.

4.3.1 Model Identification

The first step of building any stochastic model is to analyze the attributes of the time series that will be forecasted. The time series in Fig. 16 represents the single-phase current magnitudes recorded by a smart meter at the primary side of a distribution transformer. Four years of data with a resolution of 5 minutes per sample are shown in Fig. 16, which constitutes a total amount of 420,768 measurements. The data have been generated by aggregating several demands from a residential area whose individual load profiles have been randomly generated using the LoadProfileGenerator software in Pflugradt and Muntwyler (2017), Pflugradt *et al.* (2013).

Time series z_t in Fig. 16 is a non-stationary stochastic process since its mean level and

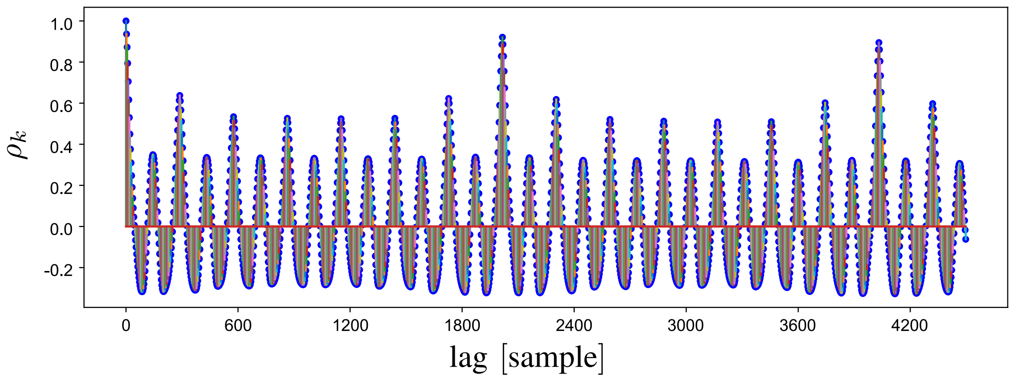

Figure 17 – Estimated autocorrelation function of series z_t.

Source: Lopez *et al.* (2019).

variance may have different values for different, sufficiently large, time intervals. However, there is a notorious interdependence between adjacent observations of the series which indicates that, in spite its randomness, aggregated demands have a tendency of following similar patterns that derive from previous outcomes, i.e., there are temporal correlations among data samples. Analyzing these correlations is the first step for model identification. Fig. 17 shows the estimated autocorrelation function of series z_t for time lags between 1 to 4,500 samples (i.e., up to two weeks).

The estimated autocorrelation function in Fig. 17 seems to oscillate without visible reduction, with two notorious spikes at lags 2,016 and 4,032, i.e., at exactly one and two weeks, which suggests a periodic time series with period $s = 2,016$. Fig. 18 shows a detailed section of time series z_t that illustrates its seasonal component. Aggregated demands usually follow a period of one week because human activities are conditioned to the hour of the day and the day of week. Other slow periods, such as annual seasons or tropical temperature oscillations, that depend on the geographic location of the loads, can also be identified following a similar analysis. However, for the sake of simplicity and generality, only a one-weekly period will be considered in this chapter, keeping in mind that all subsequent procedures for model identification can be extended to time series with multiple periods following analogous methods.

Fig. 19 shows the estimated autocorrelation function of time series $\Delta_s z_t = z_t - z_{t-s}$, with $s = 2,016$. A small version of the resulting time series is also shown in Fig. 19. Note that, after removing the periodic component of the series, most of the estimated autocorrelations are reduced. However, strong oscillating autocorrelations remain, suggesting non-stationarity.

The next step in model identification is checking whether the time series is homogeneous or not. Homogeneity is perceived when different, sufficiently large, intervals of the time

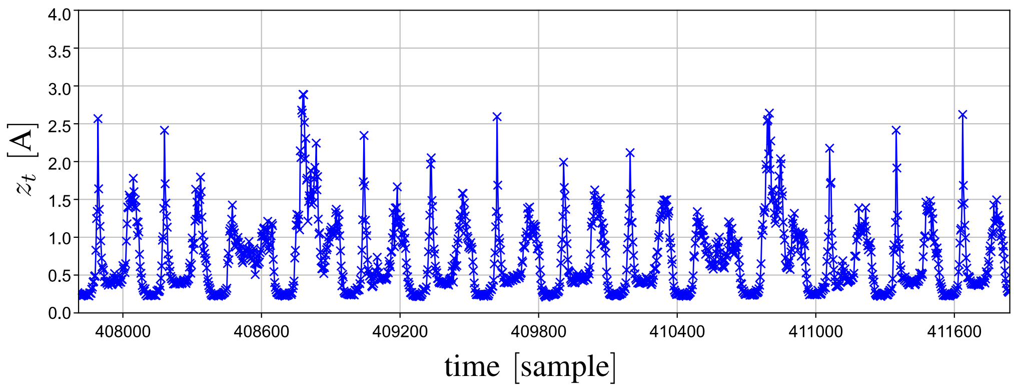

Figure 18 – Detailed section of time series z_t that shows its seasonality.

Source: Lopez *et al.* (2019).

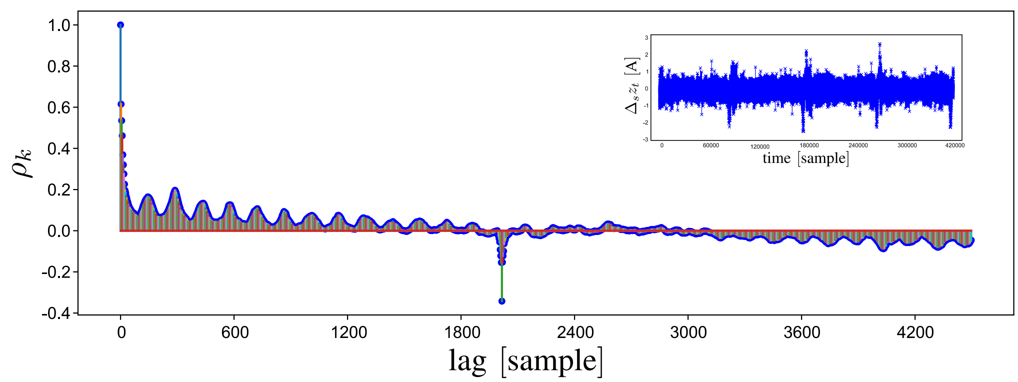

Figure 19 – Estimated autocorrelation function of series $\Delta_s z_t$, with $s = 2,016$.

Source: Lopez *et al.* (2019).

series show similar patterns in terms of level and slope. Large portions of $\Delta_s z_t$ show similar mean levels which indicates a first degree of homogeneity, i.e., each outcome is highly influenced by its previous realization. Thus, Fig. 20 shows the estimated autocorrelation function of the time series $\Delta\Delta_s z_t = z_t - z_{t-s} - (z_{t-1} - z_{t-s-1})$ and a small version of the resulting time series $\omega_t = \Delta\Delta_s z_t$, with $s = 2,016$.

Time series ω_t in Fig. 20 is a stationary time series whose estimated autocorrelations can be considered significant for lags 0, 1, 2,015, 2,016, and 2,017. Furthermore, lags 1 and 2,016 are negative, whereas lags 2,015 and 2,017 are positive which is consistent with a moving average process given by the following regression model:

$$\omega_t = \Delta\Delta_s z_t = a_t - \theta a_{t-1} - \Theta a_{t-s} + \theta\Theta a_{t-s-1}, \tag{4.1}$$

where stochastic variables ω_t and a_t's have zero mean. Equation (4.1) is known as univariate multiplicative ARIMA model (BOX *et al.*, 2008), and only three parameters need to be

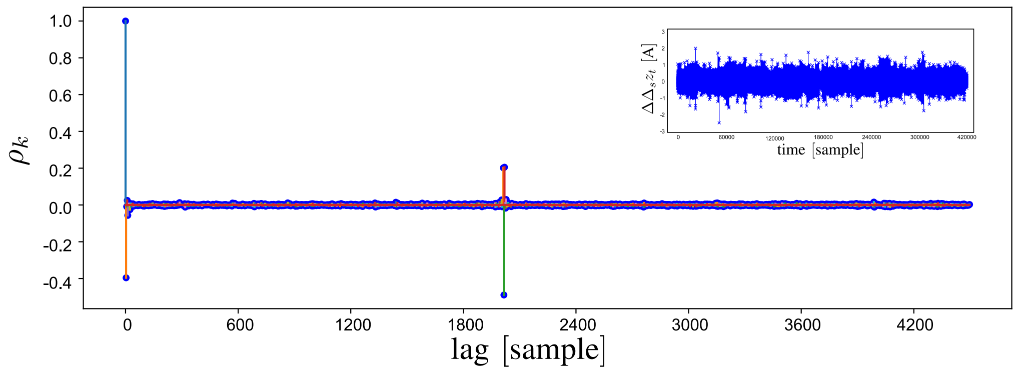

Figure 20 – Estimated autocorrelation function of stationary series $\omega_t = \Delta\Delta_s z_t$, with $s = 2,016$.

Source: Lopez *et al.* (2019).

estimated in order to start generating forecasts with (4.1): parameters θ, Θ, and the variance of the a_t's, i.e, σ_a^2.

4.3.2 Preliminary Estimation

Parameters a_t's in (4.1) are independent and identically distributed (IID) random variables whose linear regression predicts the values of the future outcomes of ω_t. Thus, the autocovariance function of (4.1), for lags $k = 0, 1, ..., \infty$, is given by (4.2).

$$\gamma_k = E\left[\left(a_t - \theta a_{t-1} - \Theta a_{t-s} + \theta\Theta a_{t-s-1}\right)\left(a_{t-k} - \theta a_{t-k-1} - \Theta a_{t-k-s} + \theta\Theta a_{t-k-s-1}\right)\right] \quad (4.2)$$

Since a_t's are IID, the analytical autocovariances of ω_t are given by (4.3)–(4.8). Note that, since $\rho_k = \frac{\gamma_k}{\gamma_0}$, (4.3)–(4.8) are consistent with the estimated autocorrelations in Fig. 20.

$$\gamma_0 = \left[1 + \theta^2 + \Theta^2 + (\theta\Theta)^2\right]\sigma_a^2 = \left(1 + \theta^2\right)\left(1 + \Theta^2\right)\sigma_a^2 \quad (4.3)$$

$$\gamma_1 = \left[-\theta - \Theta\left(\theta\Theta\right)\right]\sigma_a^2 = -\theta\left(1 + \Theta\right)^2\sigma_a^2 \quad (4.4)$$

$$\gamma_{s-1} = \theta\Theta\sigma_a^2 \quad (4.5)$$

$$\gamma_s = \left[-\Theta - \theta\left(\theta\Theta\right)\right]\sigma_a^2 = -\Theta\left(1 + \theta\right)^2\sigma_a^2 \quad (4.6)$$

$$\gamma_{s+1} = \theta\Theta\sigma_a^2 \quad (4.7)$$

$$\gamma_k = 0; \text{ Otherwise} \quad (4.8)$$

Providing that the series ω_t is stationary, and given the autocovariances in (4.3)–(4.8), the preliminary estimation of parameters θ and Θ can be obtained by (4.9) and (4.10), respectively.

$$\rho_1 = \frac{\gamma_1}{\gamma_0} = \frac{-\theta}{1+\theta^2} \tag{4.9}$$

$$\rho_s = \frac{\gamma_s}{\gamma_0} = \frac{-\Theta}{1+\Theta^2} \tag{4.10}$$

Thus, based on the empirical results from Fig. 20, the preliminary parameters are $\hat{\theta} = 0.4916$ and $\hat{\Theta} = 0.8122$, where the accent $\hat{a}$ stands for "estimated value of a". Finally, an unbiased estimation of σ_a^2 may be obtained from the time series data and the ARIMA model as discussed in the following subsection.

4.3.3 Forecasting

Once initial values for $\hat{\theta}$ and $\hat{\Theta}$ have been obtained, the ARIMA model in (4.1) can be used to dynamically generate forecasts from the time series. Consider a lag time l, such that l can go from 5 minutes-ahead to any practical value of l. Forecast values $\tilde{z}_t$ can be produced by sequentially solving (4.11) for $t \in \{\tau+1, \tau+2, \ldots, \tau+l\}$, where τ is the current time from which forecasts are taken and the accent $\tilde{a}$ stands for "forecasted value of a".

$$\tilde{z}_t = z_{t-1} + z_{t-s} - z_{t-s-1} + a_t - \hat{\theta}a_{t-1} - \hat{\Theta}a_{t-s} + \hat{\theta}\hat{\Theta}a_{t-s-1} \qquad \forall t \in \{\tau+1, \tau+2, \ldots, \tau+l\} \tag{4.11}$$

In (4.11), the values for $z_{t\leq\tau}$ are obtained directly from the time series, whereas the vales for $z_{t>\tau}$ are returned from previous forecasts. On the other hand, the values for $a_{t\leq\tau}$ are obtained by using the conditional estimation method shown in Algorithm 1, whereas the values for $a_{t>\tau}$ are set to zero.

Algorithm 1 is called *conditional estimation* because it approximates the individual outcomes of a_t's based on the ARIMA model and the historical information of the time series ω_t. Considering that the known values of ω_t start at $t = 1$ and end at $t = \tau$, back-forecasts of ω_t (regarded as $\tilde{\omega}_t$) are first calculated using the recursive procedures in lines 4 to 7, where e_t are the random coefficients of the back-forecasted series $\tilde{\omega}_t$. Once the values of $\tilde{\omega}_{-s-1\leq t\leq 0}$ have been obtained, the recursive forward method in lines 8 to 12 is used to estimate the a_t's. Note that the Algorithm 1 estimates the values of $a_{-s-1\leq t\leq\tau}$, i.e., it also provides the random coefficients of the back-forecasts.

Pseudocódigo 4.1 Conditional Estimation of a_t's

$e_t \leftarrow 0;\ t \in \{-s-1, -s, \ldots, \tau+s, \tau+s+1\}$
$\tilde{\omega}_t \leftarrow 0;\ t \in \{-s-1, -s, \ldots, -1, 0\}$
$a_t \leftarrow 0;\ t \in \{-2s-2, -2s-1, \ldots, \tau-1, \tau\}$
for each $t \in \{\tau, \tau-1, \ldots, 2, 1\}$ **do**
    $e_t = \omega_t + \hat{\theta} e_{t+1} + \hat{\Theta} e_{t+s} - \hat{\theta}\hat{\Theta} e_{t+s+1}$
for each $t \in \{-s-1, -s, \ldots, -1, 0\}$ **do**
    $\tilde{\omega}_t = e_t - \hat{\theta} e_{t+1} - \hat{\Theta} e_{t+s} + \hat{\theta}\hat{\Theta} e_{t+s+1}$
for each $t \in \{-s-1, -s, \ldots, \tau-1, \tau\}$ **do**
    if $t \leq 0$ **then**
        $a_t = \tilde{\omega}_t + \hat{\theta} a_{t-1} + \hat{\Theta} a_{t-s} - \hat{\theta}\hat{\Theta} a_{t-s-1}$
    else if $t > 0$ **then**
        $a_t = \omega_t + \hat{\theta} a_{t-1} + \hat{\Theta} a_{t-s} - \hat{\theta}\hat{\Theta} a_{t-s-1}$

Once the values of $a_{t \leq \tau}$ have been calculated, the unbiased estimator of the variance $\hat{\sigma}_a^2$ is obtained by averaging over the sum-of-square values of a_t given by (4.12), where N is the number of samples in the time series w_t.

$$\hat{\sigma}_a^2 \approx \frac{1}{N} \sum_{t=1}^{\tau} a_t^2 \tag{4.12}$$

Fig. 21 shows the forecasts of the series z_t in Fig. 16, obtained using the aforementioned technique for a lag $l = 2,016$, i.e., one-week ahead. The forecasts in yellow are compared with the real outcomes in blue to demonstrate the accuracy of the proposed ARIMA model when using preliminary values of $\hat{\theta} = 0.4916$ and $\hat{\Theta} = 0.8122$. The estimated variance $\hat{\sigma}_a^2 \approx 10.2$ is obtained by (4.12). Note that the forecasted demands follow a similar pattern as the real consumption. Through the estimated variance $\hat{\sigma}_a^2$, the standard deviation of the forecast errors at any lag l can be assessed, and they increase with the length of l (see Chapter 5 in Box *et al.* (2008)).

4.4 Model estimation

Together, the seasonal ARIMA model in (4.1) and the forecasting algorithm in Section 4.3.3, provide a parsimonious short-term load forecasting technique that can be programmed in each individual meter of an EDS with an AMI. As shown in Fig. 21, rough values of $\hat{\theta}$ and $\hat{\Theta}$ already provide suitable forecasts for a one-week lag. However, as more data become available, and considering that consumption is a dynamic stochastic process that continuously reacts to exogenous factors, e.g., new circuits that are installed to energize new demands, socioeconomic activities that change in an area, unexpected events that lead

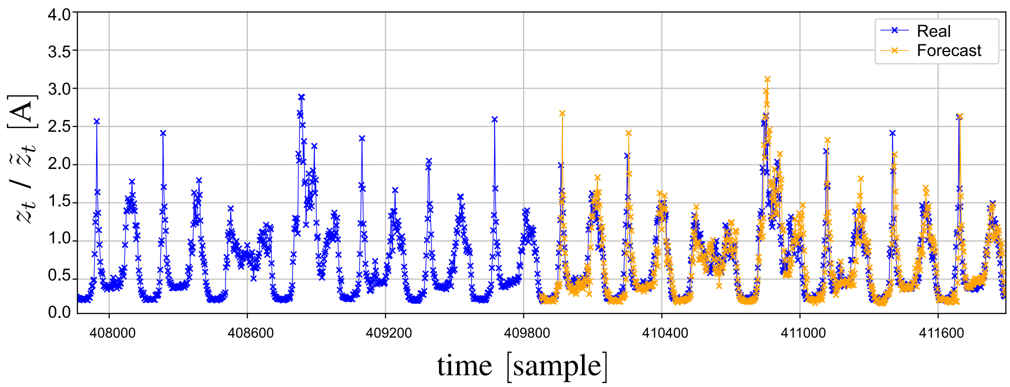

Figure 21 – Forecasts of time series z_t for a lag time of one week, with $\hat{\theta} = 0.4916$ and $\hat{\Theta} = 0.8122$.

Source: Lopez *et al.* (2019).

to different operating points and topologies of the EDS, etc. Thus, in order to be parsimonious, the proposed short-term load forecasting method must be able to adapt itself to the ever-changing nature of demands by updating the values of the parameters $\hat{\theta}$ and $\hat{\Theta}$ when new measurements of the series are obtained.

Two approaches are presented in this section to optimized the values of $\hat{\theta}$ and $\hat{\Theta}$: a frequentist and a Bayesian approach. These two methods are different strategies to optimize the model's parameters based on historical data. However, each one derives from parallel perspectives of statistics. The frequentist analysis considers parameters as fixed constant values of the estimation model, whereas the Bayesian analysis considers parameters as random variables of the estimator with given prior distributions (WAKEFIELD, 2013).

4.4.1 Frequentist Approach

In the frequentist approach, an iterative non-linear programming method is used to optimize the values of $\hat{\theta}$ and $\hat{\Theta}$ every time new data is attained, as follows:

Step 1 Let $k \leftarrow 0$. Use initial estimations of $\hat{\theta}^k \leftarrow \hat{\theta}$ and $\hat{\Theta}^k \leftarrow \hat{\Theta}$.

Step 2 Use Algorithm 1 for calculating the a_t^k's of the time series for a set of updated measurements of z_t, and use (4.12) to estimate the variance $\hat{\sigma}^2_{a^k}$.

Step 3 Determine the negative derivatives $x_t^{\hat{\theta}^k}$ and $x_t^{\hat{\Theta}^k}$, in which each term is calculated using (4.13) and (4.14), for $t \in \{1, \ldots, \tau\}$ and a small δ.

$$x_t^{\hat{\theta}^k} = \frac{1}{\delta}\left[a_t^k|_{\hat{\theta}^k,\hat{\Theta}^k} - a_t^k|_{\hat{\theta}^k+\delta,\hat{\Theta}^k}\right] \tag{4.13}$$

$$x_t^{\hat{\Theta}^k} = \frac{1}{\delta}\left[a_t^k|_{\hat{\theta}^k,\hat{\Theta}^k} - a_t^k|_{\hat{\theta}^k,\hat{\Theta}^k+\delta}\right] \tag{4.14}$$

Step 4 Update the parameters using the least square estimator as in (4.15), where coefficients f_{11}, f_{12}, f_{21} and f_{22} are given by (4.16).

$$\begin{bmatrix}\hat{\theta}^{k+1}\\ \hat{\Theta}^{k+1}\end{bmatrix} = \begin{bmatrix}\hat{\theta}^{k}\\ \hat{\Theta}^{k}\end{bmatrix} + \begin{bmatrix} f_{11}\sum_{t=1}^{\tau} x_t^{\hat{\theta}^k} a_t^k + f_{12}\sum_{t=1}^{\tau} x_t^{\hat{\Theta}^k} a_t^k \\ f_{21}\sum_{t=1}^{\tau} x_t^{\hat{\theta}^k} a_t^k + f_{22}\sum_{t=1}^{\tau} x_t^{\hat{\Theta}^k} a_t^k \end{bmatrix} \tag{4.15}$$

$$\begin{bmatrix} f_{11} & f_{12}\\ f_{21} & f_{22}\end{bmatrix}^{-1} = \begin{bmatrix} \sum_{t=1}^{\tau}\left(x_t^{\hat{\theta}^k}\right)^2 & \sum_{t=1}^{\tau} x_t^{\hat{\theta}^k} x_t^{\hat{\Theta}^k} \\ \sum_{t=1}^{\tau} x_t^{\hat{\theta}^k} x_t^{\hat{\Theta}^k} & \sum_{t=1}^{\tau}\left(x_t^{\hat{\Theta}^k}\right)^2 \end{bmatrix} \tag{4.16}$$

Step 5 If $\|\hat{\theta}^{k+1} - \hat{\theta}^k\| < \epsilon$ and $\|\hat{\Theta}^{k+1} - \hat{\Theta}^k\| < \epsilon$, then Stop. Otherwise, let $k \leftarrow k+1$ and return to Step 2.

The aforementioned frequentist approach was used to optimize parameters $\hat{\theta}$ and $\hat{\Theta}$ using the preliminary values obtained in Section 4.3.2 as initial guesses, and $\delta = \epsilon = 0.001$. After 54 iterations, the optimized values are $\hat{\theta} = 0.6033$ and $\hat{\Theta} = 0.9567$, which has an estimated variance of $\hat{\sigma}_a^2 = 8.53$, i.e., 16.4% lower than the same variance obtained with the preliminary values.

4.4.2 Bayesian Approach

Let $p(\theta,\Theta)$ be the joint probability distribution function for random variables θ and Θ, prior to the data. Then, Bayes's theorem in (4.17) states that the posterior probability distribution function of θ and Θ given a collection of data $\mathbf{z}$, i.e., $p(\theta,\Theta|\mathbf{z})$, is proportional to the product between prior distribution $p(\theta,\Theta)$ and the joint distribution of the data given parameters θ and Θ, i.e., $p(\mathbf{z}|\theta,\Theta)$.

$$p(\theta,\Theta|\mathbf{z}) \propto p(\mathbf{z}|\theta,\Theta)\, p(\theta,\Theta) \tag{4.17}$$

Assuming a_t's and w_t's are normally distributed, it can be demonstrated that the joint distribution function of data given parameters θ and Θ is (4.18), where $S(\theta,\Theta) = \sum_{-s-1}^{\tau} a_t^2$ is the conditional sum-of-squares function, and $f(\theta,\Theta)$ is a non-linear function of θ and Θ (BOX *et al.*, 2008).

$$p(\mathbf{z}|\theta,\Theta) = f(\theta,\Theta)\exp\left\{-\frac{1}{2\hat{\sigma}_a^2}S(\theta,\Theta)\right\} \tag{4.18}$$

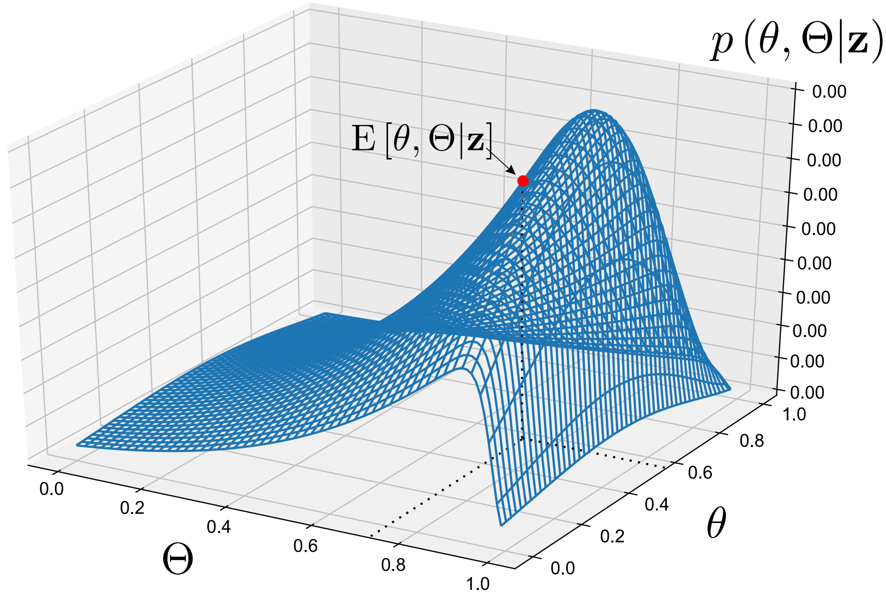

Figure 22 – Joint PDF of the posterior $p(\theta, \Theta|\mathbf{z})$ and expected value $\mathrm{E}[\theta, \Theta|\mathbf{z}]$.

Source: Lopez *et al.* (2019).

Using Jeffery's prior (JEFFREYS, 1961) for both parameters, and assuming a constant value for $\hat{\sigma}_a^2$, the posterior probability distribution function $p(\theta, \Theta|\mathbf{z})$ has the form of (4.19), where N is the number of data samples of the time series $\mathbf{z}$.

$$p(\theta, \Theta|\mathbf{z}) \propto [S(\theta, \Theta)]^{-N/2} \tag{4.19}$$

Taking samples from $0 \leq \theta \leq 1$ and $0 \leq \Theta \leq 1$, and using Algorithm 1 for calculating the a_t^k's, the posterior probability distribution function $p(\theta, \Theta|\mathbf{z})$ in (4.19) can be plotted to identify the mean values and statistical moments of θ and Θ, using the most recent available information of $\mathbf{z}$. Fig. 22 shows the resulting joint probability distribution of $p(\theta, \Theta|\mathbf{z})$ which not only indicates the expected values of $\hat{\theta} = 0.5421$ and $\hat{\Theta} = 0.7274$ but also, it provides a confidence interval of 95% for $0.4 \leq \theta \leq 0.8$ and $0.7 \leq \Theta \leq 1.0$.

4.4.3 Adaptability

In practice, the process of updating the values of $\hat{\theta}$ and $\hat{\Theta}$ using either the frequentist or Bayesian approach is done independently for each time series (and smart meter) as follows: whenever a new realization of the time series is available at time τ, use the previous N samples to deploy the model estimation approach of choice and disregard any sample before $\tau - N$. The forecasted values of $\bar{z}_t$ are only calculated when the OOP requires them using (4.11) for a lag time l.

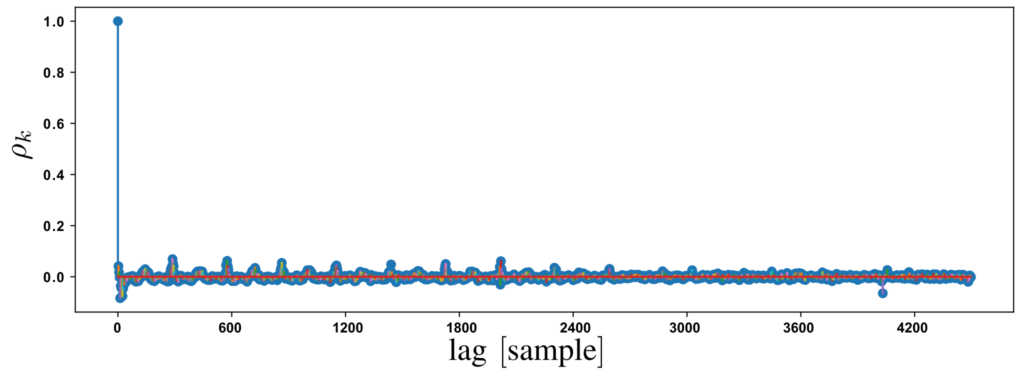

Figure 23 – Frequentist approach: Estimated autocorrelation function of the residuals a_t's.

Source: Lopez *et al.* (2019).

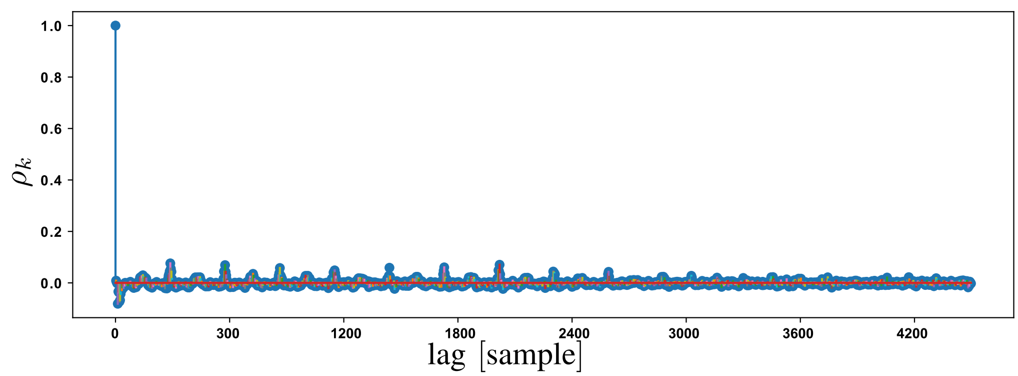

Figure 24 – Bayesian approach: Estimated autocorrelation function of the residuals a_t's.

Source: Lopez *et al.* (2019).

4.5 Model Adequacy

Low values of the estimated variances $\hat{\sigma}_a^2$ are not a sufficient indication of the forecasting method's accuracy. Checking the autocorrelation function of the residuals is also an important aspect because high autocorrelations indicate that critical information from the original series has been left behind by the model. Figs. 23 and 24 show the estimated autocorrelation function of the residuals a_t's for both model estimation approaches, frequentist and Bayesian, considering lags between 1 to 4,500 samples (i.e., up to two weeks). Despite some cyclical deviations, which are expected in random series, there are no noticeable large autocorrelations that indicate an evident lack-of-fit from both methods.

A more systematic way for checking the adequacy of the model is to assess the statistical significance of apparent deviations of the residuals. To do so, the Ljung-Box-Pierce

(LJUNG; BOX, 1978) statistic test can be performed using (4.20).

$$\bar{Q} = N\left(N+2\right)\sum_{k=1}^{K}\left(N-k\right)^{-1}\rho_k^2 \tag{4.20}$$

where N is the interval of the data series used to fit the model and K is the interval of the lags under study. If the model is appropriate the statistic $\bar{Q}$ is approximately distributed as $\chi^2\left(K-p-q\right)$, where $p = 0$ and $q = 2$ in the ARIMA model (4.1). Thus, considering $K = 4,032$ (i.e., two weeks) and fitting the model using $N = 34,944$ samples (i.e., one year) the value of $\bar{Q}$ was approximately 3,032 using the frequentist approach, and 3,472 for the Bayesian approach. Both $\bar{Q}$'s are below the adequacy level of 4,179 that corresponds to the 5%-χ^2 test, with 4,030 degrees of freedom. In his case, the Ljung-Box-Pierce statistic test does not provide any evidence of inadequacy in the model.

4.6 Tests and Results

In order to test the efficiency of the proposed short-term load forecasting technique in the context of solving OOP problems, a robust self-healing scheme was simulated. To that end, the real-size 13.2 kV EDS in Fig. 25 was used for tests. The system comprises five radial feeders that supply electricity to 38,000 users of three types: residential, commercial and industrial consumers. Individual load profiles were randomly generated using the LoadProfileGenerator software in Pflugradt and Muntwyler (2017), Pflugradt *et al.* (2013). The real-size EDS has 5,181 nodes, from which 955 are primary distribution transformers with smart meters. The meters are constantly measuring average three-phase current and voltage magnitudes with a resolution of 5 minutes per sample. Thus, each smart meter supervises at least six time series per transformer and, it is assumed that at least four years of measurements are available to the OOP system. Blue and magenta feeders in Fig. 25 are connected to a main substation of 40 MVA (nominal capacity), whereas red, yellow, and green feeders are connected to a different substation of 60 MVA. Moreover, the EDS has three 5 MVA dispatchable distributed generation (DG) units with islanded operation capabilities. The total installed capacity of the distribution transformers is approximately 81 MVA. Also, there are 32 remotely-controlled normally closed (NC) switches and 14 remotely-controlled normally open (NO) switches that participate in the self-healing scheme.

The proposed short-term load forecasting model in (4.1) is used to predict the three-phase consumption at each transformer. Thus, all the 955 meters in Fig. 25 are set to be constantly measuring at least six different time series (three-phase voltage magnitudes and load currents) and deploying one-week ahead forecasts with a lag of $l = 2,016$ samples, whenever the self-healing scheme requires them. Note that, in theory, any lag l can be used,

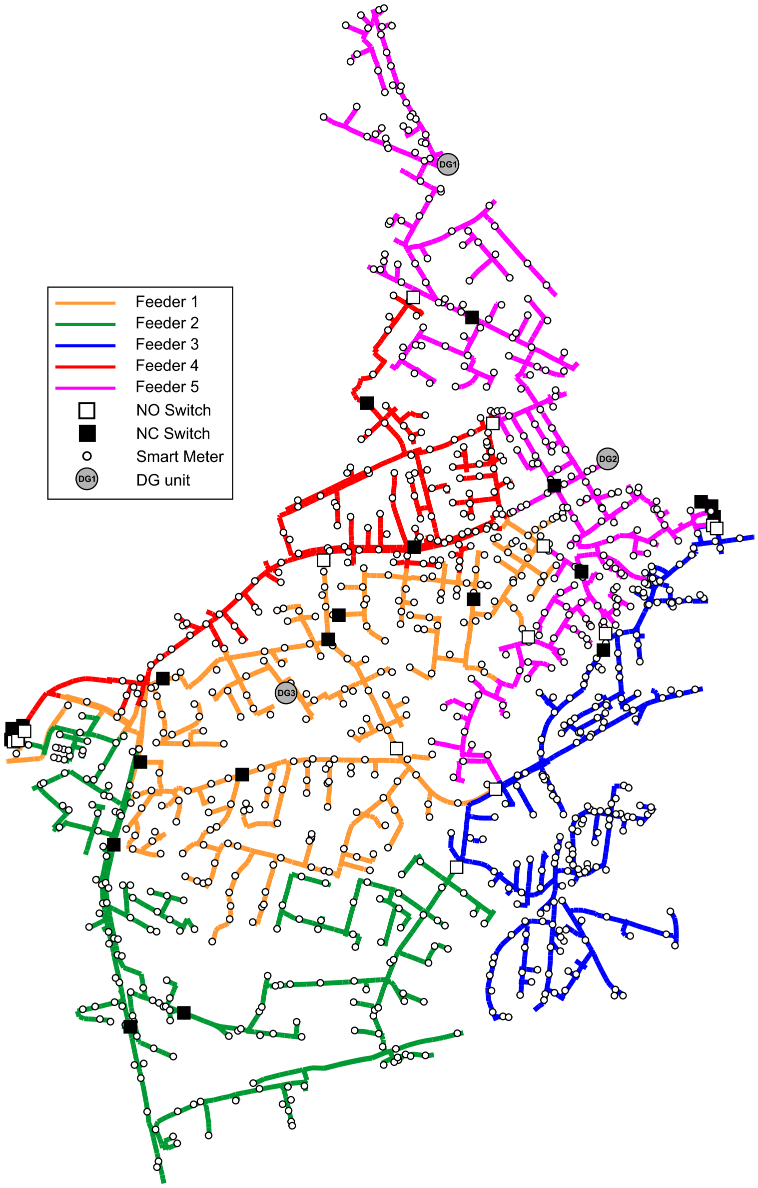

Figure 25 – Real-size 13.2 kV EDS with an AMI.

Source: Lopez *et al.* (2019).

but the standard deviation of the forecast errors increases with the length of l (BOX *et al.*, 2008). Hence, the proposed ARIMA model can only be employed for short-term planning, because the forecasted data for the next week will have larger errors than the forecasts for the next day.

Two fault scenarios are discussed in sections 4.6.1 and 4.6.2, respectively. In Case 1, the restoration after a permanent fault of the main breaker at feeder 5 (magenta) is simulated. In Case 2, a permanent fault of the main breaker of feeder 1 (yellow) is deployed. In both cases, the fault requires one day to be totally repaired. Thus, only the first 288 forecasts are

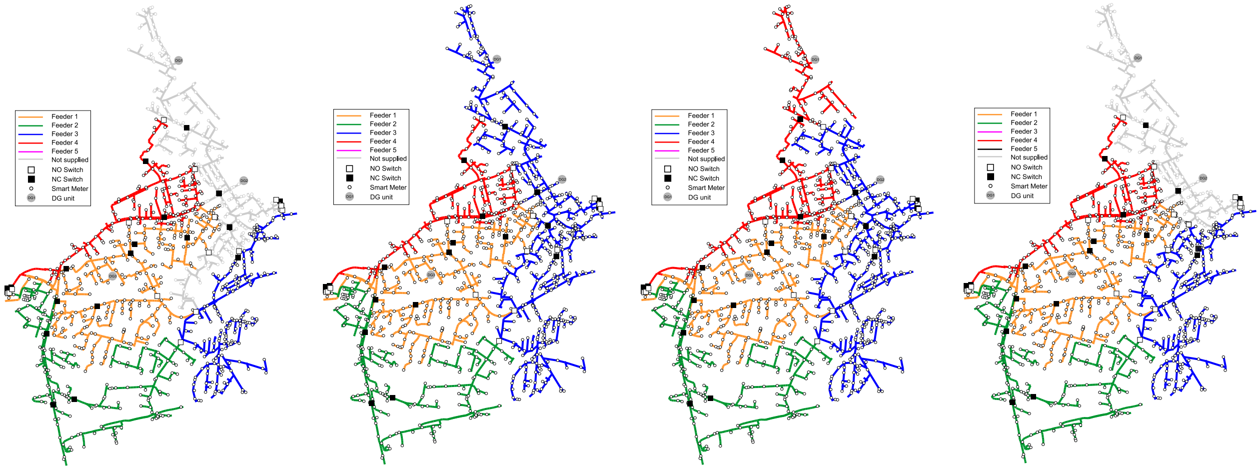

a) Nominal approach b) Day-before approach c) Frequentist approach d) Bayesian approach

Figure 26 – Self-healing solution for Case 1: a) using nominal approach; b) day-before approach; c) frequentist approach; d) Bayesian approach.

Source: Lopez *et al.* (2019).

used to deploy the self-healing system.

For each case, the two proposed methods used to estimate parameters θ and Θ, i.e., the frequentist approach in Section 4.4.1 and the Bayesian approach in Section 4.4.2, are compared with a basic restoration plan obtained either by using the nominal capacities of all transformers as conventional demands, a.k.a., the *nominal approach*, or the load diagram of the previous day as an estimation of future consumption, a.k.a., the *day-before approach*.

Finally, as mentioned in Section 4.2.1, the centralized self-healing scheme was deployed using an heuristic solution of the restoration model presented in (LOPEZ *et al.*, 2018). The heuristic is an adaptation of the Tabu Search algorithm (GROVER; LAGUNA, 1997) that returns the best restoration sequence found after 60 seconds. In all cases, the objective function minimizes the unsupplied demand and the number of switch operations, and penalizes the violations of the operational limits. The Tabu Search attribute has been set to 1 for all simulations (see Grover and Laguna (1997) for more information).

4.6.1 Case 1: Fault at the main breaker of feeder 5

A permanent fault of the main breaker in feeder 5 (magenta) disconnects all loads downstream the circuit. Thus, a restoration sequence is deployed using the load forecasts from four different approaches, as follows:

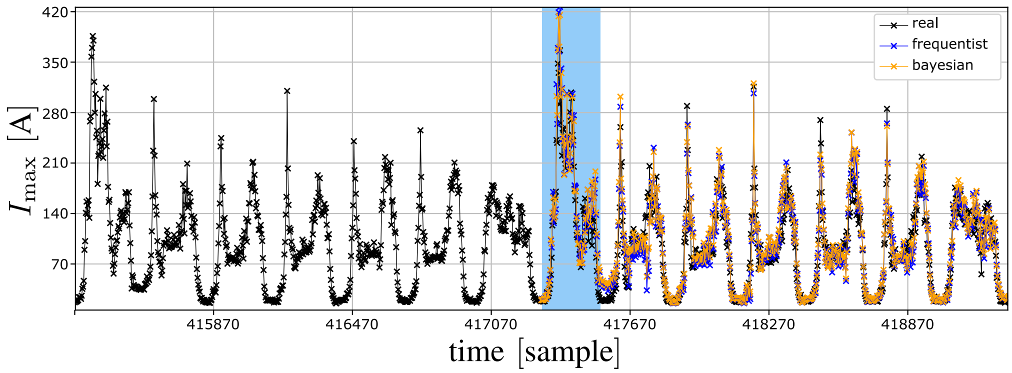

Figure 27 – Realization (black), frequentist (blue) and Bayesian (yellow) forecasts of the maximum current magnitude.

Source: Lopez *et al.* (2019).

4.6.1.1 Nominal approach

In this case, demands are considered as constant balanced three-phase active and reactive power injections, equal to the nominal capacities of the distribution transformers with an inductive power factor of 0.9. Thus, given a permanent fault of the main breaker of feeder 5 (magenta), the solution generated by the self-healing scheme using nominal capacities is shown in Fig. 26a. Note that, using the nominal capacities of the transformers, the self-healing scheme was not able to find a feasible solution that minimizes the unsupplied demand. Thus, as shown in Fig. 26a, all nodes and circuits of feeder 5 were de-energized by the opening of the main breaker at the substation, and no further restoration actions were performed.

4.6.1.2 Day-before approach

As an alternative to the nominal approach, a more simplistic method based on the load profile curve of the previous day can be used to predict the moment of maximum consumption after the fault. The solution generated by the self-healing scheme using the day-before approach is shown in Fig. 26b. In this case, the moment of maximum consumption of the previous day was 8% lower than the actual realization of the moment of maximum consumption after the fault. Thus, even though the solution in Fig. 26b transferred all demands from feeder 5 to feeder 3 (blue), the underestimation of the day-before approach produced several lines with overcurrent limits transgressions, mostly concentrated at the beginning of feeder 3, for approximately one hour during the post-fault operation. The mean absolute percentage error (MAPE) of this approach for all the 955 meters considering a one-day ahead forecast was 16%.

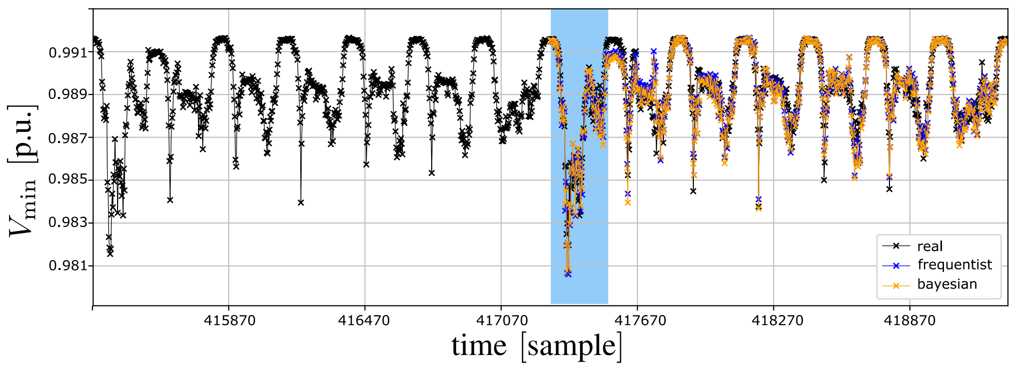

Figure 28 – Realization (black), frequentist (blue) and Bayesian (yellow) forecasts of the minimum voltage magnitude.

Source: Lopez *et al.* (2019).

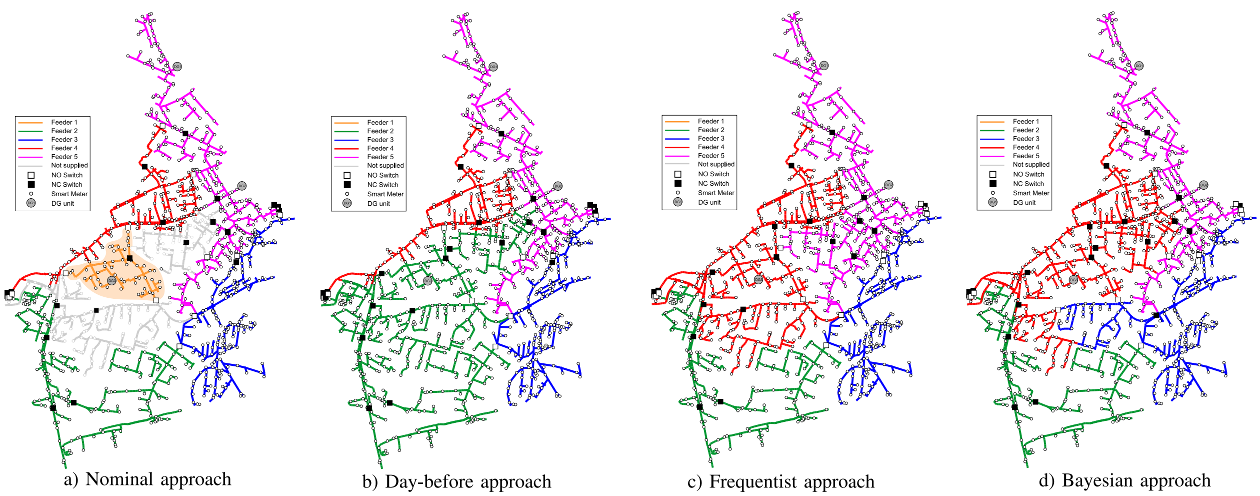

Figure 29 – Self-healing solution for Case 2: a) using nominal approach; b) day-before approach; c) frequentist approach; d) Bayesian approach.

Source: Lopez *et al.* (2019).

4.6.1.3 Frequentist approach

Clearly, assuming nominal capacities is very conservative because it is unrealistic to believe that all demands require the complete installed capacity of the EDS, simultaneously. Thus, after using the frequentist approach to generate forecasts, the moment of maximum consumption was identified by comparing the maximum forecasted currents and the minimum forecasted voltages in Fig. 27 and Fig. 28. Note that, since the expected time to repair the outage is one day, only the blue area of Fig. 27 and Fig. 28 were considered. In this case, the moment of maximum consumption occurs at lag $l = 78$, i.e., approximately after 6.5 hours after the outage. Thus, using the demands from the moment of maximum consumption, plus the standard deviation of the forecast errors provided by the ARIMA model, the restoration plan shown in Fig. 26d was obtained by the centralized self-healing scheme. In this case, all demands were supplied after transferring most of the loads from feeder 5 to feeder 3 (blue), and the remaining loads from feeder 5 to feeder 4 (red). During post-fault operation, three lines of feeder 3 have slight overcurrent of 109% of their maximum current capacities. The one-day ahead MAPE of this approach was 12%.

4.6.1.4 Bayesian approach

In this case, the Bayesian approach is used to generate the forecasts, and the moment of maximum consumption is identified as before. With the Bayesian approach, the moment of maximum consumption occurs at lag $l = 81$, i.e., approximately after 6.75 hours after the outage. Thus, using the demands from the moment of maximum forecasted consumption, plus the standard deviation of the forecast errors, the solution shown in Fig. 26c was obtained by the self-healing scheme. Unlike the frequentist approach, the restoration plan using the Bayesian estimation did not supplied all demands from feeder 5. Instead, only a portion of the consumers were transferred to feeder 3 (blue), while the rest remained de-energized. However, in terms of number of de-energized consumers, the Bayesian solution was still better than the solution using nominal transformer capacities, with no limits transgressions during post-fault operation. The one-day ahead MAPE of this approach was 12%.

A summary of all four restoration plans in Fig. 26 is shown in Table 7. The minimum voltage, maximum current and limits transgressions are taken from the post-fault operation. Thus, as evidenced by the results in Table 7, the impact and efficiency of the self-healing scheme is highly improved when suitable forecasted demands are used instead of nominal references or simplistic previous days reproductions.

4.6.2 Case 2: Fault at the main breaker of feeder 1

A permanent fault of the main breaker in feeder 1 (yellow) disconnects all loads downstream the circuit. The restoration plans for the four different load forecasting methods are shown in Fig. 29. Note that, using the nominal approach, the solution provided by the service restoration method has created an island to supply a fraction of the users in feeder 1. As shown in Fig. 29a, the island used DG unit 3 as the main supply, and it was isolated due to the opening of two NC switches. On the other hand, in the day-before, frequentist and Bayesian approaches, all users in feeder 1 were transferred to different feeders, but with unique configurations for each case. As shown in Table 8, the underestimation of the forecasted loads provided by the day-before approach leaded to overcurrent events during the post-fault operation in feeder 2. Finally, the solutions obtained with the frequentist and the

Table 7 – Self-healing results for each approach in Fig. 26.

Approach	Nominal	Day-before	Frequentist	Bayesian
Unsupplied demand [MW]	30.56	0.0	0.0	20.62
De-energized users [#]	9441	0	0	7505
Switch operations [#]	0	1	3	2
Minimum voltage [p.u.]	0.9802	0.9706	0.9788	0.9802
Maximum current [A]	417	502	458	417
Limits transgression	None	Eighteen lines with overcurrent	Three lines with overcurrent	None

Table 8 – Self-healing results for each approach in Fig. 29.

Approach	Nominal	Day-before	Frequentist	Bayesian
Unsupplied demand [MW]	15.23	0.0	0.0	0.0
De-energized users [#]	10697	0	0	0
Switch operations [#]	2	1	3	3
Minimum voltage [p.u.]	0.9802	0.9680	0.9709	0.9744
Maximum current [A]	417	455	430	417
Limits transgressions	None	Three lines with overcurrent	None	None

Bayesian approaches supplied all demands of feeder 1 and they did not lead to any operational limits transgressions during the post-fault operation.

4.6.3 Frequentist approach vs Bayesian approach

In this case, if future outcomes of the series ω_t behave mostly as a Gaussian process with zero mean and lower values of $\hat{\sigma}_a^2$, then the frequentist approach should be used because it is based on the least-square estimator that minimizes the variance of the forecast errors. However, if large portions of the series ω_t present non-homogeneous behavior (see Section 4.3.1) or large values of $\hat{\sigma}_a^2$ are obtained, then the non-informative nature of Jeffery's prior used in the Bayesian approach could produce more accurate results because there might be an underlying randomness in the nature of Θ and θ, that is not captured by the frequentist approach. Thus, a good rule-of-thumb would be to use the frequentist approach first, and then, depending on the range of the recurring values of $\hat{\Theta}$ and $\hat{\theta}$, the Bayesian approach can be deployed using tight intervals for both unknown parameters.

From the statistical point-of-view, there are no good reasons for using one inference method over the other (WAKEFIELD, 2013). However, some practical aspects might be considered for implementation. For example, the convergence of the iterative process in Section 4.4.1 is not always guaranteed, whereas the Bayesian estimation does not rely on any convergence process. One major drawback of the Bayesian approach in Section 4.4.2 is that, for large data samples, the posterior in (4.19) can result in extremely low numbers that cannot be computationally handled, thus lower values of N must be required.

4.7 Conclusion

Assuming three-phase electrical measurements as univariate non-stationary seasonal time series, this chapter investigates two parsimonious short-term load forecasting techniques to estimate future aggregated demands for the OOP of EDS: a frequentist and a Bayesian multiplicative seasonal ARIMA model. Both approaches are shown to satisfy the four parsimonious requirements: low computational complexity, fair accuracy in terms of expected value and residuals, few tuning parameters, and adaptability. Thus, they are suitable for solving OOP problems in highly supervised EDS. Results show that the use of the proposed parsimonious short-term forecasting techniques have a significant impact on the quality of the OOP methods, such as the centralized self-healing scheme, especially compared with other approaches that use nominal references or simplistic day-before approaches.

5 Designing and Implementation of a Self-Healing Scheme for Modern Electrical Distribution Systems

Abstract

In case of a permanent fault at the electrical distribution system (EDS), a centralized self-healing scheme (SHS) is deployed to automatically identify the location of the fault and to restore the electrical service to as many users as possible, in a short amount of time and with minimal human intervention. The service restoration must be done while considering topological and operational constraints, such as radiality, current and voltage magnitude limits, substation capacities, distributed generation (DG) units operation, among others. A fully automated SHS is only possible within a smart grid context, wherein electrical and topological variables of the network are supervised via smart meters, and remotely controlled via supervisory control and data acquisition (SCADA) system. Thus, this chapter presents a centralized SHS that continuously gathers and analyzes data from the SCADA to estimate the location of a permanent fault, to forecast the maximum post-fault demand, and to restore the service. Once a fault has been located, the SHS will automatically return a set of sequenced actions that isolate the faulty section of the network and maximize the supplied demand. The proposed SHS has been simulated in real distribution networks and uses a geographic information system (GIS) to display results.

Acronyms of Chapter 5

AMI	Advanced metering infrastructure
ARIMA	Autoregressive integrated moving average
DG	Distributed generation
EDS	Electrical distribution system
GIS	Geographic information system
GUI	Graphical user interface

MINLP Mixed-integer nonlinear programming

NLP Nonlinear programming

RMSE Root-mean-square error

SCADA Supervisory control and data acquisition

SHS Self-healing scheme

5.1 Introduction

In the context of modern electrical distribution systems (EDS), a centralized self-healing scheme (SHS) is a set of equipment, software and communication technologies that, after a permanent fault, can determine and deploy a sequence of restorative actions, aiming to isolate the faulted section of the network and to minimize the total unsupplied demand (AGUERO, 2012). Among those restorative actions, the operation of remote-controlled switching devices and the injections of the dispatchable distributed generation (DG) resources are the most common. A truly automated SHS does not only restore the EDS in case of a fault, but also, it is able to identify the location of the fault and estimate the total amount of unsupplied demand that needs to be minimized by the restoration process (CAVALCANTE *et al.*, 2016). As shown in Fig. 30, a centralized SHS uses the information gathered by the SCADA system (e.g., field measurements and status of switching devices) to identify the most probable location of a permanent fault and respond to it as soon as possible, with minimal human intervention. Finally, once the faulted section of the zone has been isolated, maintenance crews can be sent to find and repair the outage's cause (LIU *et al.*, 2014).

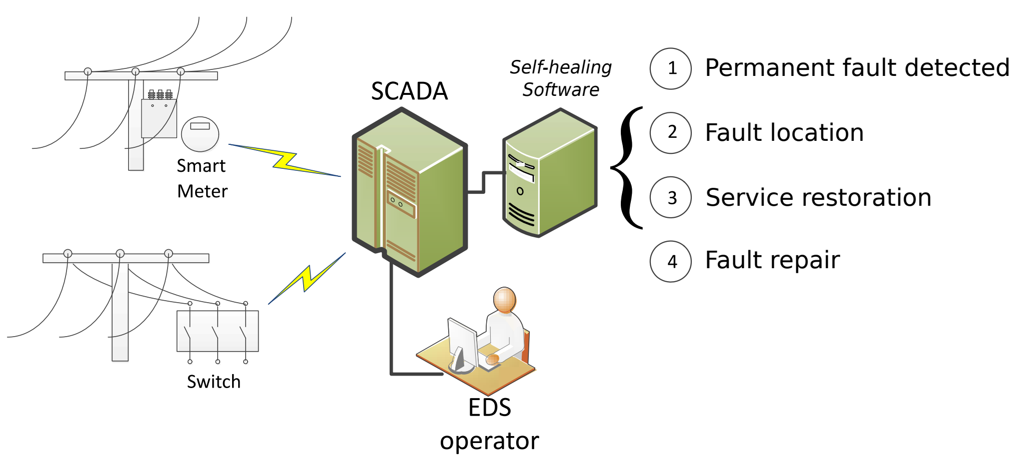

Figure 30 – Centralized self-healing scheme.

Source: author.

The term *self-healing* has been mostly coined to name sophisticated service restoration algorithms in EDS. Authors in Srivastava and Butler-Purry (2007) used it for the first time in 2007 to name a rule-based restoration approach for shipboard power systems, whose functionality needs to be preserved during battle. More recently, various multi-agent systems have been proposed as plausible SHS (ZIDAN; EL-SAADANY, 2012; ELMITWALLY *et al.*, 2015; ERIKSSON *et al.*, 2015; HAFEZ *et al.*, 2018; SHIRAZI; JADID, 2018; SHIRAZI; JADID, 2019). These techniques have proved to be successful for deploying the service restoration aspect of the SHS, but other important aspects are not addressed, such as the fault-location method and post-fault load estimation. Since the service restoration is a combinatorial optimization problem, modern heusritic techniques and mathematical programming have been used to solve it (AREFIFAR *et al.*, 2013; WANG; WANG, 2015; GOLSHANI *et al.*, 2017). However, once again, *self-healing* encompasses other processes besides the service restoration aspect. To the best of our knowledge, only two works in Drayer *et al.* (2018) and Leite and Mantovani (2017) approximate the most to the true self-healing philosophy. Authors in Drayer *et al.* (2018) and Leite and Mantovani (2017) address the fault-location method and the service restoration aspect of the proposed SHS. However, other practicalities have been overlooked: post-fault load estimation, unbalanced three-phase networks, switching sequence and scalability assessment.

In this chapter, the designing and implementation of a true SHS for modern EDS is presented. Besides the service restoration, the proposed SHS comprises a fully automated fault-location method, post-fault load estimation based on smart meters' data, and it considers practical aspects, such as unbalanced networks, DG units and switching sequence. The software has been developed in *Python* (SUMMERFIELD, 2009), and it includes a graphical user interface (GUI) with geographic information system (GIS) functionalities. The proposed self-healing scheme has been tested in real EDS to prove its scalability and efficiency.

5.2 Proposed Self-Healing Scheme

Flowchart in Fig. 31 summarizes the steps of the proposed SHS. Using data gathered by smart meters and the EDS's topological and electrical information, the proposed SHS: a) estimates the nodal demands during pos-fault operation, using a three-phase steady-state estimator and a parsimonious short-term load forecasting method; b) efficiently identifies the zone wherein the permanent fault is located; and c) generates the sequence of switching actions and DG outputs that minimizes the total unsupplied demand. Thus, the modules of the proposed SHS work in tandem: once data from the SCADA system have been consolidated, the state estimator and the load forecasting module establishes the post-fault operating

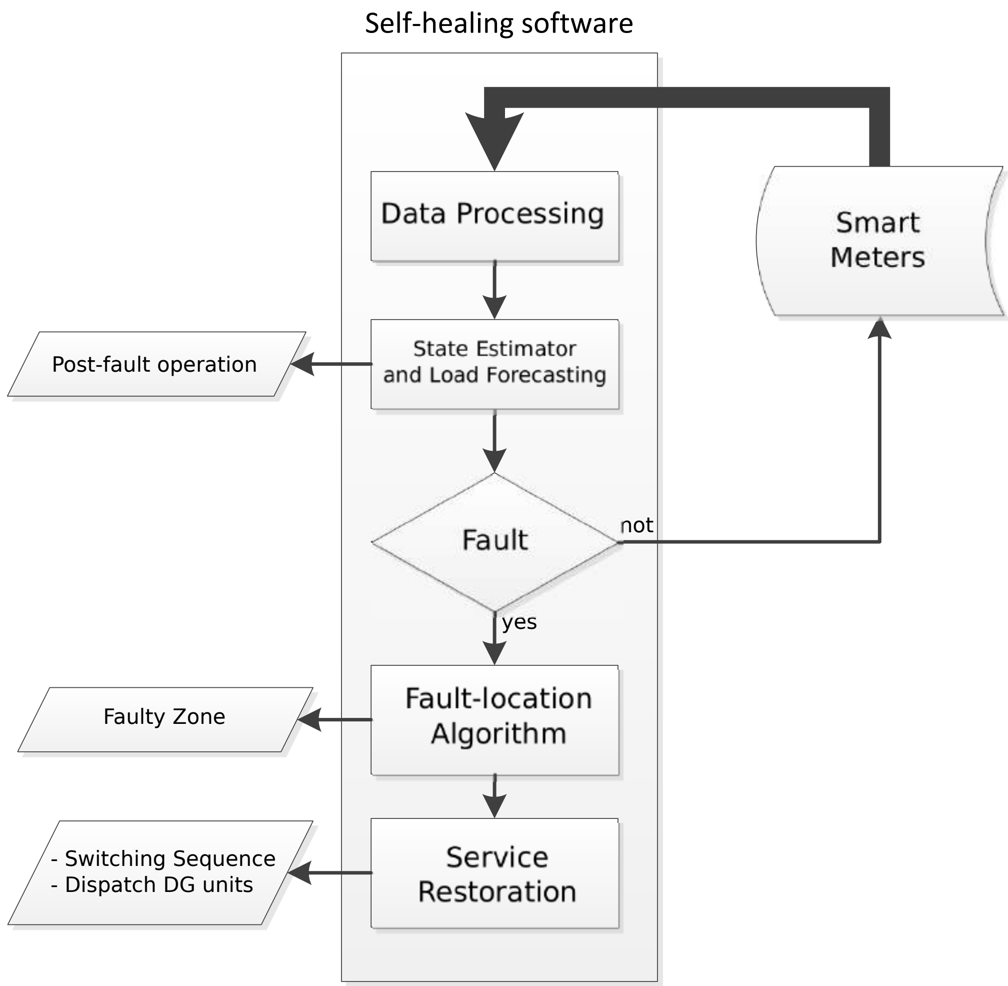

Figure 31 – Flowchart of the proposed self-healing scheme.

Source: author.

point of the EDS, based on the most recent measurements from the smart meters. Then, if a permanent fault has been identified by the protection coordination, the fault location algorithm establishes the zone of the network where the outage most probably is, a.k.a., the faulty zone. Finally, given a faulty zone and the estimation of the demands after the fault, a robust service restoration algorithm is executed.

The main characteristics of the modules will be discussed in the following subsections, i.e., the state estimation and load forecasting module, the fault-location module and the service restoration module.

5.2.1 Three-phase State Estimator

The function of a state estimator is to assess the operating point of the EDS based on available measurements (BARAN; KELLEY, 1995). In this particular case, the purpose of the three-phase state estimator is to determine the unknown active and reactive demands before the fault, based on the three-phase current and voltage magnitudes provided by smart meters. This information is used to deploy the short-term load forecasting method that estimates the post-fault demands required by the service restoration process. Most state estimators for EDS are based on weighted least square methods and require the inversion of large Jacobian matrices (PRIMADIANTO; LU, 2017). These approaches are mostly suitable for observable systems and require powerful computational resources. Thus, a generalized three-phase state estimator will be presented in this subsection based on mathematical optimization, which can be solved for any level of observability and within limited amount of time and computational resources.

The nonlinear programming (NLP) model shown in (5.1)–(5.12) is a mathematical representation of a three-phase state estimator for unbalanced EDS. Ω_b is the set of nodes, Ω_l is the set of branches, Ω_{sw} is the set of remote-controlled switches, and Ω_z is the set of measurement areas, where each area is a connected portion of the network whose nodes share a common feature. In this case, the common feature will be the upstream remote-controlled switching device of each node that participates in the service restoration process.

$$\min \left\{ \sum_{i \in \Omega_b} \sum_{f \in \{a,b,c\}} \omega_i^b \left(V_{i,f} - V_{i,f}^{\text{meas}} \right)^2 + \sum_{ij \in \Omega_l} \sum_{f \in \{a,b,c\}} \omega_{ij}^l \left(I_{ij,f} - I_{ij,f}^{\text{meas}} \right)^2 \right\} \tag{5.1}$$

subject to:

$$\sum_{ji \in \Omega_l} i^r_{ji,f} - \sum_{ij \in \Omega_l} i^r_{ij,f} + \sum_{ji \in \Omega_{\text{sw}}} {i^{\text{sw}r}}_{ji,f} - \sum_{ij \in \Omega_{\text{sw}}} {i^{\text{sw}r}}_{ij,f} = {i^{D^r}}_{i,f} - {i^{G^r}}_{i,f}; \qquad \forall i \in \Omega_b, f \in \{a,b,c\} \tag{5.2}$$

$$\sum_{ji \in \Omega_l} i^i_{ji,f} - \sum_{ij \in \Omega_l} i^i_{ij,f} + \sum_{ji \in \Omega_{\text{sw}}} {i^{\text{sw}i}}_{ji,f} - \sum_{ij \in \Omega_{\text{sw}}} {i^{\text{swsw}}}_{ij,f} = {i^{D^i}}_{i,f} - {i^{G^i}}_{i,f}; \qquad \forall i \in \Omega_b, f \in \{a,b,c\} \tag{5.3}$$

$$v^r_{i,f} - v^r_{j,f} = \sum_{h \in \{a,b,c\}} \left(R_{ij,f,h} i^r_{ij,h} - X_{ij,f,h} i^i_{ij,h} \right); \qquad \forall ij \in \Omega_l, f \in \{a,b,c\} \tag{5.4}$$

$$v^i_{i,f} - v^i_{j,f} = \sum_{h \in \{a,b,c\}} \left(X_{ij,f,h} i^r_{ij,h} + R_{ij,f,h} i^i_{ij,h} \right); \qquad \forall ij \in \Omega_l, f \in \{a,b,c\} \tag{5.5}$$

$$P^G_{i,f} = v^r_{i,f} {i^{G^r}}_{i,f} + v^i_{i,f} {i^{G^i}}_{i,f}; \qquad \forall i \in \Omega_b, f \in \{a,b,c\} \tag{5.6}$$

$$Q^G_{i,f} = -v^r_{i,f}{i^{G^i}}_{i,f} + v^i_{i,f}{i^{G^r}}_{i,f}; \qquad \forall i \in \Omega_b, f \in \{a,b,c\} \quad (5.7)$$

$$\rho_{\hat{z}_i} P^{\text{nom}}_{i,f} = v^r_{i,f}{i^{D^r}}_{i,f} + v^i_{i,f}{i^{D^i}}_{i,f}; \qquad \forall i \in \Omega_b, f \in \{a,b,c\} \quad (5.8)$$

$$\rho_{\hat{z}_i} Q^{\text{nom}}_{i,f} = -v^r_{i,f}{i^{D^i}}_{i,f} + v^i_{i,f}{i^{D^r}}_{i,f}; \qquad \forall i \in \Omega_b, f \in \{a,b,c\} \quad (5.9)$$

$$V_{i,f} = \sqrt{\left(v^r_{i,f}\right)^2 + \left(v^i_{i,f}\right)^2}; \qquad \forall i \in \Omega_b, f \in \{a,b,c\} \quad (5.10)$$

$$I_{ij,f} = \sqrt{\left(i^r_{ij,f}\right)^2 + \left(i^i_{ij,f}\right)^2}; \qquad \forall ij \in \Omega_l, f \in \{a,b,c\} \quad (5.11)$$

$$0 \le \rho_z \le 1; \qquad \forall z \in \Omega_z \quad (5.12)$$

The objective function in (5.1) is a weighted minimization of the square difference between the calculated voltage and current magnitudes ($V_{i,f}$ and $I_{ij,f}$) and their measured counterparts ($V^{\text{meas}}_{i,f}$ and $I^{\text{meas}}_{ij,f}$). Equations (5.2)–(5.9) formulate the three-phase power flow in unbalanced EDS using a rectangular form. Superscripts r and i represent the real and imaginary part of the state variables $v_{i,f}$ (nodal voltages), $i_{ij,f}$ (branch currents) and ${i^{\text{sw}}}_{ij,f}$ (switch currents). Active and reactive generation are considered by (5.6) and (5.7). Note that the nominal active and reactive consumption at each load node ($P^{\text{nom}}_{i,f}$ and $Q^{\text{nom}}_{i,f}$) are multiplied by the decision variable ρ_z in (5.8) and (5.9), where $\hat{z}_i$ maps the area of node i. Continuous variable ρ_z is a load factor at each area, bounded as in (5.12). Voltage and current magnitudes are calculated in (5.10) and (5.11), respectively. The NLP model in (5.1)–(5.12) is a non-convex optimization problem and, for practical applications, quality solutions can be obtained via modern heuristics within reasonable computational times and resources. Finally, note that the state estimator will no be necessary if an advanced metering infrastructure (AMI) is available (MOHASSEL *et al.*, 2014).

5.2.2 Short-term Load Forecasting Method

Based on the current demands obtained either by the aforementioned three-phase state estimator or the AMI, the next step of the proposed SHS is the forecasting of the post-fault demands. To do so, an adaptive version of the multiplicative autoregressive integrated moving average (ARIMA) model will be used (BOX *et al.*, 2008). The proposed seasonal ARIMA model shown in (5.13) is used to predict the three-phase consumption at each load node, given by z_t, based on its previous realizations.

$$\omega_t = z_t - z_{t-s} - (z_{t-1} - z_{t-s-1}) = a_t - \theta a_{t-1} - \Theta a_{t-s} + \theta\Theta a_{t-s-1} \quad (5.13)$$

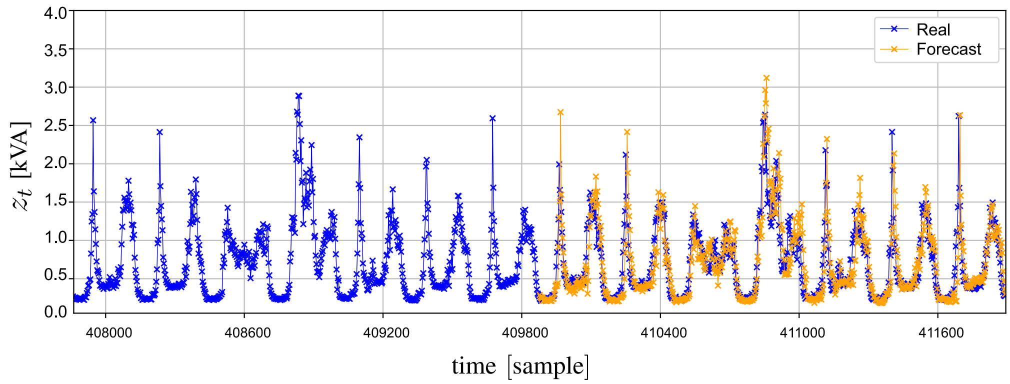

Figure 32 – Forecasting of a demand-type series z_t, obtained using the seasonal ARIMA model in (5.13) with a lag $l = 2,016$.

Source: Lopez *et al.* (2019).

Time series z_t in (5.13) is an equivalent of the three-phase active and reactive demands at each node at time t. Thus, for a resolution of 5 minutes per sample, it is expected that a stationary random signal ω_t can be obtained if the original consumption is transformed as in $\omega_t = z_t - z_{t-s} - (z_{t-1} - z_{t-s-1})$, where $s = 2,016$ for a weekly seasonal component. Aggregated demands usually follow a period of one week because human activities are conditioned to the hour of the day and the day of week. Henceforth, the seasonal ARIMA in (5.13) has been proved to be a parsimonious method for short-term load forecasting of EDS demands (LOPEZ *et al.*, 2019).

The ARIMA model in (5.13) can be used to estimate the moment of maximum consumption after the fault for any lag time l. However, the standard deviation of the forecast errors increases with the length of l (BOX *et al.*, 2008). Thus, the seasonal ARIMA is only intended for short-term load forecasting (TAYLOR; MCSHARRY, 2017). Finally, it is worth mentioning that the proposed load forecasting method is an adaptable and adequate predictor of future demands using the model estimation techniques described in Lopez *et al.* (2019). As an example, Fig. 32 shows the forecasts of a demand-type series z_t, obtained using the aforementioned technique for a lag $l = 2,016$, i.e., one-week ahead.

5.2.3 Fault-Location Method

Once a permanent fault has been identified by the protection coordination system, the next step of the proposed SHS is to immediately locate the fault. This can be done using a fault-location method in Chapter 3, based on asynchronous voltage measurements before and after the fault. The proposed fault-location method is an enhanced version of the bus-impedance-matrix-based method proposed by authors in Trindade *et al.* (2014) and

Cavalcante and Almeida (2018). Given a three-phase voltage drop at each smart meter ΔV_m^{abc} and the impedance bus matrix $Z_{n,m}^{abc}$, the origin of the fault is located by calculating the fault current at each node $n \in \Omega_b$, as perceived by each smart meter $m \in \Omega_m$, using (5.14).

$$I_{n,m}^{abc\ \text{fault}} = \left(Z_{n,m}^{abc}\right)^{-1} \Delta V_m^{abc}; \qquad \forall n \in \Omega_b, m \in \Omega_m \quad (5.14)$$

Thus, the location of the fault is identified through an index δ_n calculated using (5.15). Term $\left|\overline{I_n^{abc}}\right|^{\text{fault}}$ in (5.15) is the average fault current at node n as perceived by all meters. The node with the lowest value of δ_n is considered as the faulty node.

$$\delta_n = \sum_{m \in \Omega_m} \left| \left|\overline{I_n^{abc}}\right|^{\text{fault}} - \left|I_{n,m}^{abc}\right|^{\text{fault}} \right|; \qquad \forall n \in \Omega_b \quad (5.15)$$

This fault-location method is fast, accurate and easy to implement. Details regarding the construction of $Z_{n,m}^{abc}$ and the method's performance can be obtained at Trindade *et al.* (2014). Moreover, an enhanced version of the method is proposed in this chapter by calculating the average fault current $\left|\overline{I_n^{abc}}\right|^{\text{fault}}$ using the weighted arithmetic mean in (5.16).

$$\left|\overline{I_n^{abc}}\right|^{\text{fault}} = \sum_{m \in \Omega_m} \frac{d_{n,m}^{-1}}{\sum_{m \in \Omega_m} d_{n,m}^{-1}} \left|I_{n,m}^{abc}\right|^{\text{fault}}; \qquad \forall n \in \Omega_b \quad (5.16)$$

Where $d_{n,m}$ is the distance between node $n \in \Omega_b$ and the smart meter $m \in \Omega_m$. The weighted arithmetic mean in (5.16) is a better approach than the regular arithmetic mean because it is less susceptible to erroneous fault locations when some of the measurements are missing or unreliable.

5.2.4 Service Restoration of Unbalanced Three-phase EDS

Once the fault has been located and the post-fault maximum demands have been forecasted, the next step of the proposed SHS is to deploy the service restoration. The optimal restoration of unbalanced three-phase EDS, considering switching sequence and DGs, is given by the mixed-integer nonlinear programming (MINLP) model in (5.17)–(5.29) (LOPEZ *et al.*, 2018). Set Ω_s represents the number of sequenced steps from $\{1 \dots s^{\max}\}$ and Ω_s^{S} represents the areas with $V\Theta$ nodes, i.e., feeder root nodes.

$$\min \left\{ \sum_{z \in \Omega_z} \sum_{s \in \Omega_s} c_{z,s}^U \left(1 - x_{z,s}\right) + c^{\text{sw}} \sum_{ij \in \Omega_{\text{sw}}} \sum_{s \in \Omega_s} \left(\Delta y_{ij,s}^{+} + \Delta y_{ij,s}^{-}\right) \right\} \quad (5.17)$$

subject to:

$$(5.2)\text{–}(5.7),\ (5.10) \text{ and } (5.11); \qquad \forall s \in \Omega_s \quad (5.18)$$

$$P_{i,f}^{\max} = v_{i,f,s}^{r} {i^{D^r}}_{i,f,s} + v_{i,f,s}^{i} {i^{D^i}}_{i,f,s}; \qquad \forall i \in \Omega_b, f \in \{a,b,c\}, s \in \Omega_s \quad (5.19)$$

$$Q_{i,f}^{\max} = -v_{i,f,s}^{r} {i^{D^i}}_{i,f,s} + v_{i,f,s}^{i} {i^{D^r}}_{i,f,s}; \qquad \forall i \in \Omega_b, f \in \{a,b,c\}, s \in \Omega_s \quad (5.20)$$

$$|V_{i,f,s} - V_{j,f,s}| \leq \overline{V}\left(1 - y_{ij,s}\right); \qquad \forall ij \in \Omega_{\text{sw}}, f \in \{a,b,c\}, s \in \Omega_s \quad (5.21)$$

$$\underline{V} x_{\hat{z}_i,s} \leq V_{i,f,s} \leq \overline{V} x_{\hat{z}_i,s}; \qquad \forall i \in \Omega_b, f \in \{a,b,c\}, s \in \Omega_s \quad (5.22)$$

$$0 \leq I_{ij,f,s} \leq \overline{I_{ij}} x_{\hat{z}_{ij},s}; \qquad \forall ij \in \Omega_l, f \in \{a,b,c\}, s \in \Omega_s \quad (5.23)$$

$$0 \leq I_{ij,f,s}^{\text{sw}} \leq \overline{I_{ij}^{\text{sw}}} y_{ij,s}; \qquad \forall ij \in \Omega_{\text{sw}}, f \in \{a,b,c\}, s \in \Omega_s \quad (5.24)$$

$$y_{ij,s} - y_{ij,s-1} = \Delta y_{ij,s}^{+} - \Delta y_{ij,s}^{-}; \qquad \forall ij \in \Omega_{\text{sw}}, s \in \Omega_s|_{y_{ij,0}=s_{ij}^{\text{ini}}} \quad (5.25)$$

$$\sum_{ij \in \Omega_{\text{sw}}} \left(\Delta y_{ij,s}^{+} + \Delta y_{ij,s}^{-}\right) \leq 1; \qquad \forall s \in \Omega_s \quad (5.26)$$

$$\left| x_{\hat{z}_i,s} - x_{\hat{z}_j,s} \right| \leq 1 - y_{ij,s}; \qquad \forall ij \in \Omega_{\text{sw}}, s \in \Omega_s \quad (5.27)$$

$$\sum_{ij \in \Omega_{\text{sw}}} y_{ij,s^{\max}} x_{\hat{z}_{ij},s^{\max}} = \sum_{z \in \Omega_s \backslash \Omega_s^{\text{S}}} x_{z,s^{\max}}; \quad (5.28)$$

$$y_{ij,s}, x_{z,s}, \Delta y_{ij,s}^{+}, \Delta y_{ij,s}^{-} \in \{0,1\}; \qquad \forall ij \in \Omega_{\text{sw}}, z \in \Omega_z, s \in \Omega_s \quad (5.29)$$

In order to model the service restoration problem in (5.17)–(5.29), binary decision variables $y_{ij,s}$ and $x_{z,s}$ are required. $y_{ij,s}$ represents the status of each remote-controlled switch $ij \in \Omega_{\text{sw}}$ at step $s \in \Omega_s$, either open ($y_{ij,s} = 0$) or closed ($y_{ij,s} = 1$). $x_{z,s}$ represents the status of each area $z \in \Omega_{\text{sw}}$ at step $s \in \Omega_s$, either energized ($x_{z,s} = 1$) or de-energized ($x_{z,s} = 0$).

The objective function in (5.17) minimizes the unsupplied demand at each step of the restoration process, using a cost of de-energization $c_{z,s}^{U}$. Furthermore, the second term of the objective function minimizes the cost of swtiching operations using a cost c^{sw}, and auxiliary binary variables $\Delta y_{ij,s}^{+}$ and $\Delta y_{ij,s}^{-}$, both of which are related to $y_{ij,s}$ due to (5.25). The unbalanced three-phase load flow at each step of the restoration process is calculated in (5.18). Equations (5.19) and (5.20) establish the relationship between the forecasted maximum active and reactive demands ($P_{i,f}^{\max}$ and $Q_{i,f}^{\max}$) and the state variables (i.e., three-phase nodal voltages and demand currents). Constraint (5.21) guarantees that nodal voltages at closed switches share the same magnitude. Constraint (5.22) limits the voltage magnitudes at all nodes, considering that de-energized nodes (i.e., $x_{\hat{z}_i,s} = 0$) have zero voltage. Likewise, constraint (5.23) limits the current magnitudes at all branches, considering that de-energized branches (i.e., $x_{\hat{z}_{ij},s} = 0$) have zero current. Current magnitude limits are given by (5.23), considering that open switches (i.e., $y_{ij,s} = 0$) have zero current. As mentioned before, (5.25) relates $y_{ij,s}$ with $\Delta y^+_{ij,s}$ and $\Delta y^-_{ij,s}$, considering that $y_{ij,0} = s^{\text{ini}}_{ij}$, where s^{ini}_{ij} represents the initial status of the remote-controlled switches. Constraint (5.26) guarantees that one, and only one switching action will be performed at each step of the process. Constraint (5.27) guarantees that two areas interconnected by a closed switch (i.e., $y_{ij,s} = 1$) will share the same status. Constraint (5.28) assures that a radial topology will be obtained at the end of the restoration process. The binary nature of $y_{ij,s}$, $x_{z,s}$, $\Delta y^+_{ij,s}$ and $\Delta y^-_{ij,s}$ is given by (5.29). Finally, in order to isolate the fault during the restoration process, the binary variable $x_{z,s}$ must be fixed to zero for the area z that contains the faulty node. A comprehensive discussion of the characteristics and performance of the optimal restoration model for unbalanced three-phase EDS can be found at Lopez *et al.* (2018).

Similar to the three-phase state estimator, the MINLP model in (5.17)–(5.29) is a non-convex combinatorial optimization problem and, for practical applications, quality solutions can be obtained via modern heuristics within reasonable computational times and resources.

5.2.5 Proposed SHS software

The proposed SHS was developed as a GIS-based software, comprising the GUI developed in Python/TkInter (PYTHON, 2019). A snapshot of the GUI's prototype is shown in Fig. 33. All aforementioned modules: the three-phase state estimator, the short-term load forecasting module, the fault-location method and the service restoration were developed and executed in the proposed SHS software. Optimization problems in (5.1)–(5.12) and (5.17)–(5.29) where solved using an adaptation of the Tabu Search algorithm (GROVER; LAGUNA, 1997) that returns the best solution after 60 seconds. To do so, the continuous decision variable ρ_z in (5.12) was discretized and the remaining state variables (voltages and currents) were calculated using a backward/forward three-phase unbalanced load flow in Cheng and Shirmohammadi (1995). A similar approach was used to solve (5.17)–(5.29) via Tabu Search, considering the binary nature of the decision variables in (5.29) to code the solutions. The workstation used to run the SHS software has a standard Intel® Core™ i7-4510U, with a 2.00 GHz CPU and 8.00 GB RAM, running on Microsoft® Windows 8™. Maps were generated using the Google®Maps JavaScript API (GOOGLE MAPS API, 2019).

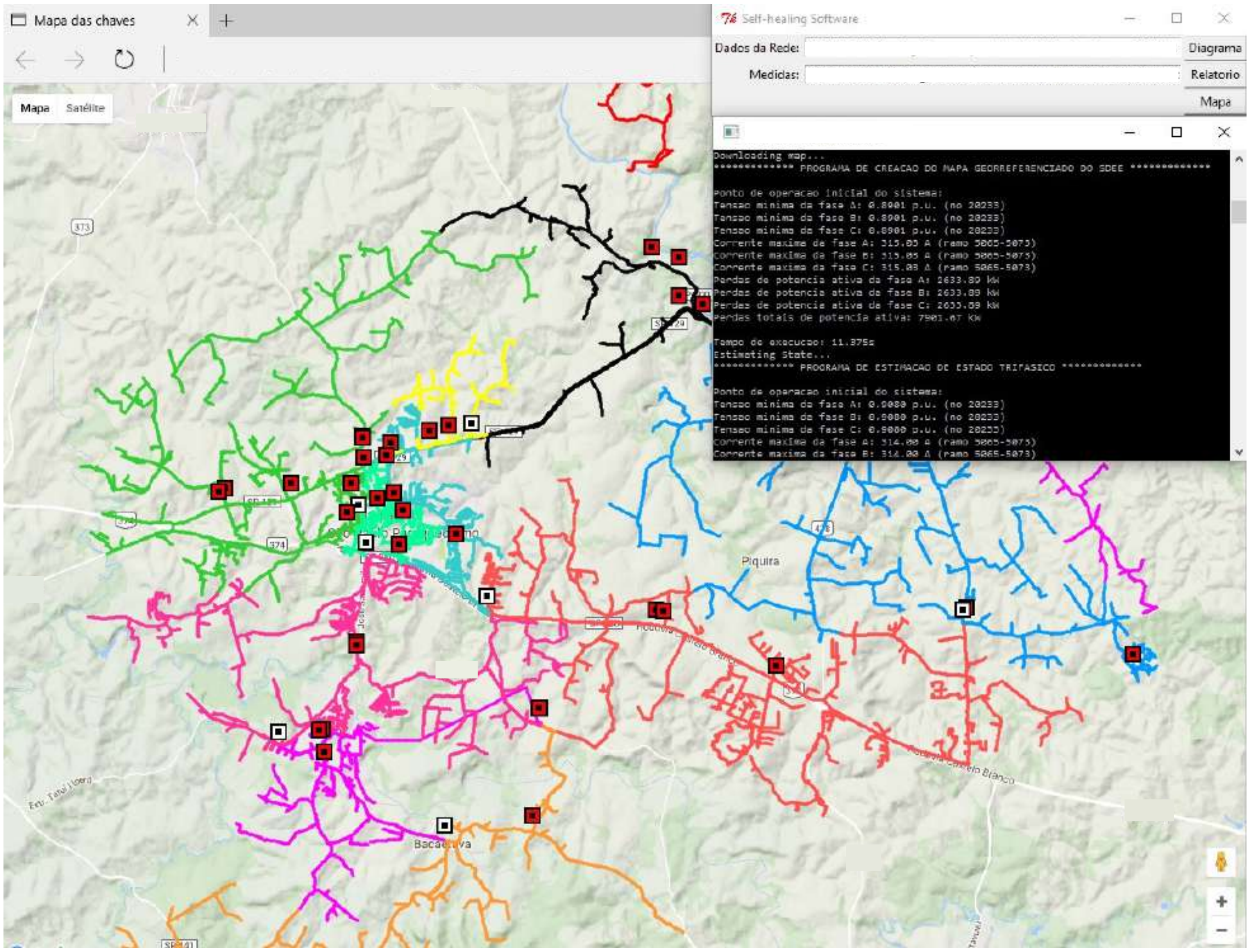

Figure 33 – GUI of the proposed SHS software.

Source: author.

5.3 Tests and Results

In order to demonstrate the performance of the proposed SHS software, the real-size 13.2 kV EDS in Fig. 34 was used for tests. The system comprises five radial feeders that supply electricity to 38,000 users of different types. The real-size EDS has 5,181 nodes, from which 955 are primary distribution transformers. The EDS has more than 115 km of distribution lines installed. Blue and magenta feeders in Fig. 34 are connected to a main substation of 40 MVA (nominal capacity), whereas red, yellow, and green feeders are connected to a different substation of 60 MVA. Moreover, the EDS has three 5 MVA dispatchable distributed generation (DG) units with islanded operation capabilities. The total installed capacity of the distribution transformers is approximately 81 MVA. Also, there are 32 remotely-controlled normally closed (NC) switches and 14 remotely-controlled normally open (NO) switches that participate in the SHS.

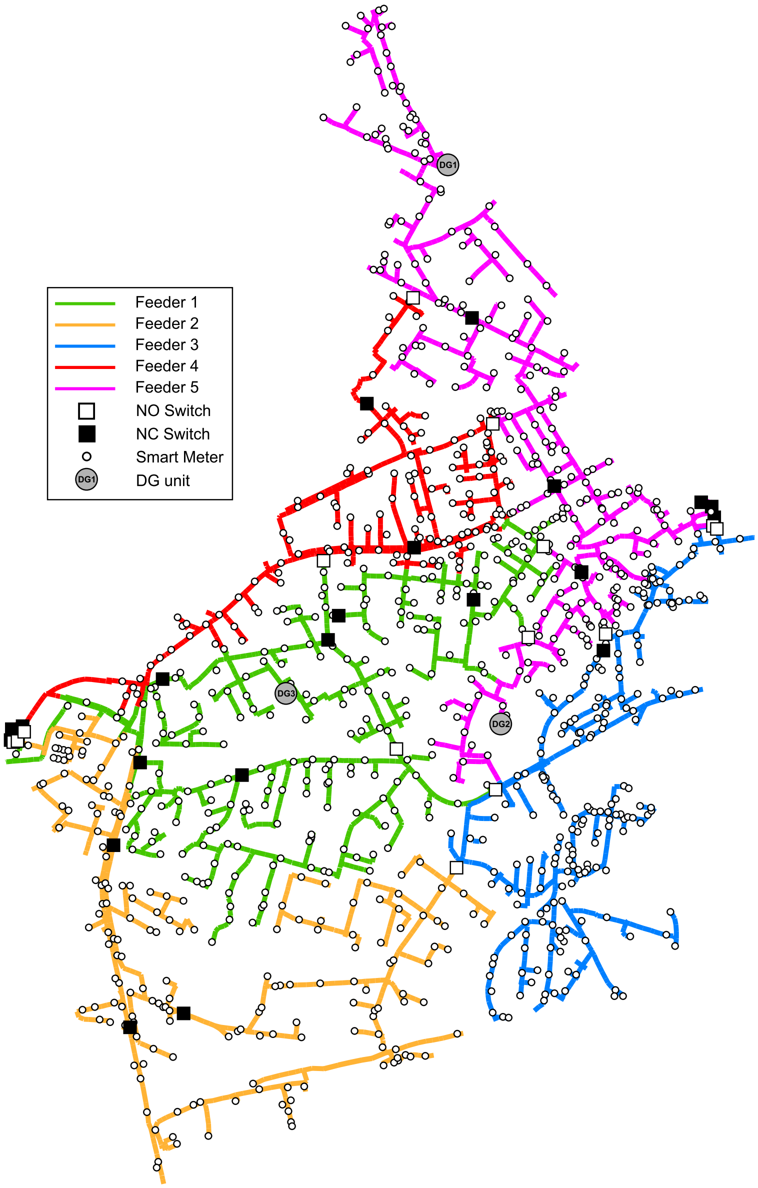

Figure 34 – Real 13.2 kV EDS with an AMI.

Source: author.

Two cases will be tested over the EDS in Fig. 34:

Case 1 Only 46 smart meters are considered to participate in the SHS. All meters are located in the same branches as the remote-controlled switches. This case will be known as the "*Basic SHS*" and its intention is to show the performance of the proposed SHS when deployed in poorly supervised systems.

Case 2 In this case, 955 smart meters are considered to participate in the SHS. All meters are located in the primary distribution transformers. This case will be known as the

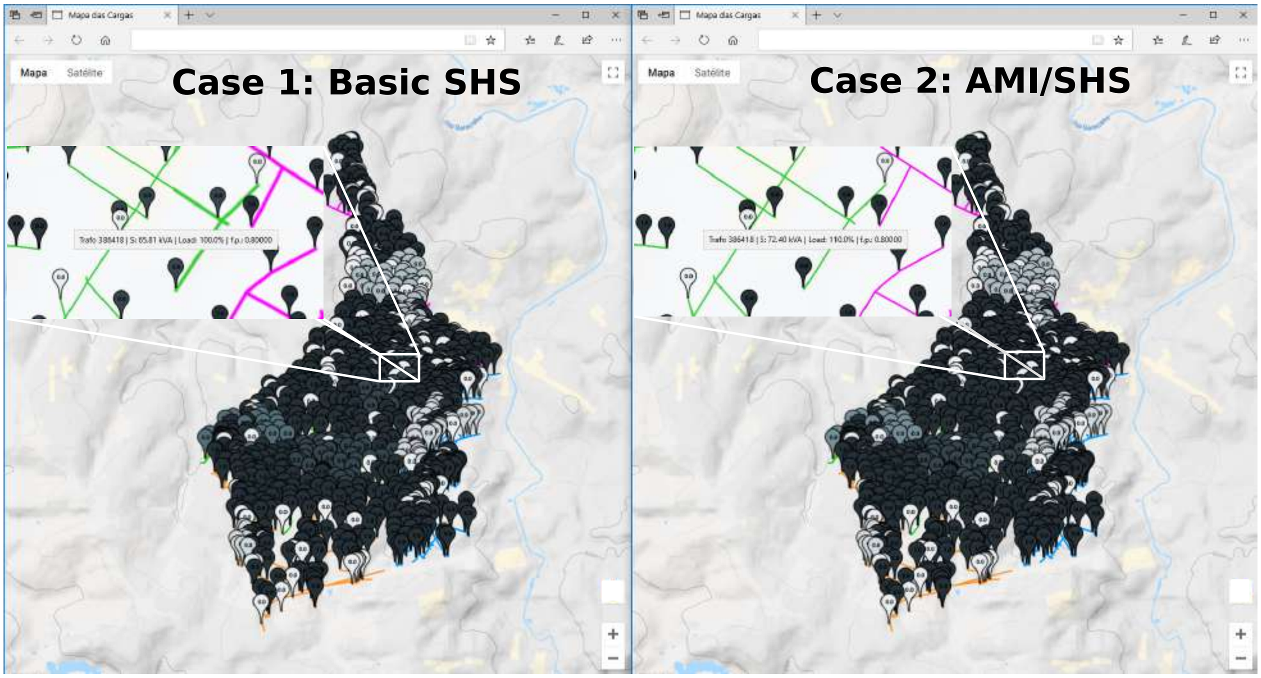

Figure 35 – Estimated loads obtained in Case 1 and 2.

Source: author.

"*AMI/SHS*" and its intention is to show the performance of the proposed SHS when deployed in highly supervised systems, i.e., with AMI.

5.3.1 Case 1: Basic SHS

As shown by the flowchart in Fig. 31, the first step of the proposed SHS is the three-phase state estimator. Considering a snapshot of the pre-fault steady-state operation, the three-phase state estimator in (5.1)–(5.12) has been solved via Tabu Search, with a stopping criterion of 30 seconds and a Tabu search attribute of 5 iterations (GROVER; LAGUNA, 1997). Each feeder is solved separately in parallel to improve the computational performance of the heuristic. The root-mean-square error (RMSE) is used to assess the quality of the three-phase state estimator for one snapshot. In this case, the RMSE of the current magnitudes was 4.2 A, and RMSE of the voltage magnitudes was 15 V. Fig. 35 compares the estimated loads obtained in Case 1 and 2. Each marker in Fig. 35 represents a distribution transformer. The lightness of each marker represents the loading factor of the transformer, where white makers have 0% loading and black markers have 120% loading. The number within each marker represents the average power factor at each transformer, obtained through the three-phase state estimator.

Once a permanent fault has been identified by the protection system, the next step of the SHS is to identify the moment of maximum consumption during the restoration time. To do so, the short-term load forecasting method discussed in section 5.2.2 is deployed. In this case, a frequentist approach has been chosen to dynamically calculate parameters θ and Θ of the ARIMA model in (5.13). However, a Bayesian approach can also be adopted as discussed in Lopez *et al.* (2019). In this case, we considered that the average restoration time is two hours after the fault has been identified.

Given the pre-fault estimation and the post-fault forecasted demands, the next step of the SHS is to identify the location of the fault and to execute the service restoration process. Thus, for each fault, the fault-location method in section 5.2.3 has been executed, considering the voltage magnitude measurements by the 46 smart meters. Then, the optimized restoration of unbalanced EDS in (5.17)–(5.29) has been solved via Tabu Search, with the same parameters as in the state estimator, i.e., a stopping criterion of 30 seconds and an attribute of 5 iterations (GROVER; LAGUNA, 1997). Three different faults have been simulated at feeder 1 (green), feeder 3 (blue) and feeder 5 (magenta) in Fig. 34. For each fault, Fig. 36 shows the real and the calculated location obtained with the fault-location method, and the final step of the restoration process.

5.3.1.1 Fault at feeder 5

As depicted by the lighting bolt in Fig. 36a, the first fault was simulated at the extreme end of feeder 5. Note that the service restoration isolated the fault by simply opening the upstream switch. The reason for this is that the isolated area contains the faulty node, and no other load can be transferred among feeders. The magnifying glass represents the location of the fault obtained by the fault-location method. Note that, with only 46 meters, the fault-location method is very unreliable. However, the faulty zone was properly identified and isolated by the SHS.

5.3.1.2 Fault at feeder 3

As shown in Fig. 36b, the fault was simulated at the origin of feeder 3. Thus, the service restoration isolated the fault by opening the feeder's main breaker at the substation, and by opening the closest downstream switch. Then, most of the unsupplied demand at feeder 3 was restored by transferring it to feeder 2 (orange) by closing the tie switch. The switching sequence was as follows: 1) open feeder 5's main breaker; 2) open downstream NC switch in feeder 5; 3) close tie switch between feeders 2 and 5.

5.3.1.3 Fault at feeder 1

Finally, a permanent fault was simulated at a middle point of feeder 1, as shown in Fig. 36c. In this case, a more complex switching sequence was generated with the aim of restoring a portion of costumers in feeder 1, by transferring them to feeder 4 (red). The restored portion is highlighted in Fig. 36c. Note that besides the faulty area, another area was de-energized by the service restoration. The reason to this is because the SHS must guarantee the operational constraints of the service restoration problem, i.e., three-phase voltage and current magnitude within their limits.

5.3.2 Case 2: AMI/SHS

Considering a snapshot of the pre-fault steady-state operation, the three-phase state estimator in (5.1)–(5.12) has been solved via Tabu Search, with the same parameters as in the previous case. The RMSE of the current magnitudes was 3.3 A, and RMSE of the voltage magnitudes was 12 V. Note that both RMSE are better than those obtained in the basic SHS. This is expected because more measurements are available (955 smart meters). Hence, they contribute with the accuracy of the state estimator. Fig. 35 compares the estimated loads obtained in Case 1 and 2. The frequentist approach has been used to dynamically estimate the moment of maximum consumption through the ARIMA model in (5.13), for a horizon of two hours after the fault.

Once again, the fault-location method in section 5.2.3 has been used, considering the voltage magnitude measurements of the AMI. The optimized restoration of unbalanced EDS in (5.17)–(5.29) has been solved via Tabu Search. The same three permanent faults have been simulated at feeder 1 (green), feeder 3 (blue) and feeder 5 (magenta). Fig. 37 shows the results of the fault-location method, and the final step of the restoration process.

Note that all three restoration actions in Fig. 37 are identical to those in Fig. 36, except for the fault at feeder 1. In Fig. 37c, the SHS transferred all unsupplied demand from feeder 1 to feeder 5 (magenta). The difference between both solutions in Fig. 37c and Fig. 36c is due to the estimated loads. As shown by the results in Fig. 35, the estimated loads obtained with and without AMI are different. As expected, the estimated and forecasted demands in Case 2: AMI/SHS are more accurate than those obtained in Case 1: Basic SHS. Thus, the SHS with AMI will be more precise and reliable.

5.3.3 DG Units Operation

The contribution of DG units in the proposed SHS software is considered as follows: given the MILP model in (5.17)–(5.29), DGs are only operated if the zones wherein the DGs are located are energized at the end of the restoration process. Nonetheless, by disregarding the topological constraint in (5.28), the service restoration can be improved if grid-forming DG units are used to create isolated energized areas. Fig. 38 shows the solution of the proposed AMI/SHS software if a fault at the beginning of feeder 5 is simulated, considering DG units operation. Note that an isolated area, called “DG Zone”, was created to reduce the impact of the outage and to alleviate the load transferring among feeders during the restoration process. The location of the fault and the switching sequence are also presented by the GIS-based GUI in Fig. 38.

5.4 Conclusion

This chapter presents the design and implementation of a GIS-based SHS software for modern EDS. In the presence of a permanent fault, the proposed SHS software is able to dynamically estimate the demands after the fault, using a state-of-the-art three-phase state estimator and a parsimonious short-term load forecasting method. Then, the location of the fault is identified, based the operation of the protection coordination system and an enhanced bus-impedance-matrix-based fault-location method. Finally, a holistic service restoration for unbalanced three-phase EDS is deployed in less than one minute, to obtain the switching sequence that minimizes the impact of the outage and that isolates the faulty zone. Results have been conducted over a real EDS and displayed using a GIS-based GUI. The proposed SHS software is shown to be more efficient and reliable under the paradigm of AMI networks with grid-forming DG units. However, it can also be implemented in EDS with basic SCADA systems.

a) Fault at feeder 5

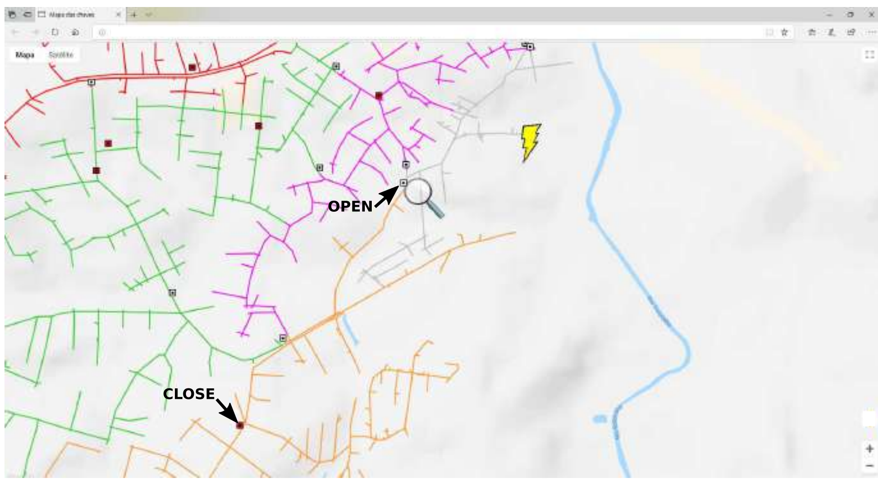

b) Fault at feeder 3

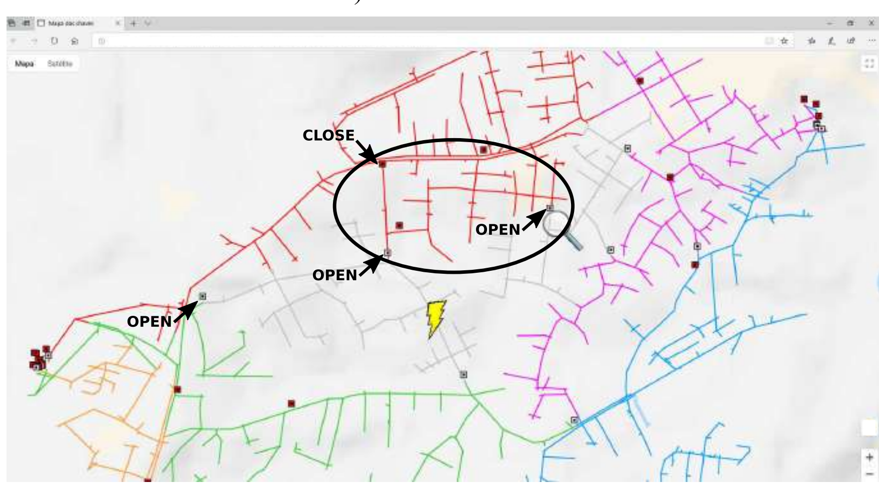

c) Fault at feeder 1

Figure 36 – Results of the Basic SHS (Case 1): a) Fault location and restoration due to a fault at feeder 5. b) Fault location and restoration due to a fault at feeder 3. c) Fault location and restoration due to a fault at feeder 1.

Source: author.

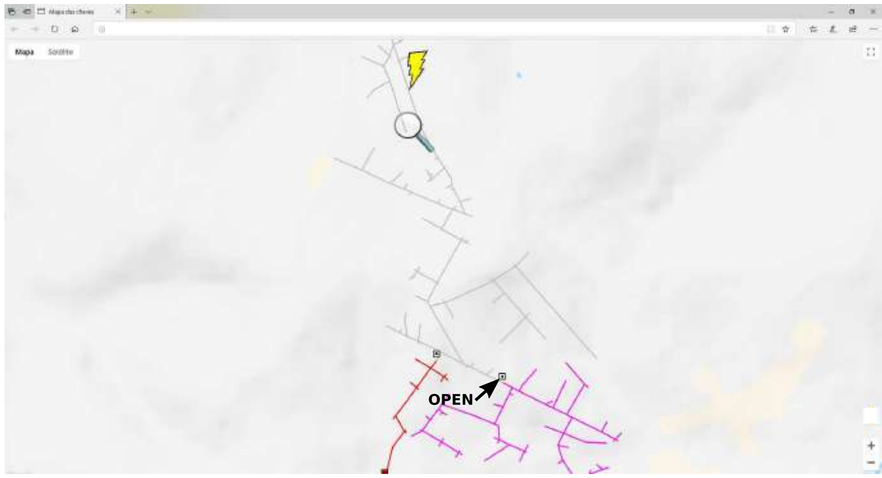

a) Fault at feeder 5

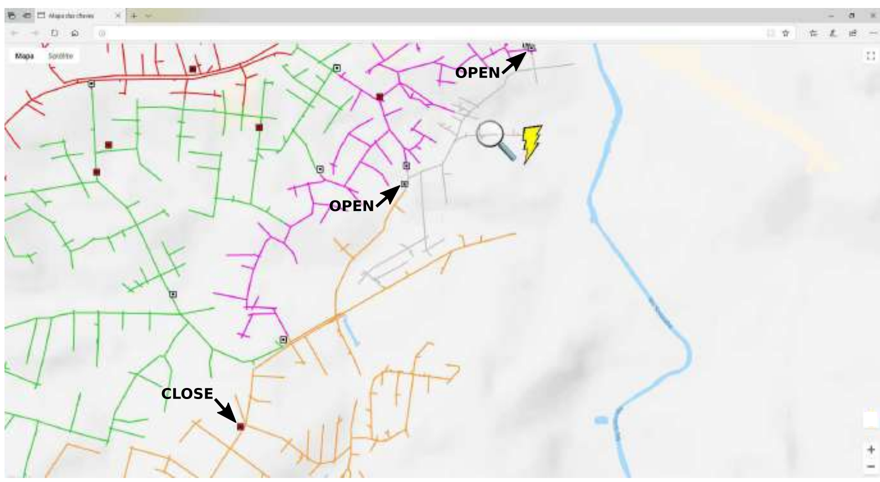

b) Fault at feeder 3

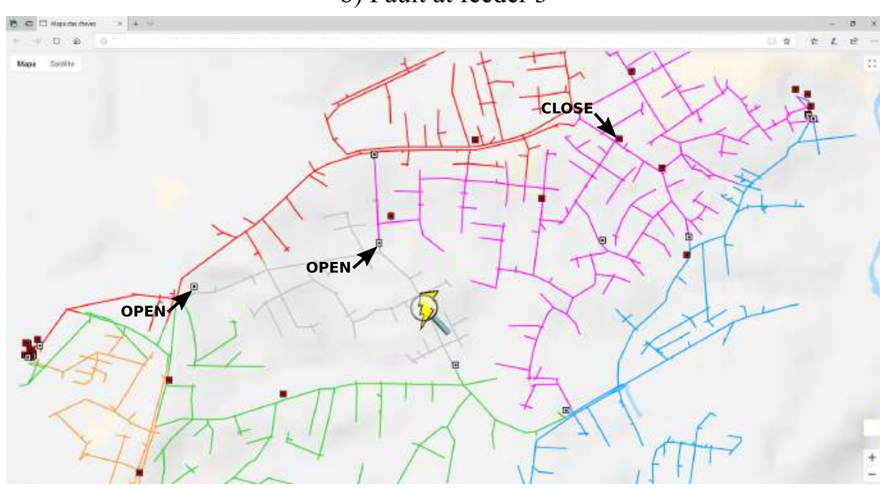

c) Fault at feeder 1

Figure 37 – Results of the AMI/SHS (Case 2): a) Fault location and restoration due to a fault at feeder 5. b) Fault location and restoration due to a fault at feeder 3. c) Fault location and restoration due to a fault at feeder 1.

Source: author.

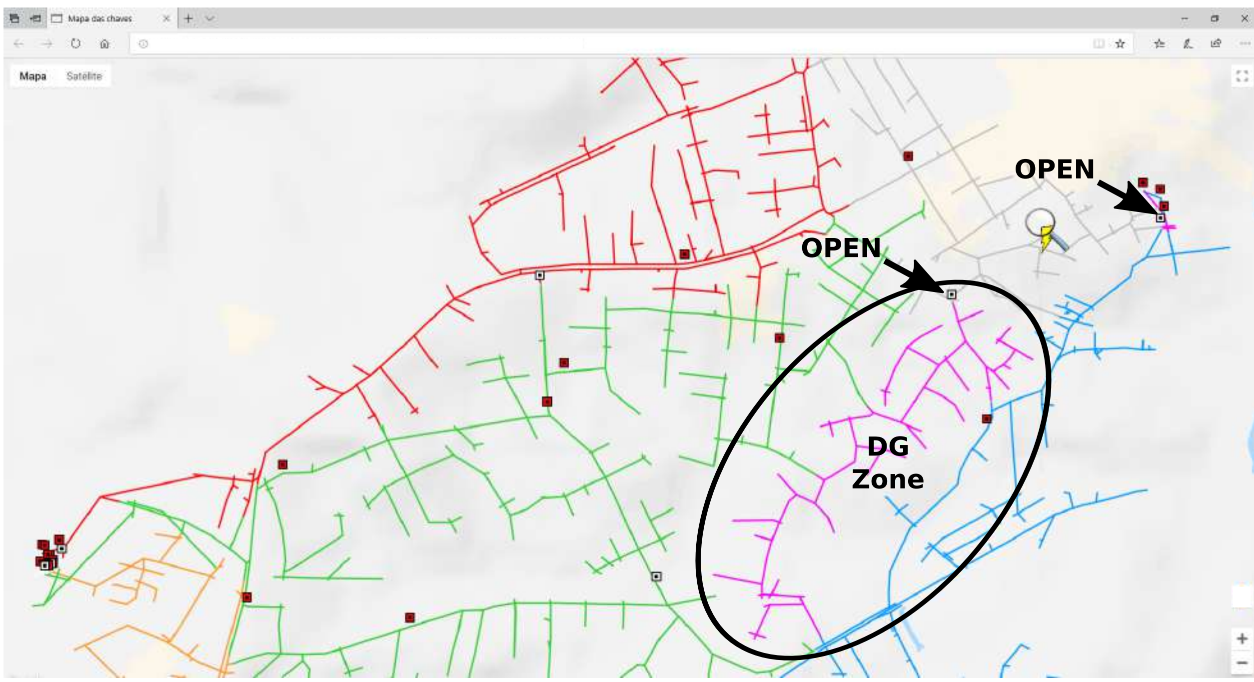

Figure 38 – Results of the AMI/SHS considering DG operation.

Source: author.

6 Conclusions and Future Works

6.1 Conclusions

In this thesis, a truly automated self-healing scheme for unbalanced three-phase EDS, considering DG units and switching sequence, has been designed and implemented through a GIS-based GUI software developed in Python. The proposed self-healing system is able to: a) estimate the nodal demands during the pre and post-fault status, using a three-phase state estimator and a short-term load forecasting algorithm, b) efficiently identify the zone where a permanent fault is located, and c) generate the sequence of operations that must be preformed by the remote-controlled switches installed along the system. Ultimately, the self-healing scheme will isolate the faulty zone of the network and restore the service of as many customers as possible, in the least amount of time and with minimal human intervention. Mathematical optimization models were used to represent the state estimator and the three-phase restoration aspect of the self-healing scheme. An enhanced fault-location method based on smart meters was also implemented. The methodology used to solve the optimization models was the metaheuristic *Tabu Search*. The short-term load forecasting method is a parsimonious seasonal ARIMA model. The proposed self-healing scheme was tested using real EDS, with thousands of consumers and distributed energy resources.

As shown by the results Chapter 5, the proposed self-healing system can be deployed in networks with different levels of automation. Either low level, i.e., minimum deployment of smart meters and remote-controlled switching devices, or high level, i.e., AMI-based networks. In both cases, the software is able to produce quality restorative actions for real EDS, within limited computational resources and minimum time (less than 1 minute).

Several contributions to the state-of-the-art in self-healing systems have been achieved during the implementation of this PhD project: the approach in Chapter 2 is a holistic service restoration model that considers the unbalanced nature of three-phase EDS, in the presence of DG units and coordinated remote-controlled switches. The fault-location method in Chapter 3 uses a simple strategy to enhance the well-behaved bus-impedance-matrix-based fault-location method proposed by Trindade *et al.* (2014). A parsimonious short-term load forecasting method has been implemented in Chapter 4 to determine the maximum demand that needs to be considered by the service restoration. Finally, a true self-healing scheme has been designed, implemented, and tested in Chapter 5 using real EDS.

As expected, technical challenges and concerns arose during the designing and implementation of the proposed self-healing system. The solution method for the service restoration and the three-phase state estimation is a key component that needs to be properly selected and adjusted in order to obtain quality solutions in reasonable time. *Tabu search* is a well-known, easy to adapt and implement metaheuristic, but other methods might be suitable as well. Another concern is the reliability of the fault-location method. Clearly, the proposed fault-location method is proved to be efficient, but it does not mean that it will be infallible. Finally, the cyber-security aspect of the proposed self-healing system has not been addressed in this project, but it is a critical issue that must to be regarded in real-world applications.

6.2 Future Works

1. A comparison of different methods used to solve the optimization models developed in this project (i.e., the service restoration process and the three-phase state estimator) and their efficiency in terms of computational complexity and solution quality.

2. Considering other flexibility assets during the service restoration, such as capacitor banks, voltage regulators, controllable loads, storage units, mobile DG units, electric vehicles, microgrids, among others.

3. Besides the short-term load forecasting method, an additional short-term renewable generation forecasting engine can be developed, in order to integrate distributed renewable resources into the net demand that must be considered by the service restoration.

4. Instead of a centralized approach, the self-healing system could also be deployed in a distributed fashion, by considering the most recent advances in distributed optimization and point-to-point telecommunication technologies.

5. Finally, the proposed self-healing scheme can be integrated into a larger resiliency plan that optimizes the available energy resources during a critical event that compromises the EDS infrastructure, such as a natural disaster.

References

AGUERO, J. R. Applying self-healing schemes to modern power distribution systems. In: *2012 IEEE Power and Energy Society General Meeting*. San Diego, CA, USA: IEEE, 2012.

AOKI, K.; NARA, K.; ITOH, M.; SATOH, T.; KUWABARA, H. A new algorithm for service restoration in distribution systems. *IEEE Transactions on Power Delivery*, v. 4, n. 3, p. 1832–1839, July 1989.

AREFIFAR, S. A.; MOHAMED, Y. A. I.; EL-FOULY, T. H. M. Comprehensive operational planning framework for self-healing control actions in smart distribution grids. *IEEE Transactions on Power Systems*, v. 28, n. 4, p. 4192–4200, Nov. 2013.

AUGUGLIARO, A.; DUSONCHET, L.; SANSEVERINO, E. R. Service restoration in compensated distribution networks using a hybrid genetic algorithm. *Electric Power Systems Research*, v. 46, n. 1, p. 59–66, July 1998.

BAHMANYAR, A.; JAMALI, S. Fault location in active distribution networks using non-synchronized measurements. *International Journal of Electrical Power & Energy Systems*, v. 93, p. 451 – 458, May 2017.

BAHMANYAR, A.; JAMALI, S.; ESTEBSARI, A.; BOMPARD, E. A comparison framework for distribution system outage and fault location methods. *Electric Power Systems Research*, v. 145, p. 19 – 34, April 2017.

BARAN, M. E.; KELLEY, A. W. A branch-current-based state estimation method for distribution systems. *IEEE Transactions on Power Systems*, v. 10, n. 1, p. 483–491, Feb. 1995.

BISCARO, A. A. P.; PEREIRA, R. A. F.; KEZUNOVIC, M.; MANTOVANI, J. R. S. Integrated fault location and power-quality analysis in electric power distribution systems. *IEEE Transactions on Power Delivery*, v. 31, n. 2, p. 428–436, April 2016.

BOTEA, A.; RINTANEN, J.; BANERJEE, D. Optimal reconfiguration for supply restoration with informed A* search. *IEEE Transactions on Smart Grid*, v. 3, n. 2, p. 583–593, June 2012.

BOX, G. E. P.; JENKINS, G. M.; REINSEL, G. C. *Time Series Analysis*. 4th. ed. New York: Wiley, 2008.

BUTLER, K. L.; SARMA, N. D. R.; PRASAD, V. R. Network reconfiguration for service restoration in shipboard power distribution systems. *IEEE Power Engineering Review*, v. 21, n. 11, p. 55–55, Nov. 2001.

CARVALHO, P.; FERREIRA, L.; BARRUNCHO, L. Optimization approach to dynamic restoration of distribution systems. *International Journal of Electrical Power & Energy Systems*, v. 29, n. 3, p. 222–229, March 2007.

CAVALCANTE, P. A. H.; ALMEIDA, M. C. de. Fault location approach for distribution systems based on modern monitoring infrastructure. *IET Generation, Transmission Distribution*, v. 12, n. 1, p. 94–103, June 2018.

CAVALCANTE, P. L. *et al.* Centralized self-healing scheme for electrical distribution systems. *IEEE Transactions on Smart Grid*, v. 7, n. 1, p. 145–155, Jan. 2016.

CHEN, B.; CHEN, C.; WANG, J.; BUTLER-PURRY, K. L. Sequential service restoration for unbalanced distribution systems and microgrids. *IEEE Transactions on Power Systems*, v. 33, n. 2, p. 1507–1520, March 2018.

CHEN, B.-J.; CHANG, M.-W.; LIN, C.-J. Load forecasting using support vector machines: a study on EUNITE competition 2001. *IEEE Transactions on Power Systems*, v. 19, n. 4, p. 1821–1830, Nov. 2004.

CHEN, C.-S.; LIN, C.-H.; TSAI, H.-Y. A rule-based expert system with colored Petri net models for distribution system service restoration. *IEEE Transactions on Power Systems*, v. 17, n. 4, p. 1073–1080, Nov. 2002.

CHEN, D.; CHEN, X.; LIU, J.; DONG, X.; LIAO, Y. Service restoration study of distribution system with distributed generators based on particle swarm optimization. In: *2011 International Conference on Advanced Power System Automation and Protection*. Beijing, China: IEEE, 2011. v. 2, p. 1176–1181.

CHEN, K.; WU, W.; ZHANG, B.; SUN, H. Robust restoration decision-making model for distribution networks based on information gap decision theory. *IEEE Transactions on Smart Grid*, v. 6, n. 2, p. 587–597, March 2015.

CHEN, P.; MALBASA, V.; KEZUNOVIC, M. Sensitivity analysis of voltage sag based fault location algorithm. In: *2014 Power Systems Computation Conference*. Wroclaw, Poland: IEEE, 2014.

CHEN, W. Quantitative decision-making model for distribution system restoration. *IEEE Transactions on Power Systems*, v. 25, n. 1, p. 313–321, Feb. 2010.

CHEN, X.; WU, W.; ZHANG, B. Robust restoration method for active distribution networks. *IEEE Transactions on Power Systems*, v. 31, n. 5, p. 4005–4015, Sept. 2016.

CHENG, C. S.; SHIRMOHAMMADI, D. A three-phase power flow method for real-time distribution system analysis. *IEEE Transactions on Power Systems*, v. 10, n. 2, p. 671–679, May 1995.

CHOWDHURY, A.; KOVAL, D. *Power Distribution System Reliability: Practical Methods and Applications*. New Jersey, USA: Wiley, 2011. (IEEE Press Series on Power Engineering).

CIRED WORKING GROUP WG03. *Fault Management in Electrical Distribution Systems*. Montefiore, Belgium, 1999. Available at: <http://www.cired.net/>.

CIRIC, R.; POPOVIC, D. Multi-objective distribution network restoration using heuristic approach and mix integer programming method. *International Journal of Electrical Power & Energy Systems*, v. 22, n. 7, p. 497–505, Oct. 2000.

DIMITRIJEVIC, S.; RAJAKOVIC, N. Service restoration of distribution networks considering switching operation costs and actual status of the switching equipment. *IEEE Transactions on Smart Grid*, v. 6, n. 3, p. 1227–1232, May 2015.

DRAYER, E. *et al.* Distributed self-healing for distribution grids with evolving search space. *IEEE Transactions on Power Delivery*, v. 33, n. 4, p. 1755–1764, Aug. 2018.

ELMITWALLY, A.; ELSAID, M.; ELGAMAL, M.; CHEN, Z. A fuzzy-multiagent service restoration scheme for distribution system with distributed generation. *IEEE Transactions on Sustainable Energy*, v. 6, n. 3, p. 810–821, July 2015.

ERIKSSON, M.; ARMENDARIZ, M.; VASILENKO, O. O.; SALEEM, A.; NORDSTROM, L. Multiagent-based distribution automation solution for self-healing grids. *IEEE Transactions on Industrial Electronics*, v. 62, n. 4, p. 2620–2628, April 2015.

FAN, S.; HYNDMAN, R. J. Short-term load forecasting based on a semi-parametric additive model. *IEEE Transactions on Power Systemsems*, v. 27, n. 1, p. 134–141, Feb. 2012.

FORTUNY-AMAT, J.; MCCARL, B. A representation and economic interpretation of a two-level programming problem. *Journal of the Operational Research Society*, v. 32, n. 9, p. 783–792, Sep. 1981.

FOURER, R.; GAY, D.; KERNIGHAN, B. *AMPL: A Modeling Language for Mathematical Programming*. Boston, USA: Thomson/Brooks/Cole, 2003. (Scientific Press series).

FRANCO, J. F.; RIDER, M. J.; LAVORATO, M.; ROMERO, R. A mixed-integer lp model for the reconfiguration of radial electric distribution systems considering distributed generation. *Electric Power Systems Research*, v. 97, p. 51 – 60, 2013.

FRANCO, J. F.; RIDER, M. J.; ROMERO, R. A mixed-integer linear programming model for the electric vehicle charging coordination problem in unbalanced electrical distribution systems. *IEEE Transactions on Smart Grid*, v. 6, n. 5, p. 2200–2210, Sep. 2015.

GAN, L.; LOW, S. H. Convex relaxations and linear approximation for optimal power flow in multiphase radial networks. In: *2014 Power Systems Computation Conference*. Wroclaw, Poland: IEEE, 2014.

GARCES, A. A linear three-phase load flow for power distribution systems. *IEEE Transactions on Power Systems*, v. 31, n. 1, p. 827–828, Jan. 2016.

GOLSHANI, A.; SUN, W.; ZHOU, Q.; ZHENG, Q. P.; TONG, J. Two-stage adaptive restoration decision support system for a self-healing power grid. *IEEE Transactions on Industrial Informatics*, v. 13, n. 6, p. 2802–2812, Dec. 2017.

GOOGLE INC. *Google Maps JavaScript API V3 Reference*. [S.l.], 2019. Available at: <https://developers.google.com/maps/documentation/javascript/reference/>.

GOUDE, Y.; NEDELLEC, R.; KONG, N. Local short and middle term electricity load forecasting with semi-parametric additive models. *IEEE Transactions on Smart Grid*, v. 5, n. 1, p. 440–446, Jan. 2014.

GROVER, F.; LAGUNA, M. *Tabu Search*. 1. ed. Boston, MA, USA: Springer, 1997.

GUO, J.; WANG, L. Self-healing resilience strategy to active distribution network based on benders decomposition approach. In: *IEEE PES Asia-Pacific Power and Energy Engineering Conference (APPEEC)*. Xi'an, China: IEEE, 2016. p. 1491–1495.

HAFEZ, A. A.; OMRAN, W. A.; HEGAZY, Y. G. A decentralized technique for autonomous service restoration in active radial distribution networks. *IEEE Transactions on Smart Grid*, v. 9, n. 3, p. 1911–1919, May 2018.

HAGAN, M. T.; BEHR, S. M. The time series approach to short term load forecasting. *IEEE Transactions on Power Systems*, v. 2, n. 3, p. 785–791, Aug. 1987.

HERNANDEZ, L. *et al.* A survey on electric power demand forecasting: Future trends in smart grids, microgrids and smart buildings. *IEEE Commun. Surveys Tutorials*, v. 16, n. 3, p. 1460–1495, Mar. 2014.

HIJAZI, H. L.; THIEBAUX, S. Optimal AC distribution systems reconfiguration. In: *2014 Power Systems Computation Conference*. Wroclaw, Poland: IEEE, 2014.

HIPPERT, H. S.; PEDREIRA, C. E.; SOUZA, R. C. Neural networks for short-term load forecasting: a review and evaluation. *IEEE Transactions on Power Systems*, v. 16, n. 1, p. 44–55, Feb. 2001.

HONG, T. Energy forecasting: Past, present, and future. *Foresight: The International Journal of Applied Forecasting*, n. 32, p. 43–48, 2014.

HONG, T.; FAN, S. Probabilistic electric load forecasting: A tutorial review. *International Journal of Forecasting*, v. 32, n. 3, p. 914–938, Sept. 2016.

HONG, T.; PINSON, P.; FAN, S. Global energy forecasting competition 2012. *International Journal of Forecasting*, v. 30, n. 2, p. 357–363, April–June 2014.

HONG, T.; WANG, P. Fuzzy interaction regression for short term load forecasting. *Fuzzy Optimization and Decision Making*, v. 13, n. 1, p. 91–103, Mar. 2014.

HOSSAN, S.; CHOWDHURY, B. Data-driven fault location scheme for advanced distribution management systems. *IEEE Transactions on Smart Grid*, 2019. To be published.

HSIAO, Y.-T.; CHIEN, C.-Y. Enhancement of restoration service in distribution systems using a combination fuzzy-GA method. *IEEE Transactions on Power Systems*, v. 15, n. 4, p. 1394–1400, Nov. 2000.

HSU, Y. *et al.* Distribution system service restoration using a heuristic search approach. *IEEE Transactions on Power Delivery*, v. 7, n. 2, p. 734–740, April 1992.

HSU, Y.-Y.; KUO, H.-C. A heuristic based fuzzy reasoning approach for distribution system service restoration. *IEEE Transactions on Power Delivery*, v. 9, n. 2, p. 948–953, April 1994.

HUANG, C.-M. Multiobjective service restoration of distribution systems using fuzzy cause-effect networks. *IEEE Transactions on Power Systems*, v. 18, n. 2, p. 867–874, May 2003.

IBM CORP. *User's Manual for CPLEX*. New York, USA, 2009.

IEEE POWER AND ENERGY SOCIETY. *Distribution Test Feeders: 123-bus Feeder*. [S.l.], 2013. Available at: <http://ewh.ieee.org/soc/pes/dsacom/testfeeders/>.

JAMALI, S.; BAHMANYAR, A. A new fault location method for distribution networks using sparse measurements. *International Journal of Electrical Power & Energy Systems*, v. 81, p. 459 – 468, Oct. 2016.

JAMALI, S.; BAHMANYAR, A.; BORHANI-BAHABADI, H. A fast and accurate fault location method for distribution networks with DG using genetic algorithms. In: *2015 Smart Grid Conference (SGC)*. Tehran, Iran: IEEE, 2015. p. 110–114.

JARVENTAUSTA, P.; VERHO, P.; PARTANEN, J. Using fuzzy sets to model the uncertainty in the fault location process of distribution networks. *IEEE Transactions on Power Delivery*, v. 9, n. 2, p. 954–960, April 1994.

JEFFREYS, H. *Theory of Probability*. 3rd. ed. Clarendon: Oxford, 1961.

JIANG, Y.; LIU, C.; DIEDESCH, M.; LEE, E.; SRIVASTAVA, A. K. Outage management of distribution systems incorporating information from smart meters. *IEEE Transactions on Power Systems*, v. 31, n. 5, p. 4144–4154, Sep. 2016.

KEZUNOVIC, M. Smart fault location for smart grids. *IEEE Transactions on Smart Grid*, v. 2, n. 1, p. 11–22, March 2011.

KHOTANZAD, A.; AFKHAMI-ROHANI, R.; MARATUKULAM, D. ANNSTLF - Artificial neural network short-term load forecaster generation three. *IEEE Transactions on Power Systems*, v. 13, n. 4, p. 1413–1422, Nov. 1998.

KHUSHALANI, S.; SOLANKI, J. M.; SCHULZ, N. N. Optimized restoration of unbalanced distribution systems. *IEEE Transactions on Power Systems*, v. 22, n. 2, p. 624–630, May 2007.

KLEINBERG, M. R.; MIU, K.; CHIANG, H. Improving service restoration of power distribution systems through load curtailment of in-service customers. *IEEE Transactions on Power Systems*, v. 26, n. 3, p. 1110–1117, Aug. 2011.

KUMAR, Y.; DAS, B.; SHARMA, J. Multiobjective, multiconstraint service restoration of electric power distribution system with priority customers. *IEEE Transactions on Power Delivery*, v. 23, n. 1, p. 261–270, Jan. 2008.

KUO, H.-C.; HSU, Y.-Y. Distribution system load estimation and service restoration using a fuzzy set approach. *IEEE Transactions on Power Delivery*, v. 8, n. 4, p. 1950–1957, Oct. 1993.

LATARE, N. A.; BHAT, S. S.; SRIVASTAVA, I. Literature review of service restoration in distribution system. In: *2017 Second International Conference on Electrical, Computer and Communication Technologies (ICECCT)*. Coimbatore, India: IEEE, 2017.

LAVORATO, M.; FRANCO, J. F.; RIDER, M. J.; ROMERO, R. Imposing radiality constraints in distribution system optimization problems. *IEEE Transactions on Power Systems*, v. 27, n. 1, p. 172–180, Feb. 2012.

LEE, S. J.; KIM, K. H.; KIM, H. Y.; LEE, J. K.; NAM, K. Y. Expert system-aided service restoration in distribution automation. In: *1992 IEEE International Conference on Systems, Man, and Cybernetics*. Chicago, IL, USA: IEEE, 1992. v. 1, p. 157–161.

LEE, S.-J.; LIM, S.-I.; AHN, B.-S. Service restoration of primary distribution systems based on fuzzy evaluation of multi-criteria. *IEEE Transactions on Power Systems*, v. 13, n. 3, p. 1156–1163, Aug. 1998.

LEITE, J. B.; MANTOVANI, J. R. S. Development of a self-healing strategy with multiagent systems for distribution networks. *IEEE Transactions on Smart Grid*, v. 8, n. 5, p. 2198–2206, Sep. 2017.

LEUVEN EMTP CENTER. *Alternative Transients Program (ATP): Rule Book*. [S.l.], 1992. Available at: <https://books.google.com.br/books?id=VmzynAEACAAJ>.

LI, J.; MA, X.; LIU, C.; SCHNEIDER, K. P. Distribution system restoration with microgrids using spanning tree search. *IEEE Transactions on Power Systems*, v. 29, n. 6, p. 3021–3029, Nov. 2014.

LIU, C. .; LEE, S. J.; VENKATA, S. S. An expert system operational aid for restoration and loss reduction of distribution systems. *IEEE Transactions on Power Systems*, v. 3, n. 2, p. 619–626, May 1988.

LIU, S.; HOU, Y.; LIU, C.; PODMORE, R. The healing touch: Tools and challenges for smart grid restoration. *IEEE Power and Energy Magazine*, v. 12, n. 1, p. 54–63, Jan. 2014.

LJUNG, G. M.; BOX, G. E. P. On a measure of lack of fit in time series models. *Biometrika*, v. 65, n. 2, p. 297–303, Aug. 1978.

LLOYD, J. R. Gefcom2012 hierarchical load forecasting: Gradient boosting machines and gaussian processes. *International Journal of Forecasting*, v. 30, n. 2, p. 369–374, June 2014.

LOPES, H. S.; RODRIGUES, L. C. d. A.; STEINER, M. T. A. (Ed.). *Meta-heurísticas em pesquisa operacional*. Curitiba, PR: Ominipax, 2013. 472 p. Available at: <http://www.omnipax.com.br>.

LOPEZ, J. C.; FRANCO, J. F.; RIDER, M. J.; ROMERO, R. Optimal restoration/maintenance switching sequence of unbalanced three-phase distribution systems. *IEEE Transactions on Smart Grid*, v. 9, n. 6, p. 6058–6068, Nov 2018.

LOPEZ, J. C.; RIDER, M. J.; WU, Q. Parsimonious short-term load forecasting for optimal operation planning of electrical distribution systems. *IEEE Transactions on Power Systems*, v. 34, n. 2, p. 1427–1437, March 2019.

LUAN, W. P.; IRVING, M. R.; DANIEL, J. S. Genetic algorithm for supply restoration and optimal load shedding in power system distribution networks. *IEE Proceedings - Generation, Transmission and Distribution*, v. 149, n. 2, p. 145–151, March 2002.

MAJIDI, M.; ARABALI, A.; ETEZADI-AMOLI, M. Fault location in distribution networks by compressive sensing. *IEEE Transactions on Power Delivery*, v. 30, n. 4, p. 1761–1769, Aug. 2015.

MAJIDI, M.; ETEZADI-AMOLI, M. A new fault location technique in smart distribution networks using synchronized/nonsynchronized measurements. *IEEE Transactions on Power Delivery*, v. 33, n. 3, p. 1358–1368, June 2018.

MAJIDI, M.; ETEZADI-AMOLI, M.; FADALI, M. S. A novel method for single and simultaneous fault location in distribution networks. *IEEE Transactions on Power Systems*, v. 30, n. 6, p. 3368–3376, Nov. 2015.

MANJUNATH, K.; MOHAN, M. A new hybrid multi-objective quick service restoration technique for electric power distribution systems. *International Journal of Electrical Power & Energy Systems*, v. 29, n. 1, p. 51 – 64, 2007.

MARQUES, L. T.; DELBEM, A. C. B.; LONDON, J. B. A. Service restoration with prioritization of customers and switches and determination of switching sequence. *IEEE Transactions on Smart Grid*, v. 9, n. 3, p. 2359–2370, May 2018.

MIU, K. N.; CHIANG, H.-D.; MCNULTY, R. J. Multi-tier service restoration through network reconfiguration and capacitor control for large-scale radial distribution networks. In: *21st International Conference on Power Industry Computer Applications*. Santa Clara, USA: IEEE, 1999. p. 153–159.

MOHASSEL, R. R.; FUNG, A.; MOHAMMADI, F.; RAAHEMIFAR, K. A survey on advanced metering infrastructure. *International Journal of Electrical Power & Energy Systems*, v. 63, p. 473–484, Dec. 2014.

MORA-FLOREZ, J. J.; HERRERA-OROZCO, R. A.; BEDOYA-CADENA, A. F. Fault location considering load uncertainty and distributed generation in power distribution systems. *IET Generation, Transmission Distribution*, v. 9, n. 3, p. 287–295, Jun. 2015.

MORELATO, A. L.; MONTICELLI, A. J. Heuristic search approach to distribution system restoration. *IEEE Transactions on Power Delivery*, v. 4, n. 4, p. 2235–2241, Oct. 1989.

NAGATA, T.; SASAKI, H. A multi-agent approach to power system restoration. *IEEE Transactions on Power Systems*, v. 17, n. 2, p. 457–462, May 2002.

NAGATA, T.; SASAKI, H.; YOKOYAMA, R. Power system restoration by joint usage of expert system and mathematical programming approach. *IEEE Transactions on Power Systems*, v. 10, n. 3, p. 1473–1479, Aug. 1995.

NGUYEN, C. P.; FLUECK, A. J. Agent based restoration with distributed energy storage support in smart grids. *IEEE Transactions on Smart Grid*, v. 3, n. 2, p. 1029–1038, June 2012.

NORTHCOTE-GREEN, J.; WILSON, R. *Control and Automation of Electrical Power Distribution Systems*. Boca Raton, FL: CRC Press, 2017.

OROZCO-HENAO, C.; BRETAS, A.; CHOUHY-LEBORGNE, R.; HERRERA-OROZCO, A.; MARIN-QUINTERO, J. Active distribution network fault location methodology: A minimum fault reactance and fibonacci search approach. *International Journal of Electrical Power & Energy Systems*, v. 84, p. 232 – 241, 2017. ISSN 0142-0615.

PAPALEXOPOULOS, A. D.; HESTERBERG, T. C. A regression-based approach to short-term system load forecasting. *IEEE Transactions on Power Systemsems*, v. 5, n. 4, p. 1535–1547, Nov. 1990.

PEREIRA, R. A. F.; DA SILVA, L. G. W.; KEZUNOVIC, M.; MANTOVANI, J. R. S. Improved fault location on distribution feeders based on matching during-fault voltage sags. *IEEE Transactions on Power Delivery*, v. 24, n. 2, p. 852–862, April 2009.

PEREZ-GUERRERO, R.; HEYDT, G. T.; JACK, N. J.; KEEL, B. K.; CASTELHANO, A. R. Optimal restoration of distribution systems using dynamic programming. *IEEE Transactions on Power Delivery*, v. 23, n. 3, p. 1589–1596, July 2008.

PFLUGRADT, N.; MUNTWYLER, U. Synthesizing residential load profiles using behavior simulation. *Energy Procedia*, v. 122, p. 655–660, Sept. 2017.

PFLUGRADT, N.; TEUSCHER, J.; PLATZER, B.; SCHUFFT, W. Analysing low-voltage grids using a behaviour based load profile generator. In: *International Conference on Renewable Energies and Power Quality*. Bilbao, Spain: RE&PQJ, 2013. p. 1–5.

POPOVIC, D. S.; POPOVIC, Z. N. A risk management procedure for supply restoration in distribution networks. *IEEE Transactions on Power Systems*, v. 19, n. 1, p. 221–228, Feb. 2004.

PRIMADIANTO, A.; LU, C. A review on distribution system state estimation. *IEEE Transactions on Power Systems*, v. 32, n. 5, p. 3875–3883, Sep. 2017.

PYTHON SOFTWARE FOUNDATION. *Graphical User Interfaces with Tk*. [S.l.], 2019. Available at: <https://docs.python.org/3/library/tk.html>.

RECHE, E. A.; SOUSA, J. V. de; COURY, D. V.; FERNANDES, R. A. S. Data mining-based method to reduce multiple estimation for fault location in radial distribution systems. *IEEE Transactions on Smart Grid*, 2019. To be published.

ROBSON, S.; HADDAD, A.; GRIFFITHS, H. Fault location on branched networks using a multiended approach. *IEEE Transactions on Power Delivery*, v. 29, n. 4, p. 1955–1963, Aug. 2014.

ROBSON, S.; HADDAD, A.; GRIFFITHS, H. Traveling wave fault location using layer peeling. *Energies*, v. 12, n. 126, p. 1–23, Jan. 2019.

ROMERO, R.; FRANCO, J. F.; LEAO, F. B.; RIDER, M. J.; DE SOUZA, E. S. A new mathematical model for the restoration problem in balanced radial distribution systems. *IEEE Transactions on Power Systems*, v. 31, n. 2, p. 1259–1268, March 2016.

RUI, L.; CHENGLEI, L.; NAN, P.; MENGHAN, C.; FEI, W. Fault location for power grid based on transient travelling wave data fusion via asynchronous voltage measurements. *International Journal of Electrical Power & Energy Systems*, v. 93, p. 426 – 439, Dec. 2017.

SABILLON-ANTUNEZ, C.; FRANCO, J. F.; RIDER, M. J.; ROMERO, R. A new methodology for the optimal charging coordination of electric vehicles considering vehicle-to-grid technology. *IEEE Transactions on Sustainable Energy*, v. 7, n. 2, p. 596–607, April 2016.

SANCHES, D. S. *et al.* Multiobjective evolutionary algorithm with a discrete differential mutation operator developed for service restoration in distribution systems. *International Journal of Electrical Power & Energy Systems*, v. 62, p. 700 – 711, 2014.

SARMA, N. D. R.; PRASAD, V. C.; RAO, K. S. P.; SANKAR, V. A new network reconfiguration technique for service restoration in distribution networks. *IEEE Transactions on Power Delivery*, v. 9, n. 4, p. 1936–1942, Oct. 1994.

SHARMA, A.; SRINIVASAN, D.; TRIVEDI, A. A decentralized multiagent system approach for service restoration using dg islanding. *IEEE Transactions on Smart Grid*, v. 6, n. 6, p. 2784–2793, Nov. 2015.

SHEN, F. *et al.* Review of service restoration methods in distribution networks. In: *2018 IEEE PES Innovative Smart Grid Technologies Conference Europe (ISGT-Europe)*. Sarajevo, Bosnia-Herzegovina: IEEE, 2018.

SHIRAZI, E.; JADID, S. Autonomous self-healing in smart distribution grids using multi agent systems. *IEEE Transactions on Industrial Informatics*, 2018. To be published.

SHIRAZI, E.; JADID, S. A multiagent design for self-healing in electric power distribution systems. *Electric Power Systems Research*, v. 171, p. 230 – 239, June 2019.

SHIRMOHAMMADI, D. Service restoration in distribution networks via network reconfiguration. *IEEE Transactions on Power Delivery*, v. 7, n. 2, p. 952–958, April 1992.

SOLANKI, J. M.; KHUSHALANI, S.; SCHULZ, N. N. A multi-agent solution to distribution systems restoration. *IEEE Transactions on Power Systems*, v. 22, n. 3, p. 1026–1034, Aug. 2007.

SONG, K.-B.; BAEK, Y.-S.; HONG, D. H.; JANG, G. Short-term load forecasting for the holidays using fuzzy linear regression method. *IEEE Transactions on Power Systems*, v. 20, n. 1, p. 96–101, Feb. 2005.

SRIVASTAVA, S.; BUTLER-BURRY, K. L. Expert-system method for automatic reconfiguration for restoration of shipboard power systems. *IEE Proceedings - Generation, Transmission and Distribution*, v. 153, n. 3, p. 253–260, May 2006.

SRIVASTAVA, S. K.; BUTLER-PURRY, K. l. Probability-based predictive self-healing reconfiguration for shipboard power systems. *IET Generation, Transmission & Distribution*, v. 1, n. 3, p. 405–413, May 2007.

SUMMERFIELD, M. *Python 3*. Anaya Multimedia, 2009. (Anaya multimedia). Available at: <https://books.google.com.br/books?id=qzJ2QgAACAAJ>.

SUN, K.; CHEN, Q.; GAO, Z. An automatic faulted line section location method for electric power distribution systems based on multisource information. *IEEE Transactions on Power Delivery*, v. 31, n. 4, p. 1542–1551, Aug. 2016.

SUN, Q. *et al.* A comprehensive review of smart energy meters in intelligent energy networks. *IEEE Internet of Things Journal*, v. 3, n. 4, p. 464–479, Aug. 2016.

TAIEB, S. B.; HYNDMAN, R. J. A gradient boosting approach to the kaggle load forecasting competition. *International Journal of Forecasting*, v. 30, n. 2, p. 382–394, June 2014.

TAYLOR, J. W.; MCSHARRY, P. E. Short-term load forecasting methods: An evaluation based on european data. *IEEE Transactions on Power Systems*, v. 22, n. 4, p. 2213–2219, Nov. 2007.

TAYLOR, J. W.; MCSHARRY, P. E. Univariate methods for short-term load forecasting. In: EL-HAWARY, M. E. (Ed.). *Advances in Electric Power and Energy Systems: Load and Price Forecasting*. New York: Wiley, 2017. chap. 2, p. 17–39.

TOUNE, S.; FUDO, H.; GENJI, T.; FUKUYAMA, Y.; NAKANISHI, Y. Comparative study of modern heuristic algorithms to service restoration in distribution systems. *IEEE Transactions on Power Delivery*, v. 17, n. 1, p. 173–181, Jan. 2002.

TOUNE, S.; FUDO, H.; GENJI, T.; FUKUYAMA, Y.; NAKANISHI, Y. Comparative study of modern heuristic algorithms to service restoration in distribution systems. In: *2002 IEEE Power Engineering Society Winter Meeting. Conference Proceedings*. New York, NY, USA: IEEE, 2002. v. 2, p. 787.

TRINDADE, F. C. L.; FREITAS, W.; VIEIRA, J. C. M. Fault location in distribution systems based on smart feeder meters. *IEEE Transactions on Power Delivery*, v. 29, n. 1, p. 251–260, Feb. 2014.

TSAI, M. Development of an object-oriented service restoration expert system with load variations. *IEEE Transactions on Power Systems*, v. 23, n. 1, p. 219–225, Feb. 2008.

U.S. DEPARTMENT OF ENERGY. *Advanced Metering Infrastructure and Customers Systems: Results from the Smart Grid Investment Grant Program*. Washington D.C., USA, 2016. Available at: <https://www.energy.gov/>.

WAKEFIELD, J. *Bayesian and Frequentist Regression Methods*. New York: Springer, 2013.

WANG, Z.; WANG, J. Self-healing resilient distribution systems based on sectionalization into microgrids. *IEEE Transactions on Power Systems*, v. 30, n. 6, p. 3139–3149, Nov. 2015.

WERON, R. *Modeling and Forecasting Electricity Loads and Prices: A Statistical Approach*. New York: Wiley, 2013.

WILLIS, H. *Power Distribution Planning Reference Book*. 2. ed. Boca Ratón, USA: CRC Press, 2004. (Power Engineering).

WU, J. S.; TOMSOVIC, K. L.; CHEN, C. S. A heuristic search approach to feeder switching operations for overload, faults, unbalanced flow and maintenance. *IEEE Transactions on Power Delivery*, v. 6, n. 4, p. 1579–1586, Oct. 1991.

ZADSAR, M.; HAGHIFAM, M. R.; LARIMI, S. M. M. Approach for self-healing resilient operation of active distribution network with microgrid. *IET Generation, Transmission Distribution*, v. 11, n. 18, p. 4633–4643, Nov. 2017.

ZHANG, S.; LIN, S.; HE, Z.; LEE, W. Ground fault location in radial distribution networks involving distributed voltage measurement. *IET Generation, Transmission Distribution*, v. 12, n. 4, p. 987–996, April 2018.

ZIDAN, A.; EL-SAADANY, E. F. A cooperative multiagent framework for self-healing mechanisms in distribution systems. *IEEE Transactions on Smart Grid*, v. 3, n. 3, p. 1525–1539, Sept. 2012.

ZIDAN, A. *et al.* Fault detection, isolation, and service restoration in distribution systems: State-of-the-art and future trends. *IEEE Transactions on Smart Grid*, v. 8, n. 5, p. 2170–2185, Sept. 2017.

APPENDIX A – List of Publications

International Journal Papers:

1. P. L. Cavalcante, **J. C. López**, J. F. Franco, M. J. Rider, A. V. Garcia, M. R. R. Malveira, L. L. Martins and L. C. M. Direito, "Centralized self-healing scheme for electrical distribution systems," *IEEE Transactions on Smart Grid*, vol. 7, no. 1, pp. 145–155, Jan. 2016. DOI: 10.1109/TSG.2015.2454436.

2. **J. C. López**, M. Lavorato, J. F. Franco and M. J. Rider,"Robust optimisation applied to the reconfiguration of distribution systems with reliability constraints," *IET Generation, Transmission & Distribution*, vol. 10, no. 4, pp. 917–927, March 2016. DOI: 10.1049/iet-gtd.2015.0558.

3. **J. C. López**, M. Lavorato, and M. J. Rider,"Optimal reconfiguration of electrical distribution systems considering reliability indices improvement," *International Journal of Electrical Power & Energy Systems*, vol. 78, pp. 837–845, June 2016. DOI: 10.1016/j.ijepes.2015.12.023.

4. **J. C. López**, J. F. Franco and M. J. Rider,"Optimisation-based switch allocation to improve energy losses and service restoration in radial electrical distribution systems," *IET Generation, Transmission & Distribution*, vol. 10, no. 11, pp. 2792–2801, Aug. 2016. DOI: 10.1049/iet-gtd.2015.1509.

5. P. P. Vergara, **J. C. López**, L. C.P. da Silva and M. J. Rider,"Security-constrained optimal energy management system for three-phase residential microgrids," *Electric Power Systems Research*, vol. 146, pp. 371–382, May 2017. DOI: 10.1016/j.epsr.2017.02.012.

6. **J. C. López**, P. P. Vergara, C. Lyra, M. J. Rider and L. C. P. da Silva, "Optimal operation of radial distribution systems using extended dynamic programming," *IEEE Transactions on Power Systems*, vol. 33, no. 2, pp. 1352–1363, March 2018. DOI: 10.1109/TPWRS.2017.2722399.

7. F. M. Wittmann, **J. C. López** and M. J. Rider, "Nonintrusive load monitoring algorithm using mixed-integer linear programming," *IEEE Transactions on Consumer Electronics*, vol. 64, no. 2, pp. 180–187, May 2018. DOI: 10.1109/TCE.2018.2843292.

8. J. E. Cardona, **J. C. López** and M. J. Rider,"Decentralized electric vehicles charging coordination using only local voltage magnitude measurements," *Electric Power Systems Research*, vol. 161, pp. 139–151, Aug. 2018. DOI: 10.1016/j.epsr.2018.04.003.

9. **J. C. López**, J. F. Franco, M. J. Rider and R. Romero, "Optimal restoration/ maintenance switching sequence of unbalanced three-phase distribution systems," *IEEE Transactions on Smart Grid*, vol. 9, no. 6, pp. 6058–6068, Nov. 2018. DOI: 10.1109/ TSG.2017.2703152.

10. P. P. Vergara, **J. C. López**, M. J. Rider and L. C. P. da Silva, "Optimal operation of unbalanced three-phase islanded droop-based microgrids," *IEEE Transactions on Smart Grid*, vol. 10, no. 1, pp. 928–940, Jan. 2019. DOI: 10.1109/TSG.2017.2756021.

11. **J. C. López**, M. J. Rider and Q. Wu, "Parsimonious Short-Term Load Forecasting for Optimal Operation Planning of Electrical Distribution Systems," *IEEE Transactions on Power Systems*, vol. 34, no. 2, pp. 1427–1437, March 2019. DOI: 10.1109/TPWRS.2018.2872388.

12. J. S. Acosta, **J. C. López** and M. J. Rider, "Optimal multi-scenario, multi-objective allocation of fault indicators in electrical distribution systems using a mixed-integer linear programming model," *IEEE Transactions on Smart Grid*, vol. 10, no. 4, pp. 4508–4519, July 2019. DOI: 10.1109/TSG.2018.2862905.

13. J. S. Giraldo, J. A. Castrillon, **J. C. López**, M. J. Rider and C. A. Castro, "Microgrids energy management using robust convex programming," *IEEE Transactions on Smart Grid*, vol. 10, no. 4, pp. 4520–4530, July 2019. DOI: 10.1109/TSG.2018.2863049.

14. P. P. Vergara, J. M. Rey, **J. C. López**, M. J. Rider, L. C. P. da Silva, H. R. Shaker and B. N. Jørgensen , "A Generalized Model for the Optimal Operation of Microgrids in Grid-Connected and Islanded Droop-Based Mode," *IEEE Transactions on Smart Grids*, vol. 10, no. 5, pp. 5032–5045, Sept. 2019. DOI: 10.1109/TSG.2018.2873411.

15. J. S. Giraldo, **J. C. López**, J. A. Castrillon, M. J. Rider and C. A. Castro, "Probabilistic OPF Model for Unbalanced Three-phase Electrical Distribution Systems Considering Robust Constraints," *IEEE Transactions on Power Systems*, vol. 34, no. 5, pp. 3443–3454, Sept. 2019. DOI: 10.1109/TPWRS.2019.2909404.

16. P. P. Vergara, **J. C. López**, M. J. Rider, H. R. Shaker, L. C. P. da Silva and B. N. Jørgensen , "A stochastic programming model for the optimal operation of unbalanced three-phase islanded microgrids," *International Journal of Electrical Power & Energy Systems*, to be published, 2020. DOI: 10.1016/j.ijepes.2019.105446.

Book Chapters:

1. P. P. Vergara, **J. C. López**, J. M. Rey, L. C. P. da Silva, M. J. Rider, "Energy Management in Microgrids," *Microgrids Design and Implementation*, Springer International Publishing, ch. 7, pp. 195–216, 2019. DOI:10.1007/978-3-319-98687-6.

International Conference Papers:

1. C. F. D. Moya, L. C. P. da Silva, **J. C. López** and P. P. Vergara, "GRASP model for smart home electrical loads scheduling," *International Energy and Sustainability Conference (IESC 2015)*, Farmingdale, NY, USA, 2015.

2. F. D. Moya, **J. C. López** and L. C. P. da Silva, "Model for smart building electrical loads scheduling," *IEEE 16th International Conference on Environment and Electrical Engineering (EEEIC 2016)*, Florence, Italy, 2016.

3. P. P. Vergara, **J. C. López**, C. Lyra and L. C. P. da Silva, "Optimal schedule of dispatchable DG in electrical distribution systems with extended dynamic programming," *17th International Conference on Harmonics and Quality of Power (ICHQP 2016)*, Belo Horizonte, Brazil, 2016.

4. **J. C. López**, M. J. Rider, P. L. Cavalcante, A. V. Garcia, L. L. Martins, L. F. Miranda and L. F. Silveira, "Smart Grids: self-healing and switch allocation in a real system," in *12th Latin-American Congress on Electricity Generation and Transmission (CLAGTEE 2017)*, Mar del plata, Argentina, 2017.

5. **J. C. López**, M. J. Rider, A. V. Garcia, P. L. Cavalcante, L. F. Miranda and L. L. Martins, "Optimization approach for the allocation of remote-controlled switches in real-scale electrical distribution systems," *IEEE PES Innovative Smart Grid Technologies Conference Europe (ISGT-Europe 2017)*, Torino, Italy, 2017.

6. N. B. Arias, R. Romero, **J. C. López**, M. J. Rider, "Optimal Sizing of Stationary Energy Storage Systems Participating in Primary Frequency Regulation Markets," *IEEE PES Transmission & Distribution Conference and Exhibition - Latin America (T&D-LA)*, Lima, Peru, 2018.

7. F. Shen, Q. Wu, S. Huang, **J. C. López**, C. Li and B. Zhou, "Review of Service Restoration Methods in Distribution Networks," *2018 IEEE PES Innovative Smart Grid Technologies Conference Europe (ISGT-Erope)*, Sarajevo, Bosnia-Herzegovina, 2018.

8. **J. C. López**, M. J. Rider, F. Shen, Q. Wu, “Distributed Service Restoration of Active Electrical Distribution Systems using ADMM,” *2019 IEEE PES Innovative Smart Grid Technologies Conference North-America (ISGT-NA)*, Washington DC, EEUU, 2019.

9. P. P. Vergara, **J. C. López**, L. C. P. da Silva and M. J. Rider, “Economic Impact of the Active Power Droop Gain in Droop-Based Islanded Microgrids,” *IEEE PES PowerTech Milan 2019*, Milano, Italy, 2019.

10. E. F. Alvarez, **J. C. López**, P. P. Vergara, J. J. Chavez, and M. J. Rider, “A Stochastic Market-Clearing Model Using Semidefinite Relaxation,” *IEEE PES PowerTech Milan 2019*, Milano, Italy, 2019.